SIMULTANEOUS CALIBRATION OF A MICROSCOPIC TRAFFIC SIMULATION MODEL AND OD MATRIX

A Dissertation

by

SEUNG-JUN KIM

Submitted to the Office of Graduate Studies of
Texas A&M University
in partial fulfillment of the requirements for the degree of

DOCTOR OF PHILOSOPHY

August 2006

Major Subject: Civil Engineering

SIMULTANEOUS CALIBRATION OF A MICROSCOPIC TRAFFIC SIMULATION MODEL AND OD MATRIX

A Dissertation

by

SEUNG-JUN KIM

Submitted to the Office of Graduate Studies of
Texas A&M University
in partial fulfillment of the requirements for the degree of

DOCTOR OF PHILOSOPHY

Approved by:

Co-Chairs of Committee,	Laurence R. Rilett
	Mark Burris
Committee Members,	Tim Lomax
	Cliff Spiegelman
Head of Department,	David V. Rosowsky

August 2006

Major Subject: Civil Engineering

ABSTRACT

Simultaneous Calibration of a Microscopic Traffic Simulation Model and OD Matrix.

(August 2006)

Seung-Jun Kim, B.S., Seoul National University;

M.S., Seoul National University

Co-Chairs of Advisory Committee: Dr. Laurence R. Rilett
Dr. Mark Burris

With the recent widespread deployment of intelligent transportation systems (ITS) in North America there is an abundance of data on traffic systems and thus an opportunity to use these data in the calibration of microscopic traffic simulation models. Even though ITS data have been utilized to some extent in the calibration of microscopic traffic simulation models, efforts have focused on improving the quality of the calibration based on aggregate form of ITS data rather than disaggregate data.

In addition, researchers have focused on identifying the parameters associated with car-following and lane-changing behavior models and their impacts on overall calibration performance. Therefore, the estimation of the Origin-Destination (OD) matrix has been considered as a preliminary step rather than as a stage that can be included in the calibration process.

This research develops a methodology to calibrate the OD matrix jointly with model behavior parameters using a bi-level calibration framework. The upper level seeks to identify the best model parameters using a genetic algorithm (GA). In this level, a statistically based calibration objective function is introduced to account for disaggregate form of ITS data in the calibration of microscopic traffic simulation models and, thus, accurately replicate dynamics of observed traffic conditions. Specifically, the Kolmogorov-Smirnov test is used to measure the "consistency" between the observed and simulated travel time distributions. The calibration of the OD matrix is performed in the lower level, where observed and simulated travel times are incorporated into the OD estimator for the calibration of the OD matrix. The interdependent relationship between

travel time information and the OD matrix is formulated using a Extended Kalman filter (EKF) algorithm, which is selected to quantify the nonlinear dependence of the simulation results (travel time) on the OD matrix.

The two test sites are from an urban arterial and a freeway in Houston, Texas. The VISSIM model was used to evaluate the proposed methodologies. It was found that that the accuracy of the calibration can be improved by using disaggregated data and by considering both driver behavior parameters and demand.

DEDICATION

This dissertation is dedicated to my wife Sooyoung,
who always stands by me,
and who gives me more love than I deserve.

ACKNOWLEDGEMENTS

First, I would like to express my sincere appreciation to Dr. Laurence Rilett, my academic advisor and co-chair of my committee, for his guidance and encouragement during my studies at Texas A&M University and University of Nebraska-Lincoln (UNL). I am particularly grateful that he provided all the research assistantships that allowed me to complete this dissertation. When he joined the faculty at UNL, he arranged for me to continue my studies with him in Lincoln. Very special thanks go to Dr. Mark Burris for his thoughtful guidance, who graciously agreed to serve as my co-chair when Dr. Rilett moved to UNL. Furthermore, I would like to thank Dr. Tim Lomax and Dr. Cliff Spiegelman for providing technical expertise and for taking the time to serve on my committee.

I would like to thank Dr. Joe Zietsman for his technical support. And thanks to Hanseon, Wonho, Muhammad, Justice, and Baven for the good times and constant friendships.

Finally, I am most grateful to my mother, Hansook Yoo, for her patience and encouragement throughout my study.

TABLE OF CONTENTS

Page

CHAPTER Page

CHAPTER Page

CHAPTER Page

Page

LIST OF FIGURES

Page

Page

Page

Page

Page

LIST OF TABLES

Page

Page

CHAPTER I

INTRODUCTION

1.1 BACKGROUND

Transportation engineers and researchers have come to rely on microscopic traffic simulation models in the evaluation of both traffic operations and transportation planning strategies. This is because identifying the best strategy using field tests is difficult. An appealing feature of microscopic traffic simulation models is that they can provide a visual representation of complex traffic conditions and capture the behavior and interactions of vehicles under a wide variety of scenarios. In order for microscopic traffic simulation models to represent reality, the ability to accurately and efficiently model traffic flow characteristics, driver behaviors, and traffic control operations is critical. This implies, in turn, that the model parameters are accurately calibrated to local conditions.

On account of the lack of readily available automatic calibration procedures, microscopic traffic simulation models are often used with default parameter values. If parameters are to be adjusted, these adjustments are typically based on educated guesses or a manual trial and error calibration approach. If the microscopic traffic simulation model has inaccurate or inappropriate parameters then there is a greater probability that incorrect results could be obtained and, ultimately, this could lead to faulty decisions.

The need for fine-tuning microscopic traffic simulation models has been addressed to replicate the network being modeled. Research efforts to date have mainly focused on minimizing the difference between observed and simulated traffic conditions based on the aggregate data, rather than disaggregate data. One of main reasons is related to the lack of available data for use in calibration purpose. However, with the

---

This dissertation follows the style of the Transportation Research Record.

recent nationwide deployment of intelligent transportation system (ITS) there is an abundance of data on traffic systems and thus an opportunity to use these data in the calibration process. In addition, the recent growth in computational resources now makes it possible to develop an automatic calibration process based on standard optimization theory that takes advantage of this ITS data. The improvement in ITS technology and computational resources makes the refined calibration process more attainable.

The calibration is generally defined as the process of adjusting the value of the parameters related to driver behavior in microscopic traffic simulation models such that the observed data is "consistent" with the simulated data. The objective of this research is to develop a methodology in which ITS data is incorporated into the calibration process to better represent reality. In addition, the research will develop a methodology to calibrate the OD matrix by quantifying its impacts on the simulated travel time results. Considering the fact that the estimation of an OD matrix has a profound effect on the quality of simulation results, a reliable OD estimator should exist that adequately represents true travel patterns for a successful simulation modeling. Most of the current calibration research seeks to identify driver behavior parameters separately without consideration of the traffic demand. This may pose a significant challenge in making simulation results useful because it implies perfect OD estimation that reflects true travel patterns.

1.2 PROBLEM STATEMENT

1.2.1 Need to Incorporate Disaggregate ITS Data into the Calibration of Microscopic Traffic Simulation Models

Microscopic traffic simulation models have become increasingly important in transportation operations and planning. In addition to greater computer performance, the abundance of ITS data opens further possibilities for achieving higher credibility or reliability of simulation results. There are many types of ITS data acquisition technologies and ITS data may be archived in different manners. For example, travel time of individual vehicle, the distribution of travel times, or the measure of central

tendency (i.e. mean), and dispersion (variance), all may be archived. These data can be used not only as inputs to microscopic traffic simulation models but also as calibration datasets. Therefore, there is a need to develop a methodology that can use disaggregated ITS data, rather than simply aggregated data, in the calibration of microscopic traffic simulation models.

1.2.2 Need to Adopt a Statistically Based Calibration Objective Function

If done properly, archived ITS data can provide access to disaggregate traffic flow characteristic details. All parts of these disaggregate data have specific qualities which could potentially prove useful if captured. However, to date, no approach that uses disaggregate data in the calibration process has been proposed. Also, there is no established guideline on checking as to the quality of the simulation results. The most critical and common limitation in existing calibration processes is that there is no clear guideline on the extent to which simulation models should replicate reality.

The objective function based on an aggregate form of the observed data has been adopted over the years because of its simplicity and limitation in the availability of data. Without considering other stochastic attributes of the observed data, the parameter set with the lowest average difference between the observed and simulated data is selected as the "best". In practice, traffic conditions have large variability so that aggregated performance measures, such as average travel time, may not be the most appropriate measure of effectiveness. For example, travel times are likely to deviate from their means in significant ways, especially during peak periods.

The use of the aggregated performance measure in the calibration of simulation models may cause a danger that inappropriate parameter sets may be selected. It is hypothesized that a statistically based approach, which is grounded on a more disaggregate form of the observed data, would avoid this situation. Specifically there is a need 1) to use the "closeness" of the observed travel time distribution to that of the simulated travel time distribution as the basis of the objective function; and 2) to measure this "closeness" using statistical techniques.

1.2.3 Need to Identify the "Best" Parameters among Competing Parameters

Because the calibration process is statistically based, there may be numerous parameter sets (or none) with which the observed traffic conditions are replicated in the microscopic traffic simulation model. When this occurs, an alternative selection technique may be required for identifying the best among competing parameter sets. The need for an alternative selection technique may be higher in networks that have greater congestion and more complex traffic situations. The application of a statistically based objective function does not exclude an automatic identification of the best parameter sets but rather leaves the final decision to the traffic engineer.

A single metric based on aggregate data could identify numerous different parameter set, denoted by N_{single}, which have "low" values of the mean absolute error ratio (MAER) or the root mean square error (RMSE). There are also a large number of statistically valid parameter sets, denoted by N_{stat} based on disaggregate data. Intuitively, the number of parameter sets N_{stat} from a statistically based objective function is less than that of parameter sets N_{single} from a single metric. This is because a statistically based objective function compares the distributions itself rather than central tendency only.

Note that there are numerous ways that one parameter set can be identified as the "best" from a set of potential solutions. Most commonly, the parameter set with the lowest MAER or RMSE could be selected as "best". By the same token, the parameter set with the highest *p*-value from the statistical test could be selected as the one that most closely represents the observed distribution. The statistical test could be one that tests for differences in the *mean* value of a specific variable or one that tests for differences in the *distribution* of the variable. Another selection criterion would be to select the parameter set that is the "least" different from default values. Engineering judgment could also be used. For example, the parameter set that best represents the saturation flow rate (arterial) or capacity (freeway) given by the Highway Capacity Manual (HCM) might be an appropriate.

1.2.4 Need to Perform Simultaneous Calibration of Driver Behavior Parameters and the OD Matrix

The interdependent relationship of travel demands and driver behavior parameters has not been taken into account in the calibration of simulation models. Traditionally, OD demands are assumed to be constant during the calibration process and research efforts have focused on the calibration of driver behavior parameters. However, the individual impact of these on simulation results cannot be considered separately.

In this research, it is hypothesized that the quality of the calibration results can be improved by incorporating the simulated travel times into the calibration of the OD matrix. The fact that travel time is a function of OD demands and vice versa provides a basis for the simultaneous calibration approach. Another consideration is that most OD estimators rely on the *a priori* OD matrix, sampled OD pattern, or traffic counts, which are not error-free measurements. Hence, it is plausible that the OD matrix can be calibrated to match the empirical observations. Intuitively, for a network where OD estimates may not be reliable, this approach would be particularly important.

1.3 RESEARCH OBJECTIVES

The widespread deployment of ITS technology provides a potential to archive OD patterns, travel times, and other information for use in the calibration of microscopic traffic simulation models. The objective of this research would be to develop a methodology for calibrating microscopic traffic simulation models using ITS data. The focus is placed upon the following: 1) incorporate ITS data to obtain superior calibration results; 2) apply a statistically based objective function on both a signalized arterial and an urban freeway network; 3) investigate alternative selection techniques in identifying the "best" parameter set among competing parameter sets; and 4) calibrate driver behavior parameters and the OD matrix jointly using a bi-level calibration framework,

1.4 RESEARCH FRAMEWORK

1.4.1 Perform Literature Review

Previous research pertaining to the calibration process of microscopic traffic simulation models will be comprehensively reviewed. Literature specific to the selected microscopic traffic simulation model, GA optimization theory, overall calibration process, and OD estimation techniques with emphasis on Kalman filtering will be analyzed.

1.4.2 Identify Test Networks and Collect Data

The proposed methodology will be evaluated on a signalized arterial and an urban freeway in Houston, Texas. The selected arterial is Bellaire Boulevard located in the southwest of Houston. It is a 1 km long arterial with 4 intersections. A video tape recording system will be used to obtain travel time data, and the signal timing plan is available from Houston TransStar. The freeway corridor is comprised of a 15.4 km section of eastbound Interstate 10 (I-10) leading to downtown Houston. This corridor is equipped with an AVI system from which the sampled OD pattern and other information will be derived.

1.4.3 Estimate Initial OD Matrix

After data collection, extensive data reduction is required to estimate the initial OD matrix from AVI data. This task includes obtaining the vehicle tag number, AVI station number, and passage time and date. From the ordered data, the sampled OD pattern, path information, and historical information such as the variance-covariance matrix will be derived. A Kalman filtering approach will be used to estimate the initial OD matrix. The framework for incorporating AVI data into OD estimation is based on the findings of Dixon (1).

1.4.4 Identify Travel Time Distribution

The distributions of the travel times on both test networks will be identified. If the distribution cannot be identified, non-parametric techniques will be used to compare the observed and simulated distributions.

1.4.5 Develop Automated Calibration Program

The goal of this task is to develop an automated calibration process using the Genetic Algorithm (GA). This automated process will be coded using the PERL programming language in a way that the modular structure enables flexible modifications whenever additions or changes need to be made in the program.

1.4.6 Apply a Statistically Based Objective Function

While the issue of travel time variability is clearly important from the perspective of calibration, to date there has been no methodology for addressing this issue in the literature. In general, the more popular methods focus on testing the equality of either the means or the variance of the distribution of a particular variable – in this case travel travel time. However, these tests do not examine the distribution of the travel times, which may be rather restrictive for many transportation applications. In this research, the hypothesis that the observed and simulated travel time data have the same *distribution* will be tested.

1.4.7 Perform Simultaneous Calibration of Driver Behavior Parameters and OD Matrix

It is hypothesized that simultaneous calibration of driver behavior parameters and the OD matrix would have a positive impact on the accuracy of simulation results. Because traffic conditions are not stable during the peak hour, the inclusion of travel times into the calibration of OD matrix and behavior parameters (if available) may increase the quality of overall calibration process. To calibrate the OD matrix based on the simulated

travel times, the relationship between OD matrix and travel times should be well established. Intuitively, this relationship cannot be expressed in analytical or deterministic state-space modeling form. This is because the relationship is highly non-linear and varies both spatially and temporally. In fact, while there are some simplified standard congestion functions, such as BPR or volume-density function (2, 3), there are no universally accepted formulae.

The calibration of OD matrix will be performed using the extended Kalman filter (EKF) that is designed to approximate the solution by linearization of nonlinear relationships (4, 5, 6). The EKF formulation is different from the standard KF used for estimating initial OD matrix in that the travel time data is augmented into its measurement equation.

1.5 CONTRIBUTION OF THE RESEARCH

This research provides a methodology for combining the calibration of driver behavior parameters and the OD matrix using ITS data to find-tune the microscopic traffic simulation model. To achieve this, a statistically based calibration objective function is introduced, and the observed and simulated travel time information are utilized for the calibration of the OD matrix. Some of the main contributions are: 1) use of disaggregate ITS data in the form of distribution as a target performance measure; 2) utilization of a statistically based objective function which defines a measure of effectiveness in terms of closeness of the empirical observation to the simulated results; 3) application of alternative selection techniques for identifying the “best” parameter set among the competing parameter sets; 4) development of the bi-level calibration framework where simultaneous calibration of OD matrix and driver behavior parameters are performed; and 5) the enhancement of the calibration accuracy as a result of the simultaneous calibration of the OD matrix and driver behavior parameters.

1.6 ORGANIZATION OF THE DISSERTATION

This dissertation is organized into eight chapters and three appendices. Chapter I summarizes the problems addressed by this study and establishes the objectives and scope of this dissertation. Chapter II provides a literature review of the main topic of this research. It outlines an introduction to the selected microscopic traffic simulation model, GA optimization theory, overall calibration process, and OD estimation techniques. Chapter III provides a framework of this study. It contains a description of the test networks, collection of simulation input data, and discussion on the bi-level calibration framework. Chapter IV illustrates how AVI data can be filtered in the existing AVI data filtering methods. It also proposes a method to better tracing of increasing and decreasing trends in the AVI travel time observations. Chapter V describes a methodology in which a statistically based calibration objective function is applied to incorporate disaggregate ITS data into the calibration of the microscopic traffic simulation model. In addition, Chapter V examines alternatives for selecting the best parameter set among competing parameter sets. Chapter VI presents a methodology for the simultaneous calibration of driver behavior parameters and the OD matrix using the bi-level calibration process. This section includes the mathematic formulation of the Extended Kalman filtering approach employed to relate the OD matrix and the travel time data. The calibration results of the proposed bi-level methodologies are presented and analyzed in Chapter VII. Finally, the findings and future research are provided in Chapter VIII.

CHAPTER II

LITERATURE REVIEW

The purpose of this chapter is to provide a comprehensive review of the literature necessary to achieve the statement of work addressed in Chapter I. Subsection 3.1 provides the underlying traffic flow theories of VISSIM and CORSIM microscopic traffic simulation models. Subsection 3.2 reviews the calibration procedure and optimization algorithms that have been employed in an automated calibration process. Subsection 3.3 provides a review of estimating the origin destination (OD) matrix with emphasis on the Kalman filter algorithm. The concluding remarks are presented in subsection 3.4.

2.1 MICROSCOPIC TRAFFIC SIMULATION MODELS

Traffic simulation software has been widely used to analyze transportation networks where analytical approaches are not feasible due to time and budget constraints or do not provide satisfactory results. These software can be primarily categorized into three types according to the level of details at which the fundamental traffic variables are modeled (7, 8). Macroscopic traffic simulation models describe the traffic stream in terms of an aggregate flow using continuum equations. Mesoscopic traffic simulation models describe traffic entities at a high level of detail but some component of the modeling is described at a lower level of detail. For example, vehicles may be modeled as individuals at intersections using discrete queuing theory but their travel time down links may be modeled using macroscopic speed density relationships.. Both macroscopic and mesoscopic models requires less data input and computing power and therefore they are suitable for modeling large networks.

On the other hand, microscopic traffic simulation models consider the detailed movement of individual vehicles. They use various models and algorithms to capture the

stochastic nature of individual vehicles. Even though there is slight difference between the models, the following discussion is equally relevant to all microscopic traffic simulation models. Microscopic traffic simulation models generally adopt a specific car-following and lane-changing models as well as different vehicle performance characteristics to model individual vehicle behavior. Each vehicle that enters the network is assigned different operational characteristics to allow for more realistic representation of reality. They include vehicle types and corresponding vehicle performances and driver characteristics. These characteristics are uniquely assigned to each vehicle and are maintained while it travels though the network. The interactions among system entities (vehicle to vehicle, vehicle to roadway, and vehicle to control device) are modeled based on car-following and lane-changing models. According to these interactions, the movement of an individual vehicle is updated for each scanning interval and its associated information such as position and speed are also updated.

Successful application of the microscopic traffic simulation model requires a reasonable understanding of underlying traffic flow theories as well as modeling assumptions (9). The lack of understanding makes it difficult to adequately utilize the model in its intended manner. Therefore, reviewing the theories behind the model may improve trust in the "black box" technology and, in turn, may be more likely to make best use of the microscopic traffic simulation in the following ways (9, 10): 1) identifying capabilities and limitations in terms of coding, visualization, and types of transportation networks; 2) choosing the right simulation model suitable for a certain transportation network evaluation or planning analysis being considered; 3) giving guidance on the strength and weakness regarding the development and application of the selected simulation model; and 4) selecting appropriate model parameters that can be used for calibrating the transportation network being modeled.

Of those which are currently available for modeling transportation networks, VISSIM and CORSIM are the microscopic traffic simulation models that are most frequently used in the North America for research and commercial purposes. The next

three subsections present more detailed review and comparison of VISSIM and CORSIM models.

2.1.1 VISSIM

VISSIM is a microscopic, time step, and behavior-based model that was developed by Planung Transport Verkehr (PTV) in Germany (11). VISSIM can model various components of the transportation network, including multiple modes of transportation, various types of signal operations, and different traffic composition (11, 12). As a useful tool for evaluating transportation alternatives, VISSIM provides significant flexibility in modeling transportation networks such as developing transit signal priority (TSP), allowing user to define signal control logics through the external signal generator (VAP), interfacing other signal packages for optimizing coordinated or actuated signal timing parameters, and comparing design alternatives (signalized or sign controlled intersection or roundabout).

To model traffic streams, VISSIM adopts the psycho-physical car-following model developed by Wiedemann (13, 14). This is a discrete, stochastic, and microscopic model, where a driver-vehicle-unit is defined as a single entity. A psycho-physical car-following model introduces the concept of "state" of a vehicle. The state of a vehicle is determined by the difference in distance and speed in comparison to the leading vehicle. If changes in distance and speed occur, the driver reacts and a new value for acceleration or deceleration is calculated.

This model is based on the assumption that a driver can be in one of four driving states. Table 2.1 describes how acceleration or deceleration is calculated for four different driving states. Figure 2.1 shows an observation-decision diagram of four driving states, where the x-axis represents the difference in speed with the left part indicating that the following vehicle is faster than the leading vehicle and the y-axis represents the difference in distance (headway).

- Free driving state: In this state, the influence of the leading vehicle is negligible. The driver tries to reach and maintain his/her desired speed but the speed in reality tends to oscillate around the desired speed.
- Approaching (approximating) state: The driver tends to adjust his/her speed to the lower speed of the leading vehicle. In this state, the driver decelerates until the difference in speed between the leading and following vehicles is zero at the moment when the desired safety distance is reached.
- Following state: The driver follows the leading vehicle without any conscious acceleration or deceleration, thus keeping the distance very nearly constant. Imperfect perception in the speed difference makes the distance between the leading and following vehicle oscillate around the desired safety distance.
- Braking state: The driver applies medium to high deceleration if the distance is smaller than the desired safety distance. This state happens due to lane-changer from adjacent lane or sudden braking of the leading vehicle.

TABLE 2.1 Driving States of Wiedemann Psycho-Physical Model (15)

State	Kind of drive	Acceleration
Free Driving I	Not influenced	depending on the current speed and the desired speed
Free Driving II	Direct influenced	positive acceleration until the desired distance is reached and the difference in speed is zero
Approximating I	Direct influenced	negative acceleration until the desired distance is reached and the difference in speed is zero
Approximating II	Direct influenced	negative acceleration until the risk distance is reached and the difference in speed is zero
Following	Indirect influenced	keeping acceleration until the desired distance is reached and the difference in speed is zero
Braking	Direct influenced	negative acceleration when the distance is smaller than the desired safety distance

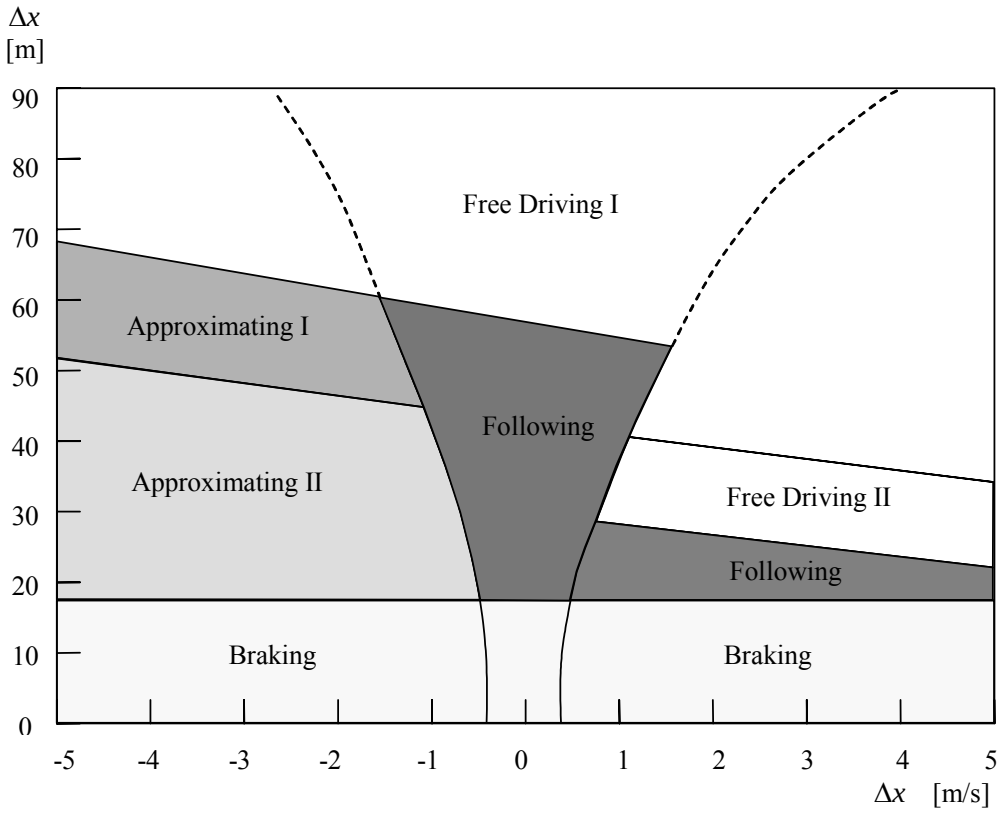

Figure 2.1 Driving State Diagram of Wiedemann Psycho-Physical Model

Each mode can be expressed as a combination of the difference in speed and distance. However, each driver's abilities to perceive or estimate the difference in speed and distance are different. Therefore, each driver has different threshold values where the driver switches from one state to another. Because the model takes into account the physical aspects (equation of vehicle motion) and physiological restrictions of individual driver's ability, it is called a psycho-physical car-following model (15).

The detailed logics of a psycho-physical car-following model are well documented in a more recent paper (16). To divide the driving state into the named area, two speed-related thresholds and four distance-related thresholds are introduced. The threshold for positive and negative speed difference is computed according to Equation 2.1.

$$\Delta v_{positiv\ or\ negative} = k_1(\Delta x - A_0)^2 + k_2 \quad (2.1)$$

$\Delta v_{positiv\ or\ negative}$ = threshold for positive or negative speed difference (m);

Δx = distance between the leading and following vehicles (m);

A_0 = standstill distance (m); and

$k_1,\ k_2$ = constants.

Besides the thresholds for speed difference, the desired distance (AD), risky distance (AR), safety distance (AS), and braking distance (AB) are introduced to describe driving behaviors with regard to the distance between the leading and following vehicles.

$$AD = A_0 + T_d \cdot v_f \quad (2.2)$$

$$AR = A_0 + T_r \cdot v_l \quad (2.3)$$

$$AS = A_0 + T_s \cdot v_f \quad (2.4)$$

$$AB = AR + \frac{\Delta v^2}{b_m} \quad (2.5)$$

v_f, v_l = speeds of the following and leading vehicles (m/s);

Δv = speed difference between the following and leading vehicles (m/s);

T_d, T_r, T_s = time headways for desired, risky, and safety distance, respectively (sec); and

b_m = deceleration rate (m/sec^2).

Based on the thresholds computed by Equation 2.1 through Equation 2.5, the driving behavior is divided into the driving states, as shown in Figure 2.1. For example,

the danger state can be defined as the case ($\Delta x \le AR$) where the distance to the leading vehicle is smaller than the risky distance (AR). Thus, it is necessary to decelerate to avoid risky situation. After identifying its present state, each driver updates his/her next position by choosing a new acceleration or deceleration. A new value for the acceleration or deceleration is computed by Equation 2.6 (15).

$$a_f = \frac{(\Delta x - A_0 - T_d v_f) a_l - 0.5\Delta v^2}{\Delta x - A_0 - T_d v_l} \quad (2.6)$$

a_f, a_l = acceleration of the following and leading vehicles (m/sec^2).

VISSIM adopts a rules-based algorithm to model lateral movements in multi-lane roadways as well as a psycho-physical car-following model for longitudinal movement. A driver is motivated to change his or her lane if the leading vehicle predictably hinders his/her movement or there is a necessity to stay within a predefined route such as an upcoming exit with a deceleration lane. A driver checks whether the present situation can be improved by the intended lane change. The following vehicle in the neighboring lane and the leading vehicles in the neighboring and direct lanes are considered in the decision structure. The conditions (position and speed) of these three vehicles decides whether a benefit arise without generating a dangerous situation.

In the VISSIM model the user can control a number of parameters associated with the car-following models to accurately mimic dynamics of traffic. They include number of observed preceding vehicles, looking ahead distance, standstill distance, and desired safety distance parameters, car-following oscillation parameter, and so on. In contrast, VISSIM provides only a few parameters that influence directly the lane-changing behavior such as lane-changing distance and maximum acceptable deceleration.

2.1.2 CORSIM

CORidor SIMuation (CORSIM), an integration of the NETSIM and FRESIM models, is a microscopic traffic simulation model designed for simulating traffic flow on integrated networks consisting of freeways and surface streets. CORSIM is a micro simulation component of the TRAF family of models developed by the Federal Highway Administration (FHWA). It combines NETSIM and FRESIM simulation models into an integrated package providing comprehensive simulation capabilities in the areas of traffic operational analysis, geometric design evaluations, congestion assessment and mitigation strategies, and assessment of transportation systems management (TMS) strategies.

CORSIM simulates the traffic behavior at a microscopic level and with detailed representation of individual vehicles and their interaction with their physical environment and other vehicles. Both NETSIM and FRESIM components of the CORSIM model have been widely used and their main simulation capabilities have been extensively discussed in a number of publications and reports (17, 19, 21, 22). It can be classified as high fidelity because it attempts to represent the spatial interaction of drivers on a continuous basis and because it attempts to model the car-following logic of drivers in detail, where the vehicle acceleration for each scanning interval is determined through difference in speed between the leading and following vehicles. Because the model is designed to mimic the dynamics of traffic the modeler has control over a large number of parameters including car following sensitivity factor, percentage of distinct vehicle types, aggressiveness of the drivers, and acceleration or deceleration capabilities.

FRESIM uses the Pitts car-following model to determine the acceleration of the following vehicle. The basic proposition is that vehicles attempt to maintain constant space headway between the leading and following vehicles, according to Equation 2.7 (17). The first two terms in the equation represent the length of the leading vehicle and the minimum vehicle separation, respectively. The third term accounts for the variability in driver space headway depending on the speed of the following vehicle and driver sensitivity factors. The final term was introduced to allow for larger space headway. A

calibration constant *b* was assigned to a value of 0.1 based on empirical studies when the speed difference between the following and leading vehicles is relatively small ($V_l - V_f \leq 10$).

$$H = L + s + kV_f + bk(V_l - V_f)^2 \quad (2.7)$$

H = space headway (ft);

L = length of the leader (ft);

k = driver sensitivity factor (sec);

s = minimum vehicle separation (ft);

V_l = speed of the leader (ft/sec);

V_f = speed of the follower (ft/sec); and

b = calibration constant.

In order to maintain the desired space headway, the following vehicle needs to react to the location and speed difference between the following and leading vehicles. The acceleration or deceleration rate of the following vehicle can be derived from Equation 2.7. The resulting acceleration or deceleration rate is shown in Equation 2.8, while its derivation can be found in the literature (18, 19).

$$a_f = \frac{2(x_l^{t+T} - x_f^t - L - s - V_f^t(k+T) - bk(V_l^{t+T} - V_f^t)^2)}{T^2 + 2\,kT} \quad (2.8)$$

a_f = acceleration rate of the follower at time t to $t+T$ (ft/sec^2);

x_l^{t+T} = position of the leader at time $t+T$ (ft);

x_f^t = position of the follower at time t (ft); and

T = time scanning interval (sec).

In this equation, the driver sensitivity factors are used to determine a desired car-following distance. A higher value of the sensitivity factor results in larger space headway and subsequently lower capacity. However, a reaction of individual driver varies from driver to driver. Therefore, CORSIM allows for the distribution of sensitivity factors to determine the various desired car-following distance for each individual driver (17, 18).

The CORSIM model adopts a lane-changing algorithm that makes drivers improve their position through gap evaluation and gap acceptance of the lane-changing decision. The leading and trailing gaps that are computed from the locations of the lane-changer and the putative leader and follower in the neighboring and direct lanes are primary factors for the lane-changing decision. The gap evaluation is made based on the deceleration rate during the lane-changing maneuver required to maintain safe positions for the lane-changer and the putative leader. The required deceleration rate should be smaller than the maximum acceptable deceleration rate and the advantage of obtaining more favorable position should be gained by the lane-changer (20).

With the premise of the basic lane-changing process, CORSIM categorizes lane-change maneuvers into three different models (20). The first is the mandatory lane-change where the driver allows higher risk to perform the lane-change for the situations such as merging from the on-ramp, exiting the network, and vacating from the dropped lane. The second is the discretionary lane-change where the driver overtakes slow moving vehicles. Discretionary lane-change is modeled based on behavioral factors associated with the lane-change. They include the intolerable speed to motivate the lane-change, the advantage or disadvantage of remaining in the current lane or moving to the neighboring lane, and the urgency for lane-changing maneuver. The last is the anticipatory lane-change that is related to lane-change maneuver upstream of on-ramps. Based on the volume and speed in the vicinity of on-ramps, the CORSIM model determines whether or not the driver performs the lane-change to avoid the downstream congestion.

CORSIM allows the user to control the parameters associated with the CORSIM lane change maneuver. They include the time delay to accelerate or decelerate, driver's aggressiveness in lane-changing process, duration of time to complete the lane-changing maneuver, and level of cooperation of the putative follower (17)

2.1.3 Comparison of VISSIM and CORSIM

The ability of the microscopic traffic simulation software is a major concern for traffic engineers who need to make decision on which software to use for the analysis. This section provides a brief comparison of the two major models, VISSIM and CORSIM based on the research conducted by the Institute for Transport Studies at the University of Leeds (23).

- Car-following and lane changing models: Driver behavior models employed in CORSIM and VISSIM have been assumed to have an implied validity in a wide range of application. Some researchers proved the validity of these models by comparing a simulated driving process with measurement data such as a probe vehicle or GPS data (24, 25). In addition, both models are well-documented, helping users clearly understand and make best use of them, while other models are often more of a black box and detailed algorithms are not shared.
- Network coding: VISSIM is more flexible since it is based on a link-connector structure while CORSIM has a link-node structure. However, the time required for coding transportation networks into CORSIM is shorter. VISSIM requires greater efforts and times for coding networks, but when exporting function is used in conjunction with other transportation software (EMME2, TransCad, GIS packages, Synchro, and SimTraffic), networks can be built relatively quickly.
- Multi-modal analysis: VISSIM can model public transits in detail and HOVs. In addition, a wide variety of transit priority rules as well as railroad preemption strategies can be modeled and analyzed. On the other hand, CORSIM does not have transit and railroad preemption modeling capabilities.

- Graphical representation: The CORSIM animation program (TRAFVU) provides a two-dimensional representation where cars, trucks, and buses are expressed as rectangular shapes with limited colors. On the other hand, VISSIM can record movie clips, with the ability to change views and perspectives. In addition, other visual elements (trees, buildings, traffic signs) can be inserted into the three-dimensional animation.
- Signal control logic: Besides the internal fixed time signal control, VISSIM provides the optional external signal generator (VAP), where users define or create their own signal control logic in a text file using a simple programming language. This function makes it easy to model actuated signal control logic as well as other signal strategies. CORSIM provides both fixed time and actuated signal control logic, but it is difficult for users to define any types of special feature including transit priority, ramp metering, and railroad preemption.
- Dynamic Traffic Assignment (DTA): VISSIM adopts the DTA approach developed by Massachusetts Institute of Technology (MIT) where a driver updates information on the traffic stream and then is reassigned accordingly as they move through entire network. COSRIM traffic assignment is limited to a single network type, meaning serious limitation if both arterial and freeway corridors are modeled at the same time. Furthermore, it uses a static trip distribution function, thus keeping the optimal path constant throughout a successive simulation run regardless of network traffic conditions.

There are several expected advantages when VISSIM is selected to model the transportation networks in this dissertation: 1) because both actuated signal control and transit priority are under operation on Bellaire arterial in Houston, one of the selected test beds in this dissertation, VISSIM is more suitable for modeling this section. As stated earlier, even though CORSIM and VISSIM have ability to model various types of transportation networks, VISSIM is more likely to be applied for modeling more complex urban network; 2) to mimic traffic dynamics a simulation time should be

incremented by a small discrete time step. VISSIM allows users to select a time step between 0.1 and 1.0 second, leading to a higher level of detail of driver behavior by smoothing the movement of simulation units while CORSIM uses a fixed time step of 1 second; and 3) both models generate a wide range of outputs that indicate network performance or traffic conditions. While CORSIM provides simulation outputs in the pre-determined output file format, VISSIM offers users additional simulation outputs by setting up an output file format. This function is very useful to obtain simulation output suitable for calibrating the simulation model in this dissertation because the model calibration requires simulation outputs for each individual driver, e.g. fully disaggregated network performance data.

2.2 CALIBRATION OF MICROSCOPIC TRAFFIC SIMULATION MODELS

Many microscopic traffic simulation models are now supporting a detailed analysis and evaluation of both traffic operations and transportation planning strategies. To recreate realistic driving behavior and, thus, increase the credibility of simulation outputs, complex traffic flow theories including car-following and lane changing models have been used. However, the application of microscopic traffic simulation models could be counter-productive if not implemented appropriately, implying a necessity of the calibration of transportation networks being modeled. In this subsection are presented the conventional and bi-level calibration procedures as well as the optimization theories employed in an automated calibration methodology.

2.2.1 Overview of the Calibration Procedure

Microscopic traffic simulation modeling consists of model development, verification, calibration, and validation. Model development involves collecting supply and demand data and coding these data into the selected simulation model. The supply data are measurable physical and control elements of the transportation network, while the demand data are the desires to transport people and freight in the form of OD matrix or

traffic count. Model verification is the process of checking that the model performs logically. This process is mainly to debug any coding errors so that the model performs in an intended manner. Model validation is the process of determining whether all elements of network being modeled are accurately represented. In this step, network performance data from the calibrated model are compared with another set of data that are not used in the model calibration using statistical tests or visualization checking (26).

Model calibration is the process of adjusting model parameters that are locally site-specific. Traditionally, this process has been concerned with identifying the "best" driver behavior parameters from a wide range of parameters related to car-following and lane-changing models. For the model calibration, the specific form of data is prepared such as a traffic count at a specific location, travel time for a small network segment, and delay at an intersection approach. These observed field data are compared with the simulation output to adjust model parameters using intrinsic guesses or automated calibration methodology.

The model calibration is very crucial in the successful application of the simulation model. This is apparent, especially, when transportation networks are geometrically complex or are congested. For example, when networks operate close to maximum capacity, slight changes in calibration parameters can have a significant effect on simulation outputs. By modifying model parameters, it is possible to obtain quite different simulation outputs. Nevertheless, due to lack of data available for the model calibration and limited applications of automated calibration methodology, the model calibration has been performed; 1) for only a few of the many model parameters; 2) for only small networks; 3) using intrinsic guesses or based on approaches that are heuristic in nature; and 4) based on aggregated field data rather than disaggregate data (27).

Park et al. summarized general requirements and a set of guidelines of the model calibration suggested by other researchers and proposed a systematic calibration procedure of microscopic traffic simulation models (28). Figure 2.2 depicts the main steps in his proposed calibration procedure. The first step comprises determination of MOEs and field data collection for the model calibration.

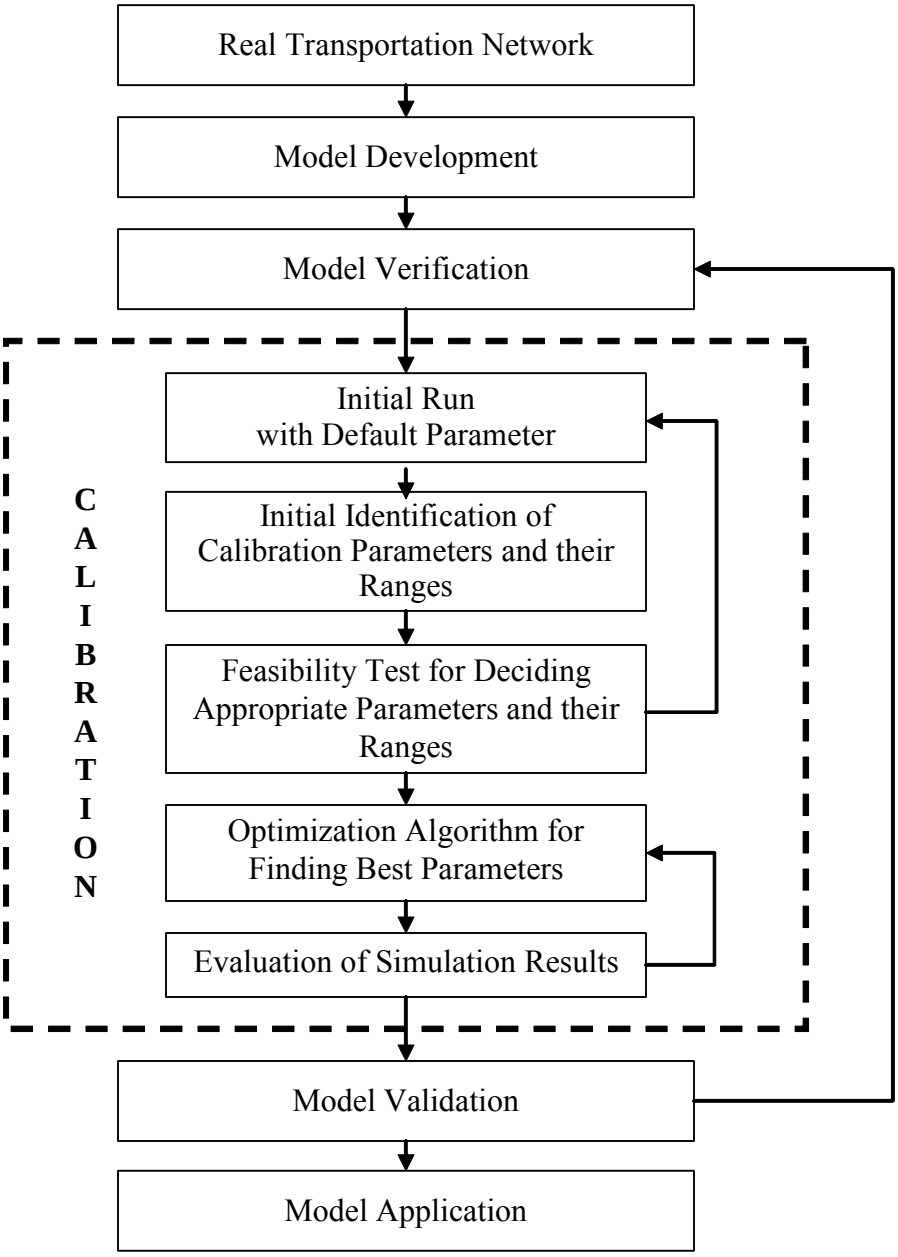

Figure 2.2 Calibration Procedure in Simulation Modeling (28)

Once the simulation model is correctly developed, the second step is to evaluate the simulation output with default parameters in comparison with the observed field data. If a close match is not found, the next calibration steps are to be performed. The third step consists of identifying influential parameters among all model parameters, constructing feasible parameter combination, and setting up the number of simulation run to reduce stochastic variability. The purpose of the fourth step is to check whether the current parameter ranges are sufficient to generate the field condition. If the field data is not covered by the simulation results, the current parameter ranges are to be adjusted. After deciding appropriate parameters and their acceptable search ranges, the fifth step is to apply optimization algorithms to find optimal parameters. In this step, optimization algorithms generate another set of new scenarios. The last step is to run multiple simulations and to evaluate the simulation results in comparison with the field data. If the evaluation is satisfactory, the model can be regarded correctly calibrated. Otherwise, the calibration procedure is repeated.

A number of research efforts in the calibration of microscopic traffic simulation models can be found in the literature. Cheu et al. calibrated INTRAS with 30 second loop detector data (29). In their study each parameter was separately calibrated while other parameters remained constant. Cheu et al. also calibrated FRESIM parameters using a genetic algorithm (30). This study was undertaken using 30 second speed and volume data over 5.6 kilometer segment of Singapore expressway. Free flow speed and FRESIM behavior parameters were calibrated by comparing FRESIM output with 30 second field data. Ma and Abdulahi calibrated the microscopic traffic simulator named GENOSIM using a genetic algorithm (31). Given initial parameters and OD flows, the calibration was carried out to obtain route-choice and lane-changing parameters. They tested GA based calibration approach in a network in Toronto, Canada and found their approach is promising for identifying better simulation parameters. Lee et al conducted a calibration study for searching best PARAMICS parameters (32). The mean headway and reaction time were calibrated for the I-5 freeway segment in California using a genetic algorithm. Average relative errors of flow and occupancy in 30 second intervals

were used as the calibration objective function to compare the simulated and observed data. Park et al. proposed a calibration procedure and demonstrated the proposed procedure in an urban arterial network in Fairfax, Virginia using VISSIM (33). They used an experimental design (Latin Hypercube Design) to reduce the number of combinations among numerous feasible model parameters. Rakha et al. modeled Salt Lake City area using INTEGRATION to demonstrate feasibility of modeling a large scale network (34). They described constructing and calibrating a large scale network microscopically. Kim et al. calibrated the I-10 freeway corridor in Houston using ITS data (35). To match the simulated and observed traffic count from CORSIM and TRANSIM under two different demand matrices, the genetic and fixed and flexible simplex algorithms were used. Gomes et al. modeled the I-210 in Pasadena, California, into VISSIM to design and implement improved on-ramp control systems (36). They assumed that driver behaviors are correlated with the position in the network. Thus, they defined different link types and VISSIM parameters were calibrated for each link type.

In the context of OD estimation, a bi-level approach has been proposed, where the OD matrix and travel-cost coefficients are calibrated at the same process (37, 38). Under a bi-level structure, the OD matrix is estimated with the travel cost coefficient constant in the first level, while the travel cost coefficient is calibrated in the second level using the calibrated OD matrix. However, even though there has been some research published in the literature pertaining to the calibration of microscopic traffic simulation models, there has been comparatively little related to the simultaneous calibration of both the OD matrix and the driver behavior parameter set. .

Kim asserted that the OD matrix has a profound impact on simulation results and, further, considered the OD matrix can be calibrated (27). In his study, the calibration of CORSIM OD matrix, which was based on a gravity model, was performed iteratively using a bi-level approach. A generalized cost function (impedance function) of a gravity model obtained using the simulated travel time was used to update CORSIM OD matrix. However, Kim's study has limited its application only to the CORSIM

model based on a simple gravity model. Consequently, the methodology used in Kim's study can not be applied to other simulation models.

Ben-Akiva et al. and Darda proposed a bi-level approach, where driver behavior and route choice parameters are calibrated jointly (39, 40). The estimation of the OD matrix requires the assignment matrix for mapping OD flows to traffic counts measured at sensors. It was addressed that the assignment matrix is a function of the route choice and path travel times, which in turn depend on the estimated OD matrix. However, these data are often unavailable in reality. Therefore, they obtained path travel times and driver behavior parameters from simulation results with a given OD matrix and subsequently updated the OD matrix iteratively using the calibrated parameters and assignment matrix.

Chu et al. conducted a calibration study in the city of Irvine, California, using PARAMICS (41). Multiple steps of calibration efforts were made including calibration of driver behavior and route choice parameters, OD estimation, and model fine-tuning. Their study mainly focused on proposing a systematic, multi-stages calibration procedure so that details of how the calibration was carried out were not clearly described. For example, they addressed the importance of calibrating route choice parameters as part of the calibration procedure but they assumed these values because of lack of available data.

2.2.2 Existing Calibration Objective Function

The calibration objective function based on an aggregate form of the observed data has been adopted over the years because of its simplicity and limitation on the availability of data. The aggregated measures such as average travel time or total traffic volume are compared to find the best parameter set that minimizes some objective functions. These functions come in many forms but the most prevalent ones are the root mean square error (RMSE), the mean absolute error ratio (MAER), and the mean absolute percentage error (MAPE). These functions are defined in Equations 2.9 through 2.11, providing information on the magnitude of errors relative to the average measurement directly.

$$RMSE = \frac{\sum_{i=1}^{n}\sqrt{(S_i - O_i)^2}}{n^2} \quad (2.9)$$

$$MAPE = \frac{\sum_{i=1}^{n}\left|\frac{S_i - O_i}{O_i}\right|}{n} \times 100 \quad (2.10)$$

$$MAER = \frac{\sum_{i=1}^{n}\left|\frac{S_i - O_i}{O_i}\right|}{n} \quad (2.11)$$

S_i = simulated measurement ;

O_i = observed measurement ; and

n = number of measurement locations.

Even though various forms of calibration objective functions have been adopted under the common goal of error minimization, they differ in some important aspects. The selection among them depends on the purpose of analysis and the availability of data. The RMSE gives the same dimensions as the observations themselves and it is sensitive to outliers in observations so that a large error has greater impact on the value of RMSE. The MAPE is the average of all the percentage errors for given observations, taken without regard to sign. The MAER is unit free and is defined as the average ratio of absolute errors to their observation (42, 43).

When an aggregated performance measure such as the MAER is used, it is automatically assumed that the parameter set which produces the minimum MAER value is the best descriptor for real traffic conditions. However, this assumption is valid only when the distributions for the simulated and observed data are identical. That is, the only difference between the results from different parameter sets is the measure of central tendency (i.e. mean or median).

2.2.3 Optimization Algorithms

Historically, the calibration of microscopic traffic simulation models was considered as a simple procedure based on manual search techniques. With greater availability of ITS data and higher speed computers, the application of optimization algorithms to the automated calibration of simulation models is now possible.

In a manual search, the selected parameters that need to be calibrated are explicitly changed based on previous knowledge and experience with microscopic traffic simulation models. It is a commonly used, less complicated and intuitive approach. The transportation engineer decides the criteria under which the search is stopped (44, 45). This search may find a set of parameters that produce better results as compared to default parameters. However, it is far more inefficient and expensive than automated optimization techniques. The main disadvantage is that there is no fixed rule for the choice of a reasonable starting and an adequate stopping point, which leads either to a premature end to the calibration procedure or the end of the search for a better solution.

Simplex algorithm (SA) is a pattern search technique, which assumes that a successful move is worth being repeated. It requires only the evaluation, not derivative of the objective function. A simplex is n-dimensional figure consisting of $n+1$ vertices, where each vertex corresponds to a parameter set. This approach takes a series of steps, reflecting, contracting, and expanding, to identify the parameter set with better function evaluation. The resulting simplex either grows or shrinks. The worst vertex is discarded and replaced with a new one. The process repeats itself until no further improvement can be made. The application of simplex algorithm can be found in the following literature (35, 46).

Genetic algorithm (GA) is a robust optimizer developed in the 1970's for intractable problems. The GA differs in many aspects from other optimization techniques, especially in that it does not require sophisticated knowledge of the objective function that is to be optimized. This feature enables the GA employed in a wide range of transportation applications, including timing traffic signals and calibrating simulation models. The application of GA for timing traffic signal logic focuses on finding optimal

signal control variables (i.e., cycle length, green split, offset, and phase sequence) under various traffic conditions and traffic signal strategies (47, 48, 49, 50, 51). A GA is ideal for the calibration of microscopic traffic simulation models because it is sometimes impossible to write out the calibration objective function mathematically while it is easy to obtain values of the function. In the calibration of simulation models, a GA has been employed to develop an automated calibration methodology, where a GA is used as an optimization tool to manipulate the model parameters that minimize the discrepancy between simulation results and real field data (27, 30, 31, 49, 52). The application of GA in other transportation field such as transit routing, ramp metering, and OD estimation can be found in the literatures (53, 54, 55, 56, 57).

In the procedure of GA application, the first step is to determine calibration parameters, function forms to calculate the fitness value, and GA control variables such as probabilities of crossover and mutation operational rules and stopping criteria. The GA is then started by generating a number of calibration parameters forming initial trial population. These parameters are encoded as binary strings called chromosomes. The second step is to decode the binary strings to real parameter values and insert these values into the simulation input file. A simulation run is then performed for each set of binary strings and simulation outputs are channeled into the analysis phase of the GA algorithm. The third step is to calculate the fitness value by evaluating the performance of each chromosome in comparison with the field data. The fitness value can be considered as a competition index within the trial population. The chromosome with higher fitness values is more likely to be selected and cloned for subsequent generation. If the comparison result does not meet the stopping criteria, a new population of candidate solutions is generated based on probabilistic rules, which are known as reproduction, crossover, and mutation. In the crossover operation, two parent chromosomes are selected based on the probabilities computed from the fitness values. The selected chromosomes exchange generic materials or genes to produce offspring chromosomes. Following the crossover, the mutation operation is performed to ensure that fresh solutions are generated. The value of the binary cell at a randomly selected

location is changed. This entire process takes place for successive generation until the stopping criteria is met (58, 59).

2.3 ESTIMATION OF AN ORIGIN-DESTINATION MATRIX

The origin-destination (OD) matrix is a fundamental input to microscopic traffic simulation models. This section reviews various approaches for estimating the origin-destination (OD) matrix with emphasis on the Kalman filter algorithm.

2.3.1 Overview of OD Estimation Techniques

There has been a considerable amount of research conducted on estimating the OD matrix on freeway and urban networks. Traditionally, the OD matrix was obtained from direct measurements, roadside interviews, or license plate surveys (60). However, these approaches are not feasible in most cases because they are often costly and time consuming. In addition, these survey based methods are inappropriate to reflect rapid changes in OD patterns, leading to the outdated OD matrix. Therefore, in recent years, most research have tried to estimate the OD matrix in an indirect way, mainly using traffic counts and sampled OD data.

The OD estimation is to find the most "likely" OD matrix that can reproduce the observed traffic count at any space-time point. Equation 2.12 describes the basic relationship between the estimated OD matrix and observed traffic counts. For a given link *a*, the sum of all OD pairs passing this link is the observed traffic count on link *a*.

$$v_a = \sum_{(ij)} p_{ij}^a \, tt_{ij} \tag{2.12}$$

v_a = traffic counts on link *a*;

p_{ij}^a = proportion of OD flows between OD pair *i* and *j* that use link *a*;

tt_{ij} = OD flows between OD pair *i* and *j*.

However, this formulation based on the observed traffic counts leads to an underdetermined OD structure (61, 62, 63). That is to say, there could be a greater number of feasible OD matrices that reproduce the observed traffic counts. This occurs because the number of OD pairs to be estimated is larger than the number of links where traffic counts are measured. Therefore, additional information is required to determine a unique solution. In general, this information is in the form of *a priori* OD information obtained by a sample OD survey or from an outdated OD matrix.

With this additional information, the problem of estimating the OD matrix can be formulated in the following general form, where the *a priori* OD matrix is used as a target OD matrix. As shown in Equation 2.13, a unique OD matrix given the target OD matrix is obtained by minimizing the deviation between the estimated and target OD matrices and deviation between the estimated and observed link traffic counts. The values of the weights are determined based on the reliability or accuracy of the target OD matrix and the observed link traffic counts. For example, if traffic counts are observed accurately, then a lager value is assigned to α_2. In turn, this leads to the estimated OD matrix that reproduces link volumes close to the observed traffic counts while allowing a larger deviation between the estimated and target OD matrices.

$$\min \quad F(T, v) = \alpha_1 F_1(T, \hat{T}) + \alpha_2 F_2(v, \hat{v}) \tag{2.13}$$

$T, \hat{T}$ = estimated and target OD matrix, respectively ;

$v, \hat{v}$ = estimated and observed traffic counts, respectively ;

F_1, F_2 = distance measures for OD matrix and traffic counts, respectively ; and

α_1, α_2 = weights for OD matrix and traffic counts, respectively.

Research on the OD estimation can be divided using several categories (64, 65). They includes: 1) time horizon; 2) treatment of congestion; 3) mathematical formulation;

and 4) network configuration. Table 2.2 summarizes important properties that distinguish various approaches. The first category is based on the time horizon. In the steady state OD estimation approach, a dynamic nature of OD patterns is overlooked and the average OD matrix for a relatively long time interval is estimated. In the dynamic model, time dependant traffic counts are taken into account to identify the time varying OD patterns. It is assumed that the travel time for a specific OD pair can span a number of different time intervals by considering various travel times consumed by individual vehicles. Therefore, it allows fractions of OD flows for the current time interval to arrive at their destinations for some future time intervals.

Table 2.2 Classification of OD Estimation Approaches

Category	Sub Division
Time Horizon	• Steady state • Time dependant
Treatment of Congestion	• Proportional assignment • Equilibrium assignment
Mathematical Formulation	• Traffic modeling approach • Statistical inference approach
Network Configuration	• Isolated intersection or freeway • Urban Network or combined network

The second category is the treatment of congestion. The proportional assignment assumes that link costs (or link travel times) are independent of link volumes. Therefore, this approach can be applied to networks with a low level of congestion. The assignment matrix is determined and given exogenously before the estimation of the OD matrix. In the presence of congestion, the equilibrium assignment model can be more representative of a reality. It assumes that link costs depend on link flows. Therefore, the assignment matrix is a function of link volumes, resulting in nonlinear relationship of v in Equation 2.12. The equilibrium assignment model generally has a bi-level structure,

where the estimation of the OD matrix is conducted on the upper level whereas a user-equilibrium problem is solved at the lower level.

The third category is based on the mathematical formulation, which is further subdivided into two categories: traffic modeling approach and statistical inference approach. The traffic modeling approach is the minimum information (or entropy maximization) model. It is assumed in this approach that the target OD matrix is typically an old OD matrix and is adjusted to meet the traffic counts. The statistical inference approach includes the maximum likelihood (ML), generalized least squares (GLS), Bayesian approach, and Kalman filtering approach. The statistical approach generally assumes that the target OD matrix is obtained from a sample survey and is considered as an observation of the true OD matrix. In turn, the true OD matrix is assumed to follow a certain probability distribution, thus the estimation of the OD matrix is obtained by estimating the parameters of the statistical distributions (65).

The last category is based on the network configuration. The estimation of the OD matrix at an isolated intersection or a freeway network is a special case. In recent years the research emphasis shifted to the development of the OD matrix estimation approach that is suitable for congested urban networks.

2.3.2 Kalman Filter Based OD Estimation

The Kalman filtering (KF) algorithms are known as a "prediction-correction" technique, which is based on the criterion of least square unbiased estimation of the state and measurement vectors (4). A common form of the KF algorithm is modeled as the random process, as shown in Equations 2.14 through 2.16.

$$x(t+1) = A(t)x(t) + \varepsilon(t) \qquad \varepsilon(t) \sim (0, Q(t)) \tag{2.14}$$

$$y(t) = B(t)x(t) + \eta(t) \qquad \eta(t) \sim (0, R(t)) \tag{2.13}$$

$$x(t+1) = x(t) + K(t)\left[y(t) - B(t)x(t)\right] \tag{2.16}$$

$x(t)$, $y(t)$	=	state and measurement matrices, respectively;
$A(t)$, $B(t)$	=	linear matrices ;
$\varepsilon(t)$, $\eta(t)$	=	state and measurement noises, respectively ;
$R(t)$, $Q(t)$	=	variance-covariance matrices for state and measurement noises, respectively; and
$K(t)$		Kalman gain matrix.

$\varepsilon(t)$ and $\eta(t)$ are, respectively, unknown state and measurement noises. It is often assumed that they follow zero-mean Gaussian white noise process and are independent of each other. The state equation estimates the state of a discrete-time random process, where the linear matrix *A(t)* relates the state for time interval *t*-1 to the state for time interval *t*. The matrix *B(t)* relates the state to the measurement *y(t).* The difference $\left[y(t) - B(t)x(t)\right]$ in Equation 2.14 is called the residual. This reflects the discrepancy between the actual measurement and the estimated measurement and determines the magnitude of the update after the measurement for time interval *t* is obtained. In the KF algorithm the determination of the Kalman gain matrix is a crucial point. This matrix is chosen such that the posterior error covariance of *x(t)* is minimized. For example, the Kalman gain matrix weights the residual heavily if measurement variance covariance matrix *R(t)* approaches zero. In other words, as *R(t)* approaches zero, larger confidence can be placed on the actual measurement. Further details regarding the KF derivation and other issues can be found in the literature (4, 5, 6).

With a few substitutions, the Kalman filter algorithm can be used as the recursive OD estimation technique, where information for the previous time intervals are used to update OD estimates for the current time interval (1). The state matrix *x(t)* in Equation 2.14 would be changed to the OD split proportion matrix *b(t)*. In addition, link traffic count matrix *v(t)* is substituted for the measurement matrix *y(t)* and the assignment matrix *P(t)* is substituted for the linear matrix *B(t)*.

In the pioneering study by Cremer and Keller, they applied the idea of dynamic OD estimation, where time dependant traffic counts were used in a recursive Kalman filter based OD estimator (60). In addition, different algorithms including an ordinary least square estimator and a constrained optimization were proposed and applied to a large intersection for comparing the accuracy of the proposed algorithms. Okutani applied the Kalman filter based OD estimator on general networks (66). This approach can be considered as the first network-oriented study. Ashok et al. suggested the improved Kalman filter based OD estimator. In their study, the concept of deviation of OD flows from target OD flows was presented instead of OD flows themselves (67). It was assumed that deviations generally have a symmetric distribution while OD flows are skewed. This approach also attempted to remove the loss of structural OD information associated with the use of autoregressive formulation in transition equation. Van der Zijpp et al. applied the Kalman filter based approach for modeling OD estimates defined in terms of a split probability instead of a fixed split proportion (68). They addressed that the assumption of a split probability can be better justifiable because OD flows are slowly moving process with a random walk rather than a fixed process and some properties related to the Kalman filter approach such as variance covariance matrix can be derived. Debashish et al. incorporated Advanced Traveler Information System (ATIS) data into an OD estimator on a freeway network (69). The Kalman filter based approach was used to update the OD matrix and associated variance covariance matrix where a route diversion behavior under ATIS system was taken into account.

2.3.3 Incorporating Travel Time Data into OD Estimator

Little research has been carried out for estimating both travel times (OD travel times or link travel times) and OD flows in one process or for estimating OD flows using travel time information as additional measurements. It is difficult to identify the relationship between these variables even though they are strongly inter-correlated. However, if this relationship is properly captured, OD estimates that reflect dynamics of traffic can be obtained with a significant improvement of estimation precision.

Chang et al. considered dynamic OD travel times for obtaining the estimates of OD flow on a freeway corridor (70). They addressed the concern that the OD estimation model, where the travel time is assumed to be either negligible or constant, can not be applicable for a long freeway segment but only for a small network or intersection. To estimate dynamic travel times, a simple method based on macroscopic traffic characteristics, that is to say the speed-density-volume relationship, were used. The extended Kalman filter based OD estimator was proposed to solve a nonlinear dynamic system. Another application of the Kalman filter based approach can be found in the study by Shou-Ren et al. (71). The simulation based model, called the adaptive Kalman filter, was developed to capture a temporal dispersion in travel times, which were in turn used to generate time-varying assignment matrices.

Hironori et al. also addressed that existing Kalman filter approaches are not applicable to a long freeway corridor and large estimation error may occur because dynamic traffic conditions are not immediately reflected in the observed traffic counts (72). They proposed a new algorithm for simultaneously estimating OD travel times as well as OD flows on a long freeway corridor, where artificial neural network (ANN) was integrated to treat nonlinear formulations of state and measurement equations of the Kalman filter model. Specifically, ANN model were used to relate the current OD flows $x(t)$ to $x(t-1)$ in Equation 2.14 and to relate the current measurement $y(t)$ to $x(t)$ in Equation 2.15. It was possible to obtain $A(t)$ and $B(t)$ matrices by taking partial derivatives of state and measurement equations, which were identified from ANN learning process, with respect to $x(t)$. In addition, a macroscopic traffic flow model was used to reduce estimation errors in OD travel times by predicting traffic conditions in advance. The proposed model was called the neural Kalman filter.

2.4 CONCLUDING REMARKS

This section provided the background literature required to simultaneously calibrate driver behavior parameters and the OD matrix. Various topics covered in this section include: 1) traffic flow theories behind VISSIM and CORSIM microscopic traffic

simulation models; 2) calibration procedure and optimization techniques; and 3) estimation of the OD matrix.

The literature review began by reviewing the underlying car following and lane changing models of VISSIM and CORSIM microscopic traffic simulation models. A reasonable understanding of these models allows for making best use of the microscopic traffic simulation models in an intended manner. This section also provided a strength and weakness regarding the application of two models through a brief comparison.

The second subsection described the procedure employed to calibrate the microscopic traffic simulation model. To reproduce realistic driver behaviors and to obtain reliable simulation outputs it is necessary to calibrate the transportation network being modeled. This can be accomplished by identifying the "best" driver behavior parameters related to car-following and lane-changing models. This subsection also discussed on the optimization techniques that have been used in an automated calibration process. They include: 1) manual search; 2) simplex algorithm; and 3) genetic algorithm. The application of optimization algorithms becomes attainable with greater availability of ITS data and higher speed computers.

The last topic in the literature review was the approach for estimating the OD matrix. The accurate OD estimates are fundamental inputs to microscopic traffic simulation models for the successful simulation modeling and further analysis. The problem of estimating the OD matrix using traffic counts was defined and associated issues were discussed. This subsection focused on reviewing the Kalman filter based OD estimation approach. The review on the application of the Kalman filter based approach will provide aid in incorporating travel time information into the OD estimation and thus developing a methodology to simultaneously calibrate driver behavior parameters and the OD matrix.

CHAPTER III

RESEARCH FRAMEWORK AND SIMULATION MODELING

The proposed calibration framework and the basic components pertaining to the microscopic traffic simulation modeling are discussed in this section. Subsection 3.1 introduces the bi-level calibration framework employed to achieve the research purposes. Subsection 3.2 describes the two specific test networks in Houston, Texas, whereas Subsection 3.3 presents the network supply and demand data required to model the test networks using the VISSIM microscopic traffic simulation. Subsection 3.4 describes some issues regarding coding the test networks. In subsection 3.4, the description of VISSIM driver behavior parameters selected for analysis is presented. Subsection 3.6 presents an application of the Genetic Algorithm, where evaluation criteria, fitness function, and stopping criteria are discussed. Finally, the concluding remarks are presented in subsection 3.7

3.1 BI-LEVEL CALIBRATION APPROACH

Conventional approaches for the calibration of the microscopic traffic simulation model assume that the OD matrix remains unchanged during the calibration procedure. However, in traffic modeling the OD matrix is usually estimated based on traffic counts. Because the calibration procedure is also based, in whole or input, on traffic counts this can be problematic. For example, an “incorrect” OD estimate might mean the potential traffic network cannot be calibrated (73). Consequently, a bi-level calibration approach is adapted where the OD matrix and the microscopic traffic simulation parameter set are calibrated in an iterative manner. A schematic of this approach is shown in Figure 3.1.

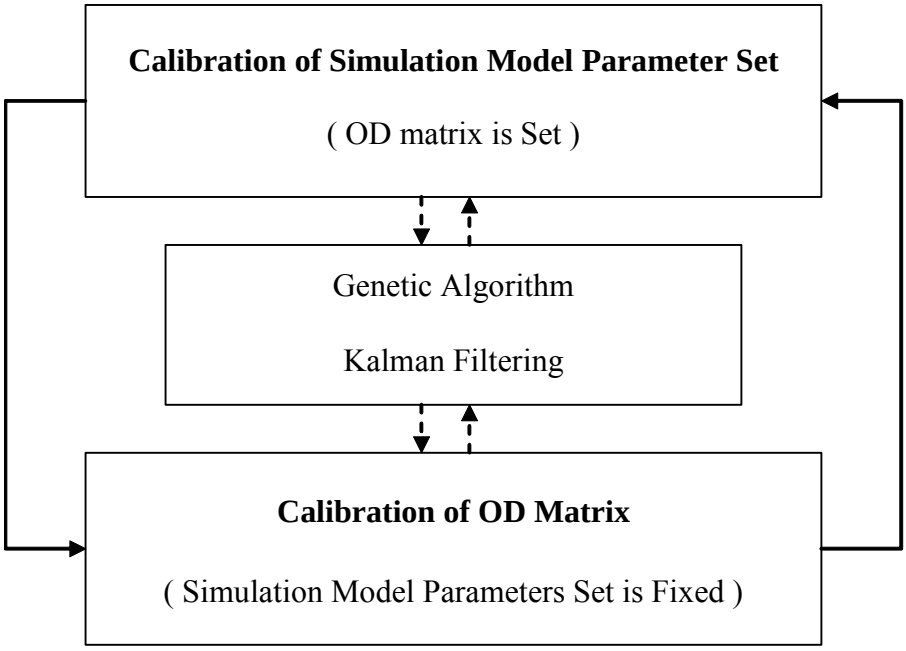

FIGURE 3.1 Concept of Bi-Level Calibration Approach

The upper level seeks to minimize the difference between observed and simulated traffic conditions by adjusting the values of the model parameters. To achieve this, a genetic algorithm is selected because of its robustness in searching the best parameters based on the statistically based objective function. The statistically based objective function is used to evaluate the selected performance measure. In this dissertation this will be the travel time in a distribution format derived from AVI data.

The lower level involves several steps for calibrating the OD matrix. The simulated travel time with the calibrated parameters are incorporated into the OD estimator by recognizing the dependence of travel time on the OD travel demand. The simulated travel time is obtained from the simulation run with the current best behavior parameters identified in the upper level. This travel time information would be incorporated into the OD estimator based on the Kalman filtering formulations. After the new OD matrix is estimated, the upper level is rerun and the iterative process continues.

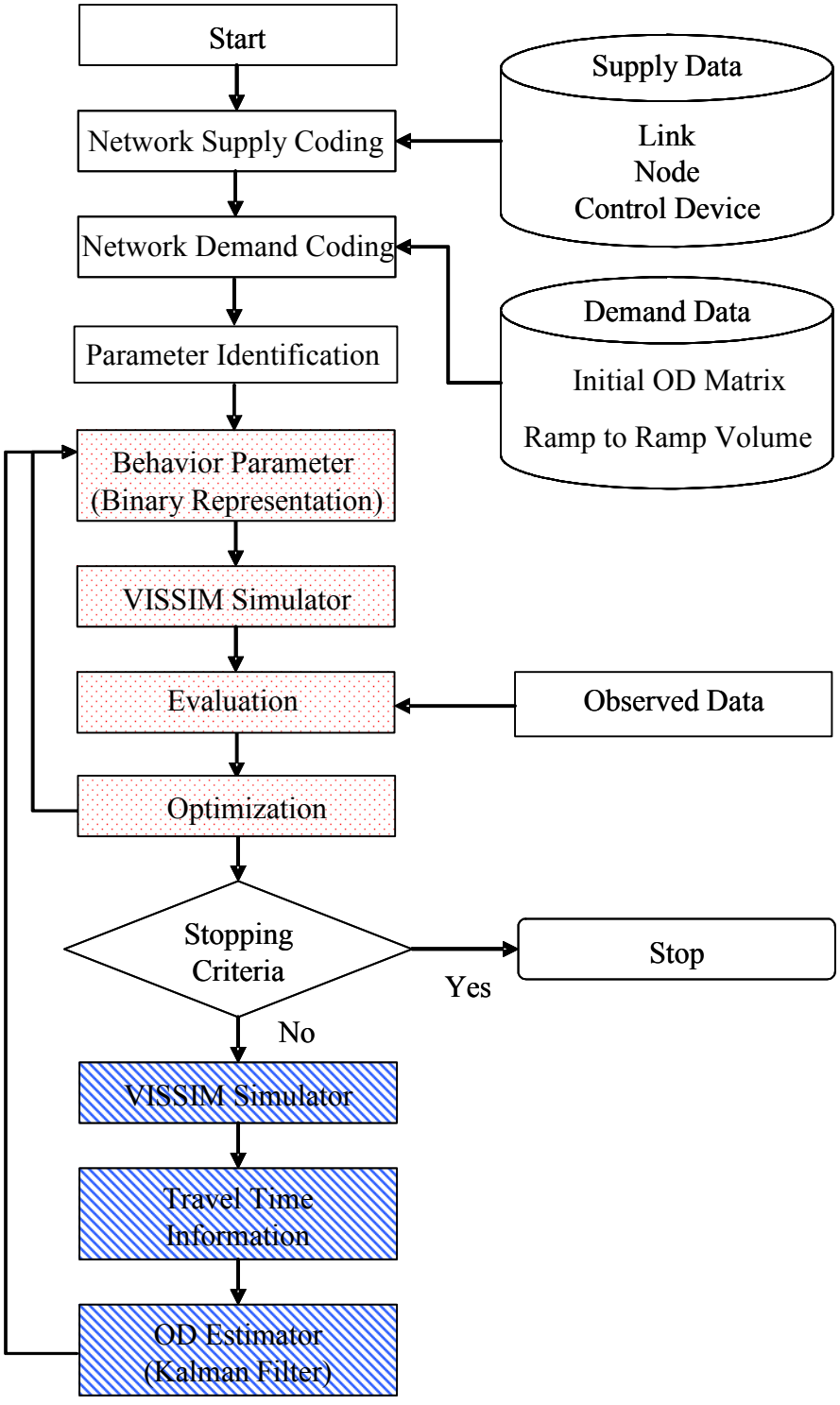

FIGURE 3.2 Flow Chart of Bi-Level Calibration Approach

Figure 3.2 illustrates the overall bi-level framework in detail. The first step is to identify a set of parameters that need to be calibrated and to translate the selected parameters into binary values. The second step involves running the VISSIM simulation with the identified parameters to generate the simulation results. These results are compared against observed data using a statistically based objective function. Based on the objective function value, fitness value, and the relative fitness, the identified parameters are optimized through the GA operation such as crossover and mutation. This procedure is continued iteratively until the predetermined stopping criteria are met.

It is ideal to identify in the upper level the behavior parameters with which the simulation results fall within acceptable range. Otherwise, the calibration of OD matrix is performed in the lower level. Given *a priori* knowledge on the effect of OD matrix on the simulated travel time, a new OD matrix is identified. This OD matrix is passed on to the upper level where the behavior parameters are calibrated.

3.2 TEST NETWORKS

One arterial and one freeway test network were selected in this dissertation to evaluate the proposed methodology. Both networks are located to the west of downtown Houston, Texas, as shown in Figure 3.3. The first test bed is the Bellaire arterial test network and the second is the I-10 freeway corridor test network.

3.2.1 Bellaire Arterial Test Network

Bellaire Boulevard, which is located in southwest Houston, Texas, is a major east-west arterial with a wide landscaped median. It is heavily traveled and serves relatively high-density residential areas. A 1.1 km section of this arterial was selected for analysis. It is comprised of 3 signalized intersections and one two-way stop controlled intersection with north-south cross streets. A traffic-actuated signal controller unit controls 3 intersections. The posted speed limit is 56 km/h (35mph) and the speed limit in the cross

streets varies between 48 km/h (30mph) and 56 km/h (35mph). Figure 3.4 shows the general layout of Bellaire Boulevard. The aerial photo map is provided in Appendix B.

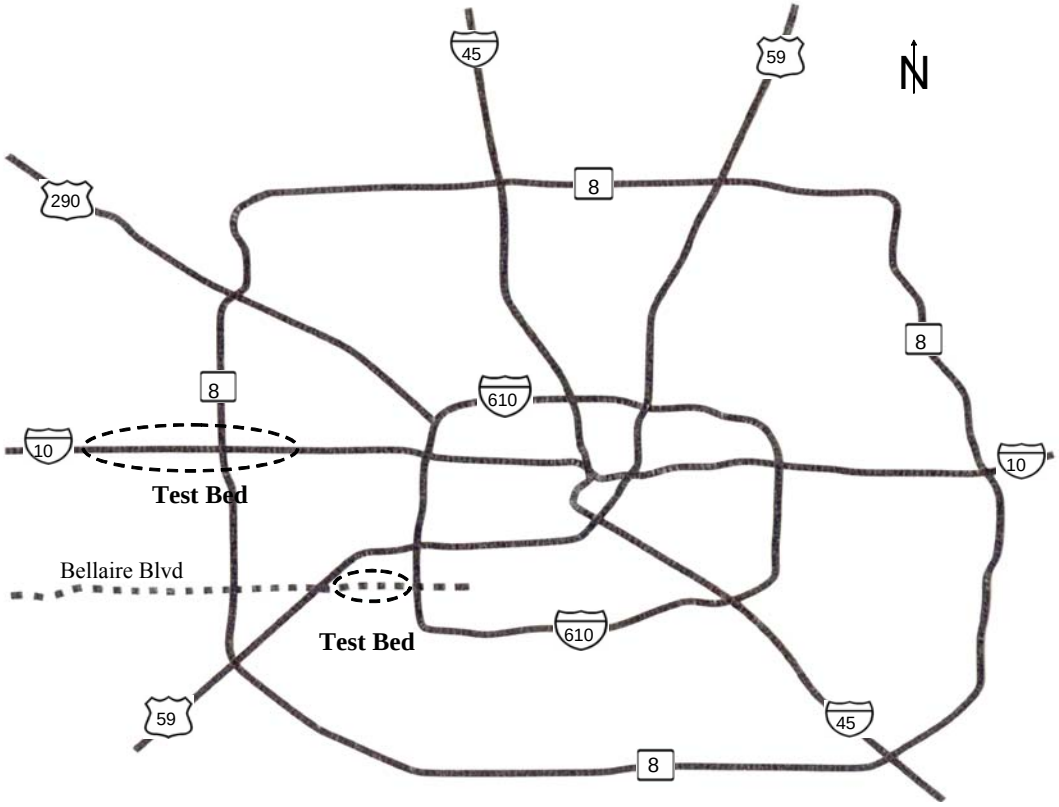

FIGURE 3.3 Test Networks Location

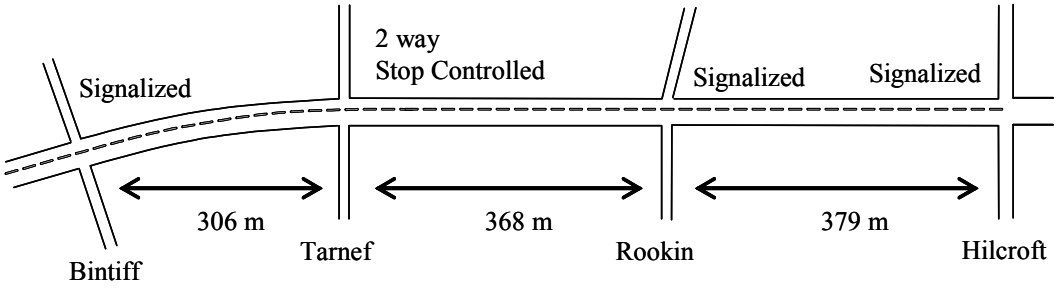

FIGURE 3.4 Layout of the Bellaire Arterial Test Network

3.2.2 I-10 Freeway Test Network

The I-10 freeway corridor functions as an "activity spine" and provides access to the central business district in Houston for east-west commuters. The I-10 freeway corridor is a full grade-separated freeway with a high occupancy vehicle (HOV) lane in the median, and AVI stations on the main freeway lanes. A 15.4 kilometer section of the corridor was selected for analysis. This selected section stretches from Baker Cypress in the west to Blalock in the east. The test network includes 10 on-ramps and 9 off-ramps, with 4 AVI stations. Figure 3.5 shows a diagrammatic layout of this test corridor. The figure also shows the distances between 4 AVI stations. Note that the network has an HOV lane although this will not be analyzed in this dissertation. The detailed link and node diagram and aerial photo map are provided in Appendix B.

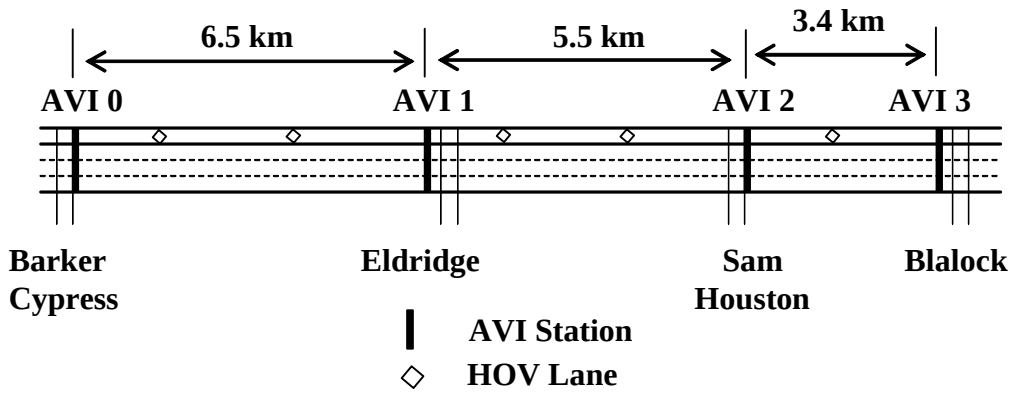

FIGURE 3.5 Layout of the I-10 Freeway Test Network

3.3 DATA COLLECTION

The data required to accurately run a microscopic traffic simulation model are quite extensive. For each test network, the following data were collected.

- Traffic volumes on all lanes;
- Turning movement at each intersection (Bellaire Blvd);

- OD matrix (I-10 Freeway);
- Lane geometry;
- Speed limit;
- Traffic signal control variable;

3.3.1 Bellaire Arterial Test Network

Traffic volume data were collected using video cameras installed at the corner of each intersection from 7:30 AM ~ 10:00 AM on October 16, 2003. The recorded video was manually retrieved and then traffic volumes were aggregated into 15 minute volumes. The traffic demand was defined in VISSIM as turning percentages at each intersection based on the observed traffic volumes. Data during the AM peak period (7:30 AM ~ 8:30 AM) was chosen in this dissertation for evaluating the proposed calibration methodology using a microscopic traffic simulation model.

The lane geometry was collected from aerial photos and direct field observation. The signal control variables were obtained from the Houston TranStar inventory. Table 3.1 summarizes the lane geometry and types of signal control on the eastbound approach at Bellaire Blvd.

TABLE 3.1 Lane Geometry and Traffic Control at Bellaire Arterial Test Network

Cross Street	Geometric	Traffic Control
Bintiff Rookin Hilcroft	• one exclusive left-turn • two through lanes • one through/right-turn shared lane	• Actuated coordinated with 120 second cycle • Protected or permissive left-turn phase
Tarnef	• one left/ through/right shared lane	• Stop Control

3.3.2 I-10 Freeway Test Network

AVI data have been collected to provide travel time information for drivers, as part of the Houston TranStar Advanced Traveler Information System (ATIS). AVI data collected in 1996 were used to derive the travel time distribution for each AVI link during the AM peak period (7:00 AM to 8:00 AM). Data for five weekdays were used to derive the travel demand in 30 minute intervals. The travel demand is the OD matrix, where split proportions of vehicles going from every origin to every destination is defined instead of OD flows. Four days were selected for constructing the historical information necessary to formulate the OD estimator based on a Kalman filter approach (1, 4, 5, 6). A remaining day was selected as the target calibration day.

Traffic volume data were collected using inductive loop detector and pneumatic tubes in 1996. The hourly traffic volumes were adjusted to estimate 15 minutes volumes based on the sampling rate at each AVI station. There was no single day in which traffic volume data on main lane and on and off ramps were collected simultaneously. As a consequence, it is assumed in this dissertation that a composite data set constructed from multiple days can be considered as typical.

3.4 NETWORK CODING

Next, the supply and demand data of the test networks were coded into the microscopic traffic simulation model. The supply data includes the link attributes (length, width, number of lanes, grade) and traffic control (type of signal control). The demand data includes the traffic volume at each entry as well as the trip movement information such as a turning percentage or an OD matrix.

3.4.1 Bellaire Arterial Test Network Coding

The successful modeling of an arterial section in the microscopic traffic simulation model hinges on how the traffic signal logic operating in the field is best emulated. The inability of existing simulation models such as CORSIM to emulate complex traffic

signal logic has limited their application in recent years. The VISSIM microscopic traffic simulation model has considerably greater flexibility in modeling actuated traffic signal control. It provides an application programming interface (API) or vehicle actuated programming (VAP) as an optional add-on module. This is a module for the simulation of programmable, phase-based, traffic-actuated signal control. VAP allows the users to program complex control strategies such as actuated signal, coordination, preemption and priority. In this dissertation, the VISSIM input file was adapted from the research performed by Kim where the signal control logic in the test network was coded in VISSIM including minimum green times, force-off, gap-out and phase sequences (74).

3.4.2 I-10 Freeway Test Network Coding

Coding a freeway network is often considered much simpler than coding an arterial network because both the supply and demand information requirements are less. However, it should be noted that more attention should be paid in coding freeway networks, particularly where there is a possibility of "incorrect" vehicular movements because of special features of the test network. Such potential coding problems are found and fixed through the preliminary simulation runs. For the I-10 freeway test network, it was found that there is a severe blockage that forms long queues in the right-most lane. This is mainly caused by a relatively short distance between on and off ramps, which makes merging or diverging vehicles unable to complete necessary lane changes. These queues were not observed in the field. Several adjustments were made to address this problem.

- In the VISSIM model, when vehicles fail to complete the necessary lane changes at off-ramps, they stop in an emergency stop position and block all of exiting vehicle in the right-most lane for a set period of time. The "waiting time before diffusion" parameter, which governs the amount of time a vehicle is stopped while waiting to make a required move, was decreased from the default 60 seconds to 3 seconds. Once this time is up, the vehicles are removed from the

simulation. It is hypothesized that this lower setting minimizes obstruction to the main-lane stream while having little impact on the total number of trip (36).

- Some on and off ramps have very short auxiliary lanes (acceleration or deceleration lane). The length of auxiliary lanes were increased in order to include the taper distance to the point where vehicles use it as a real lane rather than where it is striped.
- A speed change has to be defined on the location where vehicles are supposed to change their desired speed. Typical application in modeling is based on the fact that exiting vehicles tend to reduce their speed before they reach curves or bends at off-ramps. However, in reality, most of exiting vehicles maintain desired speed in the main-lane and only start to reduce their speed on deceleration lane. It is often the case where a speed of exiting vehicle is higher than a speed at an off ramp. Placing the "reduced speed decision" right after exiting vehicles leave the main lane causes the right lane to have a higher average speed. This, in turn, reduces the potential for bottlenecks.
- Drivers do not need to watch for ramp signs, especially during AM peak period, because commuters in large city are familiar with corridor geometry. It seems reasonable to increase the "lane change distance for connectors" at merges and diverges. However, increasing this value too much makes exiting vehicles change to the right-most lane, far upstream of their destination off ramp. Therefore, this value was included into the set of parameters being calibrated. Any unfamiliar drivers are accounted by widening the range of desired speed to include some small percentage of slower drivers.
- The desired speed is assumed to be higher than posted speed limit. In large city, drivers often attempt to go beyond a posted speed limit. Therefore, the low desired speed was assumed to be near the speed limit (8 km/h or 5 mph below) and the high desired speed was set to 30 km/h (18 mph) over the speed limit. Note that most drivers will be modeled at limits to travel in between 8 km/h to 16

km/h. Given the congested conditions in the network, this will only affect drivers on the outer edges of the networks.

- The VISSIM driver behavior model should keep most of the vehicles out of the right lane if the lane change distances for connectors are long enough. However, there are a few situations where additional modifications were required, particularly where diverge and merge sections occur sequentially within a short distance. For example, there are 7 on and off ramps in a 3.4 kilometer section of the I-10 freeway test network (Sam Houston Tollway and Blalock Road). In this case, a very short dummy connector (less than length of one car) is placed across all but the right-most lane to route some of the through vehicles over this connector. This is accomplished using a partial routing decision in VISSIM which defines a section where vehicles are re-distributed according to the routes and user-defined percentage (11). The important piece of information is that the dummy connector is placed after the critical merge and diverge sections and its lane change distance is long enough to keep vehicles out of the right-most lane before vehicles cross the connector.

In Chapter VI, the OD matrix between AVI stations will be estimated using the sampled AVI data. This matrix represents the split proportion between AVI stations. However, VISSIM requires an OD matrix with each on and off ramp as origin and destination, respectively. In the AVI system, each AVI station is associated with sets of upstream on-ramps and downstream off-ramps, as denoted by u_i and d_j. In this dissertation, the observed ramp volumes are used to generate the ramp to ramp OD matrix from the AVI OD matrix. The ratio of the ramp volume to total volume is used to approximate the probability that on-ramp *a* is an origin of the flow beginning at AVI station *i* or the probability that off-ramp *b* is a destination of flow ending a station *j*. The ramp to ramp OD matrix is computed according to Equation 3.1 and 3.2.

$$x_a(t) = \frac{V_a(t)}{\sum_{k \in u_i} V_k(t)} \quad (3.1)$$

$$y_b(t) = \frac{V_b(t)}{\sum_{k \in d_j} V_k(t)} \quad (3.2)$$

$x_a(t)$ = probability that on-ramp *a* is an origin of the flow beginning at AVI station *i* ;

$y_b(t)$ = probability that on-ramp *b* is an destination of the flow ending at AVI station *j ;*

V_k = traffic volume on ramp *k* (vehicles) ; and

u_i, d_j = set of upstream on-ramps and downstream off-ramps associated with AVI stations *i* and *j*, respectively (vehicles).

3.5 VISSIM CALIBRATION PARAMETERS

There are a variety of calibration parameters in VISSIM model that can be controlled by the users to ensure the simulated results "match" the observed data. These parameters include driver behavior and vehicle performance parameters. The former are parameters related to driver characteristics inherent in car-following and lane-changing behavior models while the latter are related to factors such as speed, acceleration, and deceleration rate associated with the simulated vehicles. The base calibration parameters selected in this dissertation are limited to driver behavior parameters. This approach was adopted because the calibration of vehicle performance parameters requires extensive performance data for the operating vehicles and consequently it is often performed by model developers rather than by model users.

To effectively calibrate a given network, it is essential to select appropriate calibration parameters. In turn, it requires knowledge regarding the internal behavioral logic of the microscopic traffic simulation. In VISSIM, two types of Wiedemann car-following models are used to deal with the stochastic nature of traffic movements. The

Wiedemann 74 model, which has relatively simple logic and has been validated with empirical data, is used for urban traffic. The more complex Wiedemann 99 model is used to model for freeway traffic and has a larger number of open parameters (11). For lane change behavior, there are also two types of lane change models (necessary and free lane changes). The free lane changing logic determines the amount of passing. The logic searches for passing opportunity in adjacent lanes. Note that in VISSIM users can not select the driver's "aggressiveness" with respect to passing. However, the "aggressiveness" of a driver is based on the desired safety distance which is a result of a combination of several relevant model parameters which can be adjusted by the modeler. In the case of necessary lane changes that drivers are required to make in order to stay on their route, the aggressiveness can be defined by specifying maximum acceptable deceleration values for the leading and following vehicles. More details on the selected calibration parameters are discussed in the following subsections.

3.5.1 Calibration Parameters for the Bellaire Arterial Test Network

The base VISSIM calibration parameters selected for the Bellaire arterial test network are provided in Table 3.2. The definitions of the parameters are also provided in the table. The table contains the parameter number, the description of the calibration parameters based on the VISSIM manual, the default values, and minimum and maximum allowable values. At this point, it is important to note that the minimum and maximum allowable values are based on engineering judgment. The calibration procedure can be considered as an optimization problem that involves the selection of the best parameter set. Such an optimization problem poses a great challenge if the parametric space to be searched is large. In addition, the allowable parameter ranges are very wide according to the VISSIM manual (typically they range from zero to infinity). Therefore, it is essential to select appropriate allowable ranges for the selected parameters to increase the optimization performance.

TABLE 3.2 VISSIM Calibration Parameters for the Bellaire Arterial Test Network

Parameter (P_i)	Description	Default	Allowable Range	
			Min	Max
P_1	Number of observed preceding vehicles	2	0	4
P_2	Look ahead distance	250	0	400
P_3	Average standstill distance	2	1	4
P_4	Additive part of desired safety distance	2	1	10
P_5	Multiplicative part of desired safety distance	3	1	10
P_6	Lane change distance	200	50	300

- Number of observed preceding vehicles (P_1): This parameter determines how many vehicles are considered when a driver reacts to other vehicles movements.
- Look ahead distance (P_2): This parameter defines the distance that a driver can see in order to react to other vehicles.
- Average standstill distance (P_3): This parameter defines the average desired distance between stopped cars.
- Desired safety distance (P_4, P_5): These parameters, additive and multiplicative parameters, mainly influence the desired safety distance, which is used for the car-following behavior.
- Lane change distance (P_6): This parameter defines the distance at which a driver begins to change lane.

3.5.2 Calibration Parameters for the I-10 Freeway Test Network

The base VISSIM calibration parameters selected for the I-10 freeway test network are provided in Table 3.3. The tables contain the parameter number, the description of calibration parameters based on the VISSIM manual, the default values, and minimum and maximum allowable values.

TABLE 3.3 VISSIM Calibration Parameters for the I-10 Freeway Test Network

Parameter (P_i)	Description	Default	Allowable Range	
			Min	Max
P_1	Maximum deceleration for the leading vehicle	-4.0	-6.5	-3.0
P_2	Reduction rate of deceleration	200	100	300
P_3	Maximum deceleration for the trailing vehicle	-3.0	-5.0	-2.0
P_4	Lane Change Distance	200	200	400
P_5	CC0, standstill distance	1.5	1.0	1.7
P_6	CC1, headway time	0.90	0.30	1.20
P_7	CC2, following variation	4.0	2.0	6.0
P_8	CC3, threshold for entering following	-8	-12	-4
P_9	CC4, following thresholds	-0.35	-0.5	-0.2
P_{10}	CC5, following thresholds	0.35	0.2	0.5
P_{11}	CC6, speed dependency of oscillation	11.44	7	15

- Maximum deceleration for the leading and trailing vehicles (P_1, P_3): These parameters are associated with the aggressiveness of lane change by defining the maximum deceleration for the leading and trailing vehicles.
- Reduction rate of deceleration (P_2): This parameters is associated with the aggressiveness of lane change by defining a reduction rate with increasing distance to the emergency stop position.
- Lane Change Distance (P_4): This parameter defines the distance at which a driver begins to attempt to change lanes before reaching the next connector of route.
- CC0 (standstill distance, P_5): This parameter defines the average desired distance between stopped cars.
- CC1 (headway time, P_6): This parameter defines time headway that a driver want to keep at a certain speed.

- CC2 (following variation, P_7): This parameter defines longitudinal oscillation while a driver follows another vehicle. The distance between the leading and trailing vehicles ranges from the desired safety distance to the sum of the desired safety distance and following variation.
- CC3 (threshold for entering following, P_8): This parameter defines when a driver starts to decelerate before reaching the safety distance.
- CC4 and CC5 (following thresholds, P_9, P_{10}): These parameters define the speed difference of the leading and trailing vehicles. The smaller the values, the vehicles are tightly coupled.
- CC6 (speed dependency of oscillation, P_{11}): This parameter defines the distance on speed oscillation. A larger value results in a greater speed oscillation.

3.6 GENETIC ALGORITHM APPLICATION

The calibration of the microscopic traffic simulation model can be considered as an optimization problem that is performed such that the simulation output "matches" the observed values. In this dissertation the Genetic Algorithm (GA) is selected as an optimization tool because it is very effective when the objective function is not explicitly known or is not expressed in a mathematical form. In addition, it searches over multiple locations and consequently has less chance of identifying a local minimum. This is important for microscopic traffic simulation modeling as the objective function is highly non-linear (75).

3.6.1 Genetic Algorithm Code

The genetic algorithm is written in the Perl language and a copy of the code is provided in Appendix A. The GA code consists of several modules, such as binary representation of the selected parameters identified in Section 3.5.

Figure 3.6 provides the sub-modules employed in the GA application. The optimization process is basically iterative in that candidate chromosomes (parameter set)

are identified, simulation results are evaluated, and then new chromosomes generated. A description of each sub-module is provided in the following sections.

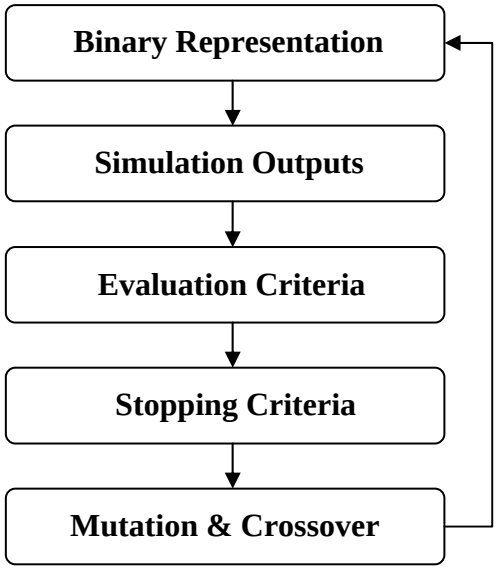

FIGURE 3.6 Overview of GA Application

- There were a total of six parameters for the Bellaire arterial test network and eleven for the I-10 freeway test network. These parameters were subsequently translated into binary values. To calculate the binary string lengths, the maximum and minimum values as well as the precision value of each parameter are taken into account.
- The candidate chromosomes are then translated into appropriate VISSIM input file format and the VISSIM simulation run is performed.
- An objective function is used to evaluate simulation results. In this dissertation a statistically based objective function is used. Once the chromosome is found statistically valid, it is not deleted but stored in the pool, opposed to the conventional GA application where only elite chromosomes are kept. Using the chromosome stored in the pool rather than the elite chromosome into generating

offspring chromosomes may encourage the GA to effectively search the parametric space and result in a reduction in computation time.

- If the stopping rules established a priori are met, the process ends. If not, the algorithm proceeds and new offspring chromosomes are generated.
- New offspring chromosomes are created based on the predetermined GA operational parameters including the population size (P), the mutation probability (P_m), and crossover probability (P_c). The total number of new offspring is the sum of the GA operation results from crossover (O_1) and mutation (O_2). In this dissertation, the following values are used. (P =30, P_m=0.3, and P_c=0.5)

3.6.2 Calibration Objective Function

The implementation of ITS technology in North America has increased the availability of disaggregate traffic data. The majority of current calibration techniques seek to minimize an objective function that is based on a single aggregated metric (i.e. mean travel time).This approach has been adopted because of lack of disaggregated data (i.e. the distribution of observed travel times). It is hypothesized that this approach only takes into account a small portion of traffic behavior (e.g. average travel time) and it would be better to use more detailed information if possible. This fact points out a need to develop a calibration objective function which uses disaggregate traffic data and to subsequently test this approach to determine if it improves the calibration accuracy and precision.

In this dissertation, a statistically based objective function is introduced as an evaluation criterion where the statistical test is used to define "consistency" between the observed and simulated traffic conditions. The selected statistically based objective function is the Kolmogorov-Smirnov (KS), which compares the equality of observed and simulated travel time distributions. This approach will be explained more detail in Chapter V.

3.6.3 Fitness Function

The evaluation result for each trial chromosome is channeled into the fitness function, which returns the probability to be selected for next reproduction. Various functions have been used in GA including exponential function, power functions, and linear function. In this dissertation, the *p*-value from the KS test is used to calculate the fitness values.

Three points need to be addressed in the selection of the fitness function. The first point is that, in this dissertation, the calibration objective function is defined as a maximization problem against the *p*-value, implying that the chromosome with higher *p*-value is stronger in a competition, while a metric that minimizes the difference between the simulated and observed data has been used in the conventional approach. Therefore, an appropriate function form needs to be selected to translate the evaluation result obtained from the maximization objective function into a measure of fitness. The second point is that the *p*-value can range from zero to one. The selected fitness function places higher weight on the chromosome with higher *p*-value, thus increasing the probability that this chromosome is chosen for the reproduction step of the GA. The third point is that the KS test is evaluated at the $100(1-\alpha)$ percent confidence level. The selected fitness function can place higher weight to the chromosome that is statistically valid (chromosome with *p*-value greater than 0.05). In this dissertation α is originally set to 0.5.

The fitness value corresponding to each chromosome and the total fitness are calculated according to Equation 3.3 and 3.4, respectively. Subsequently, the fitness relative to the total fitness is assigned to each chromosome for use in the crossover and mutation steps of the GA.

$$F(x_i) = f(g(x_i)) = \begin{cases} e^{g(x_i)} + C_1 g(x_i) & \text{if } g(x_i) \le 0.05 \\ e^{g(x_i)} + C_1 g(x_i) + C_2 & \text{otherwise} \end{cases} \quad (3.3)$$

$$TF(P) = \sum_{i=1}^{P} F(x_i) \quad (3.4)$$

$$F_R(x_i) = \frac{F(x_i)}{TF(P)} \quad (3.5)$$

$F(x_i)$ = fitness function value of *i*th chromosome (x_i) ;

$g(x_i)$ = objective function value of *i*th chromosome (*p*-value) ;

C_1, C_2 = constants ($C_1 = 3, C_2 = 5$) ;

$TF(P)$ = total fitness of P chromosome ; and

$F_R(x_i)$ = relative fitness that is used as probability in crossover and mutation GA operation.

3.6.4 Stopping Criteria

The stopping criterion that is commonly used in the GA is the maximum number of iterations, which is, by definition, established *a priori*. However, for the modified approach developed in this dissertation, two different stopping criteria are identified because the proposed calibration procedure has different features over the conventional approach. One is the statistically based objective function (KS test) and the other is the bi-level calibration structure.

In the case of a statistically based objective function, the maximum number of accepted chromosomes (N_t) is used as a stopping criterion. The typical GA, known as the elite selection method, maintains the best *P* chromosomes and passes them to next generation, where *P* is the population size. In contrast, in the proposed calibration procedure, the chromosome is stored in the pool of accepted chromosomes once it passes the KS test. As a result, the number of accepted chromosomes may keep increasing as the generation increases. Therefore, the maximum number of accepted chromosomes

(N_t) is also defined as another stopping criterion to terminate the calibration procedure when a sufficient number of "acceptable" chromosomes are obtained. Note that the conventional GA based approach commonly uses the maximum number of iterations as its stopping criterion.

In the case of the bi-level calibration structure, the convergence of the selected performance measure is used as a stopping criterion. The convergence is based on the maximum difference between the observed and traffic conditions, as shown in Equation 3.6. The algorithm stops when the percentage difference between the simulated and observed travel times is less than the pre-defined minimum ε. In this dissertation ε is originally set to five percent of the observed travel time. If either the maximum number of accepted chromosomes or the convergence of selected performance measure is met, the GA based calibration procedure ends.

$$\max \left| \frac{TT_{ij}^{obs} - TT_{ij}^{sim}}{TT_{ij}^{obs}} \right| \leq \varepsilon \tag{3.6}$$

TT^{obs} = observed travel time between AVI station *i* and *j* (sec);

TT^{sim} = simulated travel time between AVI station *i* and *j* (sec); and

ε = tolerance (5% of observed travel time)

3.7 CONCLUDING REMARKS

This section outlined the bi-level calibration framework adopted in this dissertation. As addressed in Section 2.2.1, researchers that address the joint calibration of OD matrix and driver behavior parameters are quite rare. The limited research that exists has focused on the use of the microscopic traffic simulation model to generate the simulation data required to calibrate route choice parameters or the assignment matrix because path travel times are not usually available in reality. In addition, the applicability of these

approaches is limited in a freeway network where the route choice possibility is absent. In the bi-level approach proposed in this dissertation, it is hypothesized that there is circular inter-dependence between the OD flows and driver behavior parameters. For example, if the OD flows are changed and then associated traffic conditions are changed, driver behavior parameters also need to be calibrated to capture different driver behavior trait. The upper level seeks to identify driver behavior parameters by comparing the simulated and observed traffic conditions while the OD matrix is set. In the lower level the OD matrix is calibrated by incorporating the simulated travel time into the Kalman filter OD estimator while the calibrated driver behavior parameters are fixed.

This section also outlined some issues with coding the network supply and demand data into the VISSIM microscopic traffic simulation model. For the I-10 freeway test network, a severe blockage was found due to a relatively short distance between merge and diverge sections. This problem was fixed by adjusting the waiting time before diffusion parameter, desired speed distribution, lane change distance for connectors, and dummy connector and partial route decision.

In this dissertation, the Genetic algorithm (GA) was selected as an optimization technique to find the “best” driver behavior parameters. The settings of the GA application were presented. Especially the statistically based objective function (KS test) and the corresponding fitness function were defined.

CHAPTER IV

AUTOMATIC VEHICLE IDENTIFICATION DATA

Automatic Vehicle Identification (AVI) data has been used to provide travel time information to drivers as a part of Houston Advanced Traveler Information Systems (ATIS). As a main source of travel time data AVI systems have attracted increasing attention because of their effectiveness and convenience (1, 76).

There is, however, a chance that the AVI data is contaminated. For example, AVI readings could be lost because of contamination errors. Consequently, the data needs to be screened to ensure that a suspect observation is left or removed for further analysis.

In subsection 4.1, the description of the Houston Automatic Vehicle Identification system is presented. In subsection 4.2, AVI data processing method is discussed and provided. In subsection 4.3, the existing AVI data filtering algorithms are described while subsection 4.4 provides the description of proposed model and its application results. Finally, the concluding remarks for Chapter IV are presented in subsection 4.5.

4.1 AUTOMATIC VEHICLE IDENTIFICATION SYSTEM

Automatic Vehicle Identification (AVI) technology identifies the passage of a particular vehicle at a particular point. In most applications in North America the technology is based on radio frequency identification (RFID). AVI systems have mainly been used for automatic toll collection applications. It also has been used to provide real time travel time information to motorists because it enables to collect travel information in a continuous and inexpensive way. The AVI systems, that are currently operated to collect real time travel information, include the TranStar system in Houston, the TransGuide system in San Antonio, and the Transmit system in the New York/New Jersey metropolitan area (76).

The AVI system is comprised of AVI-equipped vehicles, AVI stations, and a central computer. Vehicles are equipped with AVI tags because 1) they have been outfitted for use on the local toll roads or 2) the owner has installed the devices voluntarily. The tags have electronically encoded with a unique identification number. This information is transmitted to AVI readers as the vehicles traverse the network. The AVI readers are located on overhead structure and monitor the passage of vehicles equipped with tags. Each time an AVI-equipped vehicle enters the antenna capture range, its tag ID number, station number, and corresponding time and data are collected by the readers, and transmitted to a central computer. In Houston the AVI stations are placed in intervals from 2 to 8 kilometers along the freeway and are stationed over each lane. When a vehicle passes through successive AVI stations the central computer computes the average travel time and speed between them.

Houston is one of the first cities where AVI technology has been applied on non-toll roads. TranStar, the local traffic management center (TMC), have installed and operated an AVI monitoring system along 360 kilometers (227 miles) of interstate highway. It focuses for detecting traffic congestion and collecting real time travel information on the system. Average travel time and speed are archived as historical information and provided to public through the TranStar website and variable message sign. TranStar also provides historical speed report and chart for yearly and daily comparison as well as current traffic speed map along main freeways.

4.2 DEVELOPING THE AVI DATASET

AVI data can be used for many traffic applications. The spatial and temporal distribution of travel time between specific sections can be obtained from AVI data. In addition, paths, AVI volume, and AVI OD proportions can be indirectly sampled through appropriate AVI data processing.

The AVI data processing starts with sorting the unique vehicle identification numbers. Note that these numbers have been randomized to protect the privacy of the commuters. These data are then sorted based on the AVI station number and the time it

is read. To compute travel times, the times a vehicle with the same identification number passes consecutive AVI stations are grouped together. The link travel time is calculated by matching the times recorded by the AVI readers at the start and the end of the defined AVI links.

Through this process, the raw AVI data are turned into the dataset that are ordered by the AVI station number and the time a vehicle enters the network. These datasets would be used to extract the OD information that is necessary for estimating the OD matrix in Chapter VI. They include the individual trip OD, total AVI OD volume, and path information.

4.3 EXISTING AVI FILTERING ALGORITHMS

Although valuable information about travel times can be obtained from AVI data, the data quality should be checked prior to their use. The quality of data is mainly controlled by removing outliers. The primary source of these outliers is motorists that leave the freeway, stop for some time, and then re-enter the system. This "detour" provides large outlier readings of travel time. However, outliers may occur because of drivers traveling considerably faster (or slower) than the average. Therefore, a method for separating these two types of phenomenal needs to be identified. Ideally all "detours" would be removed while keeping all valid observations.

In this dissertation, the AVI travel times would be used to evaluate the network performance in comparison with the VISSIM simulated results. Even though the VISSIM adopts stochastic submodules that allow for different behavioral reactions of drivers subject to the same traffic conditions, the variation are limited within a certain range. Therefore, any observations that seem not to be emulated within the VISSIM should be removed.

4.3.1 Description of Existing Algorithms

Various methods have evolved to screen traffic data and increase their accuracy. In the case of loop detector, which has been a main source of collecting traffic data in North America, common approach is to remove "unreasonable" speed, volume, and occupancy data by observation against a threshold value (77, 78). If the observed data falls outside the threshold, it is not included into a valid dataset. The algorithms for AVI data control are basically similar to the approach adopted for loop detectors, except that travel time is the variable that is checked. The algorithms applied for AVI data control will be described in the following subsections.

Dixon used a rolling mean and standard deviation as a primary threshold and a median as a secondary threshold (1). It was assumed that the travel times follow a normal distribution. The travel time beyond a "reasonable" percentile was considered as invalid. A secondary threshold based on the median was used to detect the sudden onset of congestion during peak hours. When such a sudden change in traffic conditions occurs, the actual link travel time may possibly jump above the primary threshold value. To avoid successive observations being rejected, this secondary threshold was applied when 10 travel times were rejected sequentially. In his research, this secondary threshold value was computed as the product of the median and a factor equal to 1.2.

Another approach is used for estimating link travel time by the TranStar, TransGuide, and Transmit TMCs. Even though the details of these three systems are different, the basic concepts are similar. The algorithms are explained using the TranStar logic. The TranStar TMC algorithm is defined by Equation 4.1 and 4.2. Equation 4.1 defines the valid set of the observed travel times between two AVI stations *i* and *j*. The average link travel time is updated by taking average for the valid travel time observations, as shown in Equation 4.2 (76).

$$VS_{ij} = \left\{ tt_{ij} \mid t - tw \le t_j \le t \text{ and } Att_{ijt}(1-l) \le tt_{ij} \le Att_{ijt}(1+l) \right\} \quad (4.1)$$

$$tta_{ij} = tta_{ij} = \frac{\sum_{i=1}^{n_{VS}} tt_{ij}}{n_{VS}} \quad (4.2)$$

VS_{ij} = valid set of the observed travel times between AVI station *i* and *j* ;

t = time at which travel time filtering process takes place (seconds) ;

tw = rolling time window (seconds) ;

l = link travel time threshold value ;

Att_{ijt} = average link travel time between AVI stations *i* and *j* at time *t* (seconds) ;

tt_{ij} = observed travel time between AVI stations *i* and *j* (seconds) ;

t_j = time at which vehicle pass AVI station *j* (seconds) ; and

n_{VS} = number of valid observations.

The size of a rolling time window and the value of a link travel time threshold play important roles in determining the validity of travel time observations. The rolling time window relates to the time step that should be taken into account when the homogeneous set of travel time observations is decided. Therefore, a small rolling time window is more likely to define the homogeneous observations better while it reduces the number of observations that are assumed to be representative of existing traffic conditions. However, this setting makes the algorithm more sensitive to changes in traffic conditions. Another key factor for deciding the rolling time window is the AVI tag penetration rate. Higher penetration rate allows to sample more travel time observations for the same period and to trace changes in traffic conditions with increased confidence. In Houston, 150,000 tags are distributed to regular commuters for automatic toll collection (1). These cover about 9% of total vehicles operating in Houston. It results

in approximately 7 travel time observations per minute during peak hour and 5 travel time observations during off peak hour at each AVI station.

The link travel time threshold is used to determine the boundary above or below which the observed travel times are considered invalid or an outlier. If the observed travel time differs from average link travel time by a pre-specified threshold, this observation is rejected and considered invalid. There is no established guideline about the value of the link travel time threshold but the link travel time threshold of 0.2 seems to be used as a common practice by both the TranStar and the TransGuide traffic management systems.

In the TranStar system, the algorithm uses the rolling time window of 30 seconds and a link travel time threshold of 0.2. Whenever a new observation is collected, the validity of this observation is decided by comparing the upper and lower boundaries, as computed in Equation 4.1. For instance, if new observation falls outside the boundary, this data is considered invalid and removed from the valid travel time data set. In turn, the average link travel time remains unchanged. Otherwise the average link travel time is updated by taking the average of new observation and valid observations obtained in the previous 30 seconds time period.

The TransGuide TMC system is similar to the TranStar TMC. The only difference is that average link travel time is updated at a fixed time interval of 2 minutes instead of being updated whenever new observation is obtained. In Transmit TMC system, a large fixed time interval of 15 minutes is used to obtain current travel time estimates. After estimation of the current travel time, this estimate is smoothed against a historical database. This smoothing process ensures that incident data are not included in computing current average travel time. Also this smoothing against historical data results in slow response to changes which is designed to produce reliable long term average travel time (76).

4.3.2 Evaluation of Existing Algorithms

To evaluate the performance of the existing algorithms, each algorithm was applied to datasets from the Houston AVI system. The Transmit algorithm was excluded in the analysis because it requires historical travel time information. AVI data were collected along the I-10 freeway test network for five weekdays in 1996. The morning peak period (7:00AM~8:00AM.), which is identified as being congestion-recurring interval, is selected as the analysis period. For the I-10 freeway test network, approximately 3 observations per minute were made during the morning peak hour.

For the method used by Dixon, the evaluations of primary threshold and the combination of the primary and secondary thresholds were performed separately to quantify how the secondary threshold enhances the performance of the filtering algorithms. The existing filtering methods are summarized in Table 4.1, where column three describes the parameters used in each filtering method.

TABLE 4.1 Existing AVI Filtering Algorithms and Operating Parameters

Case	Description	Operating Parameters
1	Rolling Mean	• Rolling mean of 10 previous observations • Use of 95% z-score under Normal assumption
2	Rolling Mean + Median	• Use of median as secondary threshold when 10 observations are rejected sequentially
3	TranStar	• Use of 30 seconds rolling time window • Use of 0.2 link travel time threshold
4	TransGuide	• Use of 2 minutes rolling time window • Use of 0.2 link travel time threshold

In the first case, only the rolling mean was used. The upper and lower limits for the current observation were built based on the 95 percent significance level of the average travel time of the last 10 valid observations. The improvements of the filtering algorithm were tested in the second case where the median was used as the secondary

threshold when 10 observations were rejected sequentially. The third and forth cases were tested based on the same parameter settings as the TranStar and TransGuide TMC system are using. As stated earlier, a 30 seconds and a 2 minutes time window were used, respectively.

To evaluate each case from the beginning (7:00AM) of the analysis period, the first observation collected after 6:55AM was used as the starting point. During this 5 minutes initializing period, the first 10 observations were assumed to be valid. The observations for the first 30 seconds and 2 minutes periods were also considered valid and used to compute the average link travel time for the case 3 and 4, respectively.

Figure 4.1 illustrates how the case 1 filtered the AVI data. It should be noted that similar results were obtained for most of AVI travel times considered in the analysis. Figure 4.1 shows the average link travel time, the valid and invalid observations, and the upper (lower) limit of the validity window. The travel times continuously increase from 210 seconds at 7:10AM to 330 seconds at 7:27AM. The use of primary threshold was not able to trace the changes in travel time, and thus failed to produce a valid travel time dataset. The exclusion of the travel times after 7:16AM resulted in subsequent observations being rejected and the average link travel time being estimated as constant. The last valid observation was made when travel time fell inside the validity window around 7:20AM. As can be seen in Figure 4.1, the simple moving average led to extremely insensitive filtering algorithm. This was in spite of the fact that the observed travel times do not appear to be changing rapidly. Another issue is related to the size of validity window which defines the threshold boundary. The standard deviations fluctuated around 15 seconds between 7:10AM and 7:15AM and were approximately 8 seconds after 7:15AM. For instance, if a new observation is made after 7:15 AM whose travel time is deviated from the moving average travel time by more than 16 seconds (the product of 8 seconds standard deviation and 95% z-score of 1.96), this observation is considered invalid. The validity window that is constructed based on the used criteria was too small to capture the subsequent increase in travel time because of congestion.

The procedure was redone using the 99 percent significance level. The downside to this is that the probability of a "detour" outlier being accepted increases. This attempt resulted in larger validity windows. Despite the use of a larger validity window, it was found that the filtering algorithm was unable to trace the change in travel times due to congestion.

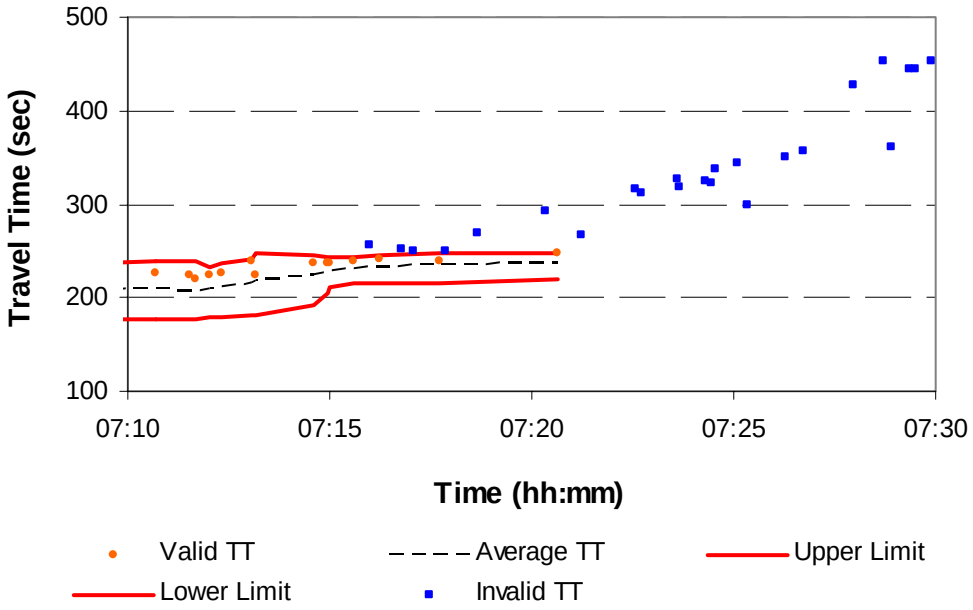

FIGURE 4.1 Application of Primary Threshold (Rolling Mean) to Houston AVI Dataset 1

The use of the rolling horizon and median values was then tried and the results are shown in Figure 4.2. The first half of Figure 4.2 was identical to that of Figure 4.1. The main difference between Figures 4.1 and 4.2 was that the observations between 7:26AM and 7:27AM were considered valid. The secondary threshold was not used, unless 10 consecutive travel time observations were found invalid. This threshold value is calculated by multiplying the median of the last ten rejected observations by a factor of 1.2. Hence, the secondary threshold was not applied for observations between

7:16AM and 7:20AM, indicating that these observations were removed from valid dataset. After the last valid observation at 7:21AM, exactly 10 observations between 7:21AM and 7:25AM were declared invalid. At 7:26AM the algorithm restarted the inclusion of observations into valid dataset.

Regarding the parameters used in case 2, the magnitude of multiplier and the number of consecutive invalid observations may have significant influences over the performance of the algorithm. Therefore, in the analysis, it is needed to carefully select these parameters in order to be associated with specific local traffic conditions. For example, a value of 1.8 was used as a multiplier in other research (79).

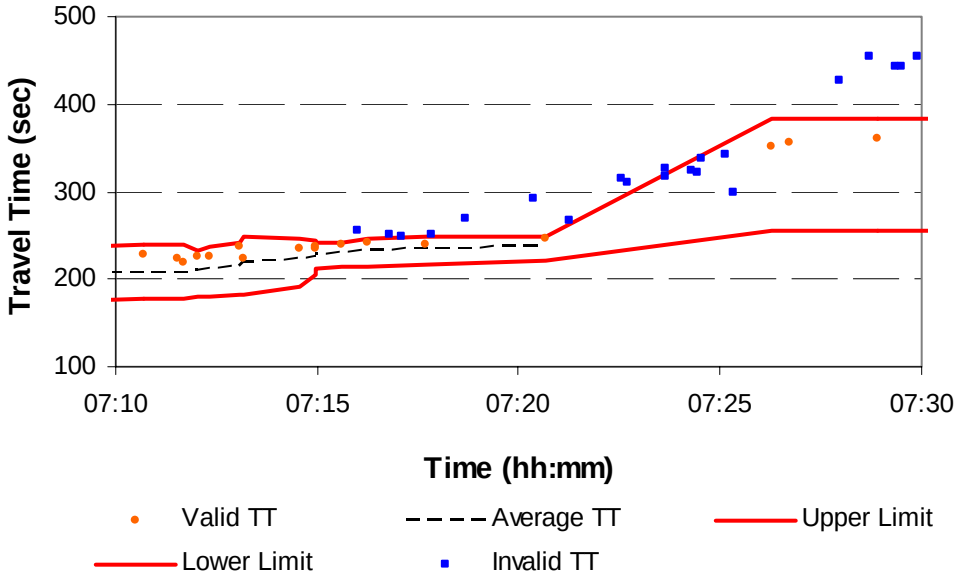

FIGURE 4.2 Application of Primary and Secondary Threshold to Houston AVI Dataset 1

The mere fact that the travel time observations are sequentially rejected raises the question as to whether they are outliers. In reality, there is a small likelihood that all of 10 rejected observations are outliers. Therefore, it is plausible that the travel time observations possibly jump due to due to sudden changes in traffic conditions.

To illustrate the overall performance of the TranStar algorithm when moderate changes in traffic conditions were observed, the TranStar algorithm was applied to different AVI datasets. Note that Figure 4.4 was generated using the same dataset used for Figures 4.1 and 4.2, but with different x and y-axes range to better visualize the overall performance during the full peak. The TranStar algorithm showed the ability to correctly trace changes in travel times and to effectively identify outliers. Any individual travel time observation between AVI stations, that differed less than 20% from the previously estimated average link travel time, was considered valid and used for updating the average link travel time. The impact of 0.2 link travel time threshold was apparent in Figure 4.3. It produced wider validity boundaries, which were 60 seconds at 7:10AM and 83 second at 7:28AM, respectively. In addition, Figure 4.3 illustrates how close the average link travel times followed individual travel time observation. Considering that there are approximately 3 AVI travel time observations per minutes in the I-10 freeway test network, only one or two previous observations were placed within a small rolling time window of 30 seconds. Therefore, the average link travel time computed by Equation 4.2 was very close to the new observation.

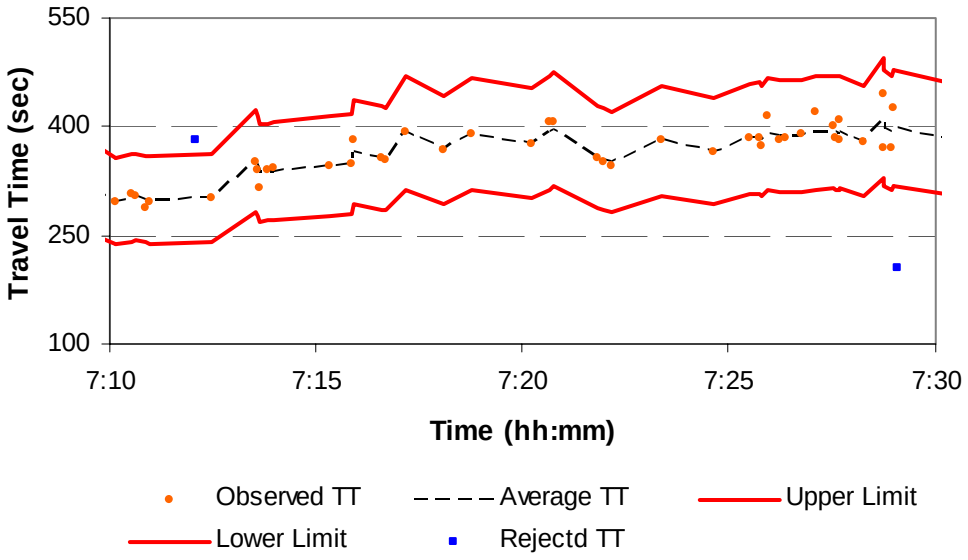

FIGURE 4.3 Application of TranStar Algorithm to Houston AVI Dataset 2

Despite wider boundaries and quick response to moderate changes in traffic conditions, the TranStar algorithm was unable to trace sudden changes, as shown in Figure 4.4. The observations before 7:28AM were filtered appropriately by the TranStar algorithm while the rolling mean and rolling mean plus median algorithms (cases 1 and 2) wrongly removed the observations after 7:15AM. However, the TranStar algorithm failed to trace the jump in the travel time from 354 seconds to 427 seconds at 7:28AM. The corresponding time interval between the two observations was 1 minute 15 seconds. This failure would be explained by the fact that travel time could be changed by more than 20% over 1 minute time interval if roadway conditions change dramatically.

Figure 4.5 was generated by applying the TransGuide algorithm to the same dataset used in Figure 4.4. The main difference between the algorithms was linked to the fact that the average link travel time was updated every 2 minutes, contrary to the TranStar algorithm that updates the average link travel time whenever a new observation is made. Therefore, the upper (lower) limits of the validity window appeared to be stepwise. The overall results of the TransGuide algorithm were very similar to those of the TranStar algorithm, especially in terms of the time when the algorithm failed and the updated average link travel time.

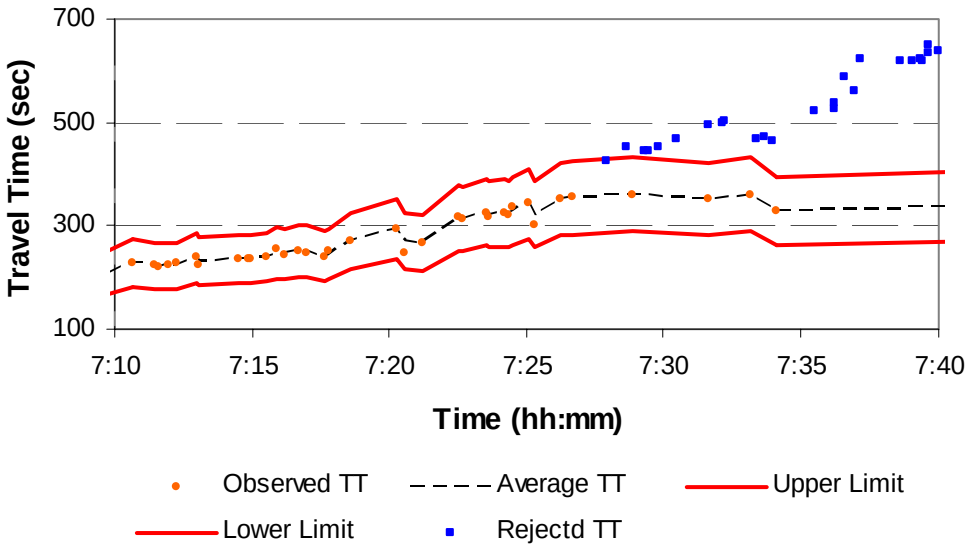

FIGURE 4.4 Application of TranStar Algorithm to Houston AVI Dataset 1

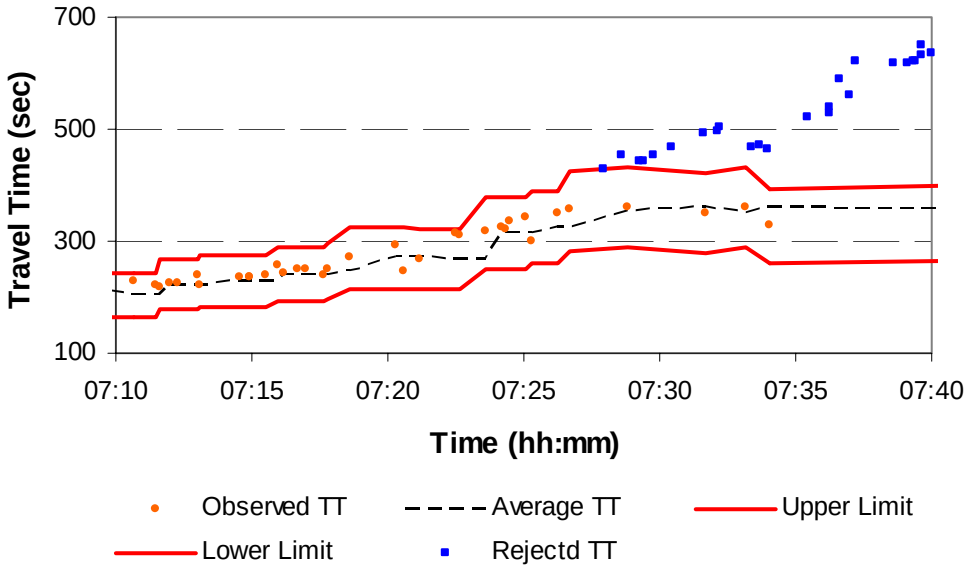

FIGURE 4.5 Application of TranGuide Algorithm to Houston AVI Dataset 1

4.4 PROPOSED AVI FILTERING ALGORITHM

Even though several problems were found in the application of the existing algorithms to the dataset from the Houston AVI system, further analysis is required determine whether the finding can be generalized to the different time and location. In particular, the impact of the algorithm parameters such as the number of sequentially rejected observations, the size of rolling time window, and the value of a link travel time threshold should examined.

In this section, based on the previous findings a better method will be proposed for better tracing of increasing and decreasing trends in the AVI travel time observations. The proposed algorithm should meet the following conditions.

- As was found in the applications of the moving average and median values, the average link travel time should not lag behind the true link travel time. The

average link travel time needs to be updated so that it "represents" underlying trends of each travel time observations.

- A link travel time threshold of 0.2 is seemed appropriate to capture moderate changes in traffic conditions, as shown in the operational performances of the TranStar and TransGuide algorithms. However, the link travel time threshold should be selected to be wide enough to allow the algorithm to respond better when sudden changes occur.
- It is desirable to reduce the number of parameters which need to be calibrated by users to be associated with specific traffic conditions, such as the number of sequentially rejected observations and the significance level for computing validity boundaries in the rolling horizon algorithm, the size of rolling time window, and the value of a link travel time threshold.
- As shown in the case 2, 10 valid observations were excluded from the set of valid observations. The modified algorithm needs to minimize this unnecessary loss of valid observations.

The proposed AVI filtering algorithm is shown in Equations 4.3 through 4.9. Equation 4.3 defines the set of valid observations. Unlike Equation 4.1, the concept of the rolling time window is not used because the previous time step to be taken into account is implicitly incorporated into Equations 4.6 and 4.9. The upper and lower limits of the validity window are computed using Equations 4.4 and 4.5. The validity window is the range encompassing the link travel time threshold from the average link travel time.

In the proposed algorithm the average link travel time is updated whenever a new travel time observation is collected. Contrary to the TranStar and TransGuide algorithms which take an average of all valid observations within the fixed rolling time window, the average link travel time is computed by weighting the new valid travel time (vehicle k) with the average link travel time (vehicle k-1) that had been previously updated.

$$VS_{ijk} = \left\{ t_{ijk} \mid tt_{ijk\,\min} \le tt_{ijk} \le tt_{ijk\,\max} \right\} \tag{4.3}$$

$$tt_{ijk\,\min} = Att_{ijk-1}(1 - l_k) \tag{4.4}$$

$$tt_{ijk\,\max} = Att_{ijk-1}(1 + l_k) \tag{4.5}$$

$$Atta_{ijk} = (1 - \alpha_k)\, Atta_{ijk-1} + \alpha_k tt_{ijk} \tag{4.6}$$

$$\alpha_k = 1 - (1 - \beta)^{\Delta DT_{k,k-1}} \tag{4.7}$$

$$l_k = \begin{cases} 0.2 \\ R_k \quad \textit{if } tt_{ijk} \textit{ is invalid} \end{cases} \tag{4.8}$$

$$R_k = \frac{\sum_{m=k-2}^{k-1} abs\left| tt_{ijm} - tt_{ijm-1} \right| / (DT_{ijm} - DT_{ijm-1})}{\sum_{m=k-10}^{k-1} abs\left| tt_{ijm} - tt_{ijm-1} \right| / (DT_{ijm} - DT_{ijm-1})} \tag{4.9}$$

VS_{ijk} = valid set of the travel times between AVI stations *i* and *j* when the observation of vehicle *k* is made ;

$tt_{ijk\,\min}$ = minimum valid travel time for vehicle *k* between AVI stations *i* and *j* ;

$tt_{ijk\,\max}$ = maximum valid travel time for vehicle *k* between AVI staions *i* and *j* ;

Att_{ijk} = average link travel time between AVI station *i* and j when the observation of vehicle *k* is made ;

tt_{ijk} = travel time observation of vehicle *k* between AVI station *i* and *j* ;

l_k = link travel time threshold value for vehicle *k* ;

α_k = weight for updating the average link travel time ;

β = sensitivity parameter ;

$\Delta DT_{k,k-1}$ = difference in detection times between vehicle *k* and *k-1* ;

DT_{ijk} = detection time of vehicle *k* between AVI stations *i* and *j* ; and

R_k = ratio of travel time changes for vehicle *k-1,…,k-10*.

As indicated in Equation 4.7, the value assigned to the weight is mainly affected by the elapsed time between two consecutive observations with the given sensitivity parameter. For instance, a larger interval increases the possibility of significant changes in traffic conditions. In turn, a larger weight is assigned to the current observation. In other words, the algorithm places higher confidence on the current observation. A wide range of parameters were investigated for various values of the elapsed times between vehicles *k* and *k-1*. From this analysis, a value of 0.002 was selected as the sensitivity parameter for β. With this parameter setting, weights of 0.33, 0.67, and 0.85 would be assigned to a new observation (vehicle *k*) with respect to the elapsed time of 20, 60, and 100 seconds, respectively.

In the proposed algorithm, two types of link travel time thresholds are used. The fixed link travel time threshold of 0.2 is used as the primary constraint to evaluate the validity of a new observation. If a new observation is found invalid, the link travel time threshold is substituted by the value computed using Equation 4.9. The secondary link travel time threshold is designed to capture changes in traffic conditions without loss of valid observations. It is based on the concept that the extent to which previous travel time observations fluctuate provides useful information to recognize underlying trends of increasing or decreasing travel times. In Equation 4.9, rates of changes in the last 2 pairs travel time observations is divided by rates of changes in the 10 pairs of previously observed travel times. If no significant variations occur, a value of about 0.2 is assigned to the secondary link travel time threshold, which is identical to the primary threshold. On the other hand, if more fluctuations are made for the most recently travel time observations, a larger value is given to the secondary link travel time threshold, and thus the validity window is expanded. It should be noted again that the secondary threshold is used only when the application of primary threshold is rejected.

To be consistently compared with the results of the existing filtering algorithms, the same dataset was used to generate Figures 4.6 and 4.7. As shown in Figure 4.6, the observations after 7:28AM (labeled as 2 and 3) were considered valid even though the travel times were changed from 354 seconds (labeled as 1) to 427 seconds (labeled as 2).

The proposed algorithm reevaluates the validity of the observation based on the validity window computed using Equation 4.9. This is because the application of 0.2 link travel time threshold is rejected. At this point, the value of link travel time threshold was increased from 0.2 to 0.24, resulting in the larger upper and lower validity window. The inclusion of data point at 7:28AM into the set of valid travel time observations led to the update of the average link travel time and the subsequent observations were not incorrectly removed. While the existing algorithms accepted new valid observations only after the travel times were reduced to the validity window at the end of peak hour, the proposed algorithm was able to identify the underlying trends in traffic conditions without a break.

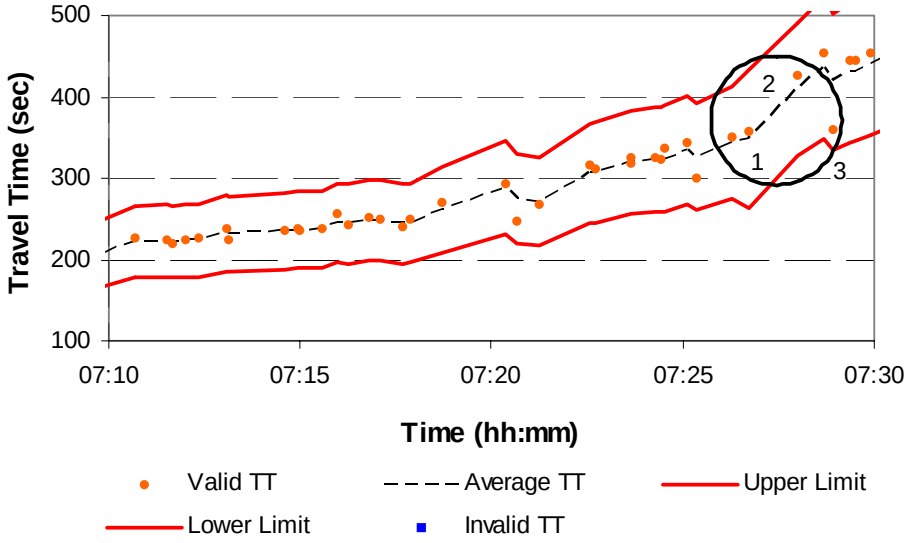

FIGURE 4.6 Application of the Proposed Algorithm to Houston AVI Dataset 1

Figure 4.7 shows the operational performance of the proposed algorithm over the entire morning peak (7:00AM~8:00AM). While incorrect inclusion or exclusion appeared to be made for a few observations which were closely located to the upper and lower boundaries, the proposed algorithm overcame the shortcomings of the existing algorithms. The algorithm adjusted the size of the validity window to be more sensitive

to sudden fluctuations in the travel time observation. The validity windows for the datapoints after 7:30AM were increased when large variations in travel times started. On the other hand, narrower upper and lower boundaries can be found for the most of data points before 7:30AM

The proposed algorithm was able to track moderate and significant travel time changes without resort to check how many consecutive data points fell outside the validity window. No data points were thus unnecessarily excluded from the set of valid observations. The impact of introducing the weighted combination of a new observation (vehicle *k*) and the average link travel time that had been previously estimated (vehicle *k-1*) was apparently visible.

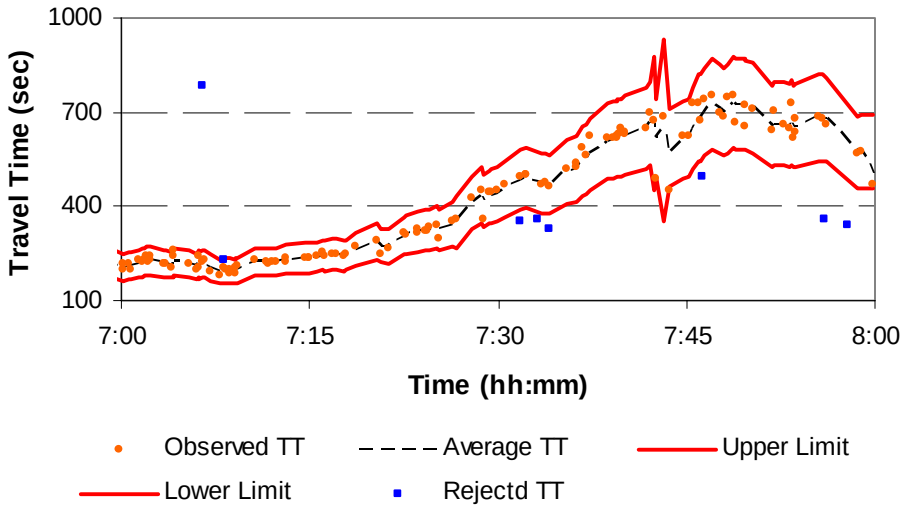

FIGURE 4.7 Application of the Proposed Algorithm to Houston AVI Dataset 1 for the Full Peak Hour

The algorithm could also control the amount of the average link travel time update in such a way that it was less sensitive to short term fluctuation but more responsive to long term changes by simply determining the sensitivity parameter, β. In addition, in the proposed algorithm, the sensitivity parameter was the only factor which

users had to calibrate to meet the local specific traffic conditions before the implementation, while the existing algorithms have various factors that affect the performance of the algorithms such as the number of sequentially rejected observations, the number of sequentially rejected observation, the size of rolling time window, and the value of a link travel time threshold.

4.5 CONCLUDING REMARKS

It was found that the existing filtering algorithms for AVI data quality control did not account for sudden variations in traffic conditions and result in the subsequent observation being declared as outliers. These were demonstrated by applying the existing filtering algorithms to AVI datasets from the TranStar TMC in the Houston, Texas.

The proposed filtering algorithm overcame these deficits in that: 1) it successfully traces the true average link travel time over the existing filtering algorithms. Contrary to a simple moving average technique, the algorithm takes into account the elapsed time between two successive observations when updating the average link travel time. A larger weight is assigned to the current observation if the elapsed time increases; and 2) it provides wider validity boundaries not to falsely exclude valid observations when AVI travel time data exhibits sudden changes in travel conditions. It was hypothesized that the variations of the previous travel time observations can be used as indicators that capture underlying trends of increasing or decreasing travel times. Therefore, the algorithm dynamically increases the upper and lower limits of the validity according to travel time variations.

Even though the proposed filtering algorithm was successfully applied to AVI dataset from the TranStar TMC, further research is required for the proposed filtering algorithms not to be restricted to specific time and location. In addition, the sensitivity parameter used for updating the average link travel time needs to be calibrated because it is a function of traffic volumes and AVI tag penetration rate (e.g. the number of observations per time period).

CHAPTER V

CALIBRATION OBJECTIVE FUNCTION BASED ON NON-PARAMETRIC STATISTICAL TEST

There has been an increasing interest in the use of microscopic traffic simulation models for transportation analysis. In order for these simulation models to represent reality, they must be calibrated to local conditions. This is particularly true when local driver behavior and/or vehicle characteristics are markedly different from the default values.

In the context of calibration, the indicators that measure "consistency" between observed and simulated traffic conditions are very important. These indicators are obtained by translating the simulation output into simple metrics on how well a given parameter set has performed. The traffic output typically includes an average of travel time or volume counts on a specific link. However, these types of indicators cannot address sufficiently certain aspects of observed field conditions. Therefore, they cannot provide sufficient evidence for deciding how well the simulation model is performing in replicating observed field conditions. To date there is no clear guideline on what "consistency" means and how "consistency" is quantified.

This chapter consists of 5 subsections. Subsection 5.1 describes the observed distributions of travel times for the test beds. Subsection 5.2 presents the statistically based calibration objective function while the results of the application are provided in subsection 5.3. Subsection 5.4 describes alternative selection technique for identifying the "best" parameter set among numerous statistically valid parameter sets. Finally, subsection 5.5 provides concluding remarks and findings.

5.1 DISAGGREGATE TRAVEL TIME DATA

5.1.1 Performance Measures at Disaggregate Level

The widespread deployment of Intelligent Transportation Systems (ITS) has allowed for the collection of traffic data in an efficient and inexpensive way. Examples of ITS include Automatic Vehicle Identification (AVI), Automatic Vehicle Location (AVL), and Global Positioning Systems (GPS). Archived ITS datasets provide an access to traffic flow characteristic details at a disaggregate level. However, they are usually aggregated or grouped in order to produce composite measures.

Kim (27) calibrated the freeway corridor using empirical ITS data. In his study, travel time data was extracted from an AVI system and the average of this data was compared to the simulated travel time. Rakha (34) observed variations in the field data due to the stochastic nature of traffic and emphasized a statistical approach that would quantify variability in the simulated data relative to the field data. However, the focus of this approach was on the variation emerging from daily flow changes and of simulation random seeds rather than use of a disaggregate data for calibrating the simulation model. Bloomberg (80) used the average speed of vehicles obtained from main lane for calibrating a parameter set that was indicative of the real system. While aggregated measures have been previously used in the calibration of microscopic traffic simulation, Brockfeld et al. used more disaggregate data that was obtained from individual probe vehicles equipped with GPS. This study focused on validating the car-following logic on which the microscopic traffic simulation model is based rather than calibrating a fully operational simulation model (81). Disaggregate data was often used only by the model developers to calibrate the individual modules implemented within traffic simulators.

The disaggregate data may have specific qualities which could prove useful if captured. It is more accurate in representing observed traffic conditions and has the added benefit of avoiding aggregation bias (82, 83). In addition, it makes it possible to determine statistical distribution of a variable. Therefore, it is hypothesized in this dissertation that the use of disaggregate data for the calibration of simulation models increases the credibility in simulation results, where disaggregate data is used as a basic

unit in deciding the quality of simulation results. A statistically based calibration objective function which can account for disaggregate data will be proposed in Section 5.2. A conceptualization of disaggregated performance measure in the calibration process is shown in Figure 5.1.

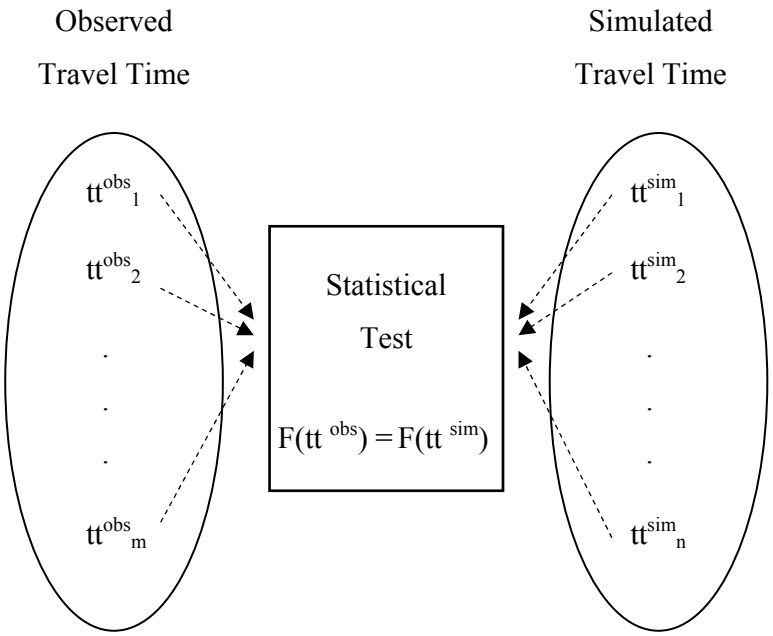

FIGURE 5.1 Disaggregate Performance Measure in Calibration Process

There are a number of traffic performance measures that may be used for quantifying the quality of the calibration. In this dissertation, the travel time is selected as a performance measure. It is not only one of the key features associated with traffic conditions but also is of critical interest for most drivers. In addition, the selection of travel time can be further justified by the fact that the calibration of simulation models against traffic counts may leads to an overestimation of the realism of the model. This occurs because the OD matrix, an important input in microscopic traffic simulation models, is often estimated based on the observed link volumes. Therefore, to obtain a higher degree of detail and accuracy in the calibration of simulation model, the calibration based on travel time is desirable (27, 84).

More importantly in this dissertation, travel time in the form of a distribution is the key decision criteria in contrast to many statistics which rely on a measure of central tendency such as the mean. This is important because travel time and its variability are important components of traffic conditions. For example, when the traffic conditions have large variability and a highly non-normal distribution, travel time may lead to poor calibration results only considering averages. Travel times are likely to deviate from their average in significant ways, especially during peak periods. Therefore, the distribution of travel time has the potential of considerably improving the accuracy of calibration results.

5.1.2 Travel Time Distribution for the Bellaire Arterial Test Network

The travel time statistics, including the average time, the standard deviation, maximum, and minimum, are summarized in Table 5.1. The average travel time was 164 seconds and the standard deviation was 54 seconds. A large variability in travel time was observed because the test bed was a signalized arterial where a coordinated signal control system was operated. Therefore, the estimate of the mean travel time was considerably different from what was actually experienced by a large portion of drivers.

TABLE 5.1 Summary Statistics of Travel Times for the Bellaire Arterial Test Network

		1st Peak	2nd Peak	Total
AVI Travel Time	Mean (seconds)	125.5	214.9	164.0
	Standard Deviation (seconds)	18.9	41.9	54.1
	Minimum (seconds)	81	166	81
	Maximum (seconds)	162	350	350
Travel Speed	Average (km/h)	31.7	18.5	24.2

This concept is illustrated in Figure 5.2, which shows a histogram of individual travel times for the arterial as a whole. Superimposed on this diagram is the normal distribution for the two regimes. It may be seen in Figure 5.2 that the observed travel times tend to exhibit a bimodal distribution. The first peak presumably results from the coordinated signal control system that is designed to favor directional flow during peak hour. On the other hand, the second peak may represent drivers who are interrupted by a red signal because they may enter the arterial from the cross street or require more than one signal cycle to pass through intersection.

It should be noted that the standard deviation in the first peak (i.e. travel time less than 165 seconds) is smaller than that in the second peak. The standard deviations of the first and second peaks are 19 seconds and 42 seconds, respectively. It is hypothesized that this occurs because the vehicles in the first peak tend to travel at a similar speed in order to stay in the progression band.

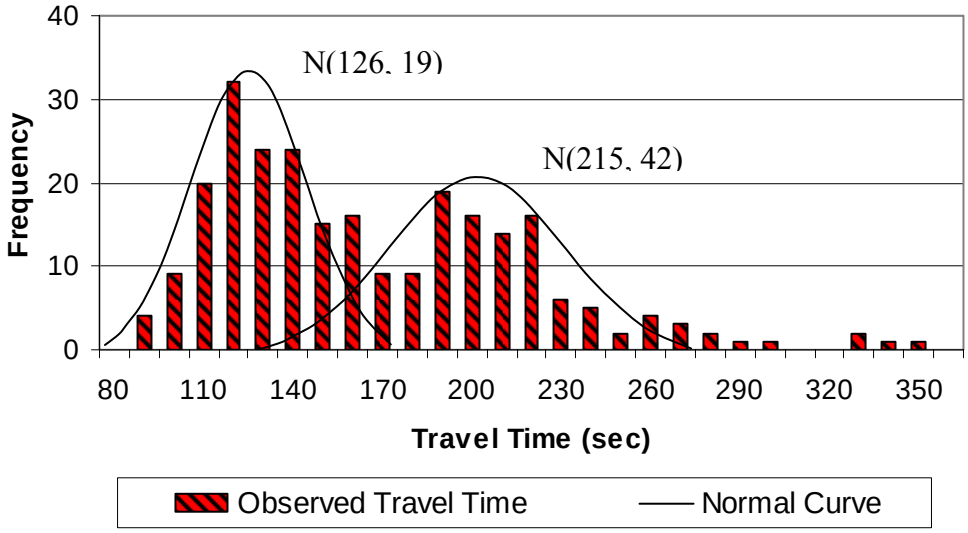

FIGURE 5.2 Histogram of Observed Travel Times for the Bellaire Arterial Test Network

The shape of histogram clearly indicates that the travel times are not normally distributed. This is confirmed with the results of the Kolmogrov-Smirinov normality test, which is provided in Table 5.2. It should be noted that that although the travel times as a whole are not normally distributed, the travel time in the first peak follows the normal distribution supported at a 95 percent confidence level.

TABLE 5.2 Normality Test of Travel Times for the Bellaire Arterial Test Network

	Kolmogorov-Smirnov Test	
	Statistics	Significance
1st Peak	0.069	0.082*
2nd Peak	0.183	0.000
Total	0.112	0.000

* The normality test is significant at the 95 percent (0.05) level

5.1.3 AVI Travel Time Distribution for the I-10 Freeway Test Network

In this section, the characteristics of travel time information that were filtered out using the methodology proposed in Chapter V are provided. The distributions of travel times will be used in further analysis for the calibration of the microscopic traffic simulation model.

The average travel time between AVI stations is obtained by taking the average of all valid observations for a given period of time. The statistics, including the average travel time, the standard deviation, maximum, and minimum, are summarized in Table 5.3. As would be expected, the closer a given link is to downtown Houston the lower is its average speed. The average speed for AVI 01 is approximately equal to the posted speed limit of 104 km/h (65mph) whereas drivers on AVI 23 have an average link speed of 62 km/h (40 mph). In addition, as the average speed decreases the standard deviation increases. It is hypothesized that this occurs because high level of congestion accompanies increasing interaction between moving vehicles.

TABLE 5.3 Summary Statistics of Travel Times for the I-10 Freeway Test Network

		AVI 01	AVI 12	AVI 23
AVI Travel Time	Mean (seconds)	242.4	261.9	201.1
	Standard Deviation (seconds)	14.4	34.4	35.6
	Minimum (seconds)	210	190	151
	Maximum (seconds)	273	347	282
Travel Speed	Average (km/h)	97.8	74.2	61.9

Histograms of the AVI travel times on each of the AVI links are provided in Figures 5.3 through 5.5. Note that using the approximate means and standard deviations, normal curves have been superimposed over these histograms. The null hypothesis, that there is no difference between the given travel time distribution and a normal distribution, is evaluated using the KS test. The results of normality test are presented in Table 5.4. The results show that the distributions of the travel times on the AVI link 12 follow a normal distribution while the distribution on AVI link 23 does not. The distribution on AVI link 01 tends to be normally distributed although it is not supported at a 95 percent confidence level. The violation of normality could be a problem for running parametric tests when comparing the given distribution with the simulated distribution. For this reason, a non-parametric statistical test will be introduced in Section 5.2, because it does not require assumptions about the underlying distribution.

TABLE 5.4 Normality Test of Travel Times for the I-10 Freeway Test Network

	Kolmogorov-Smirnov Test	
	Statistics	Significance
AVI 01	0.091	0.031
AVI 12	0.069	0.200*
AVI 23	0.200	0.000

* The normality test is significant at the 95 percent (0.05) level

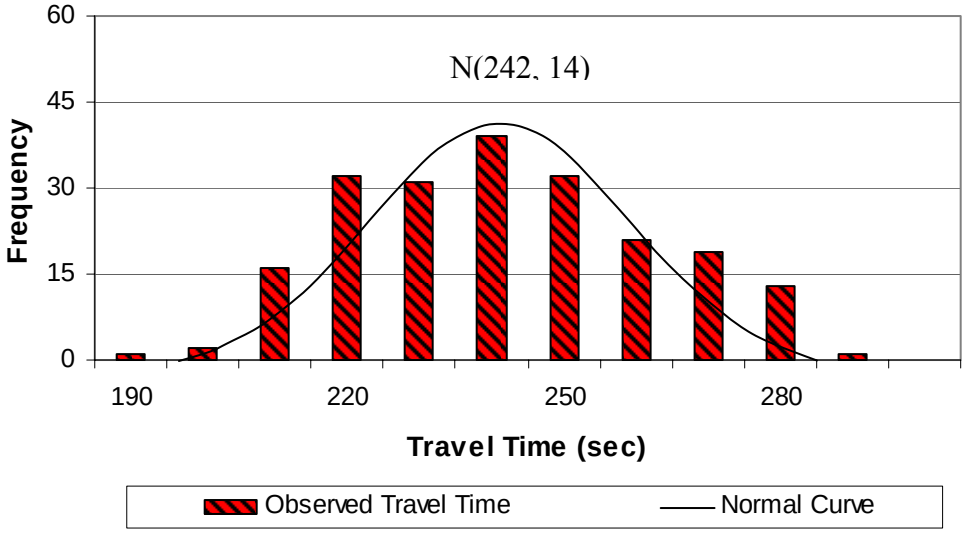

FIGURE 5.3 Histogram of Travel Time for AVI Section 01

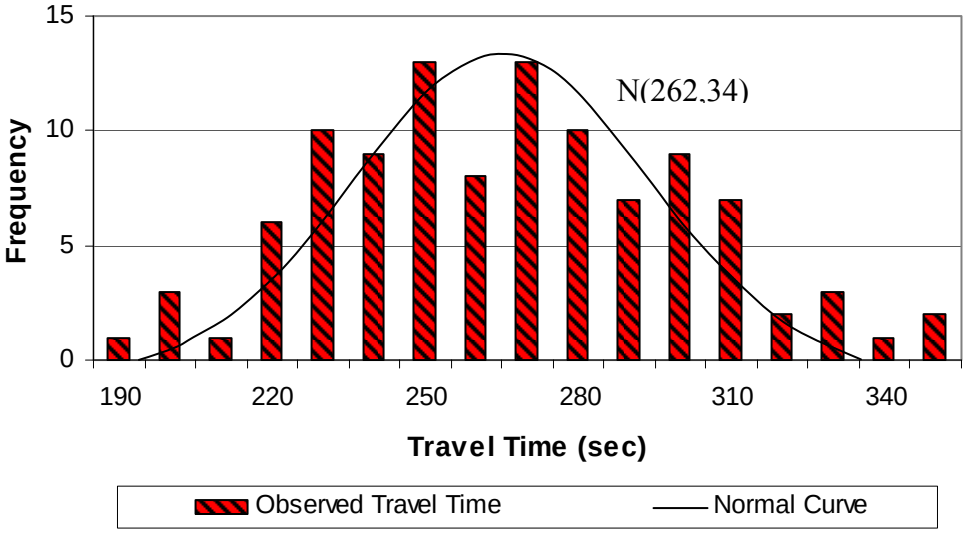

FIGURE 5.4 Histogram of Travel Time for AVI Section 12

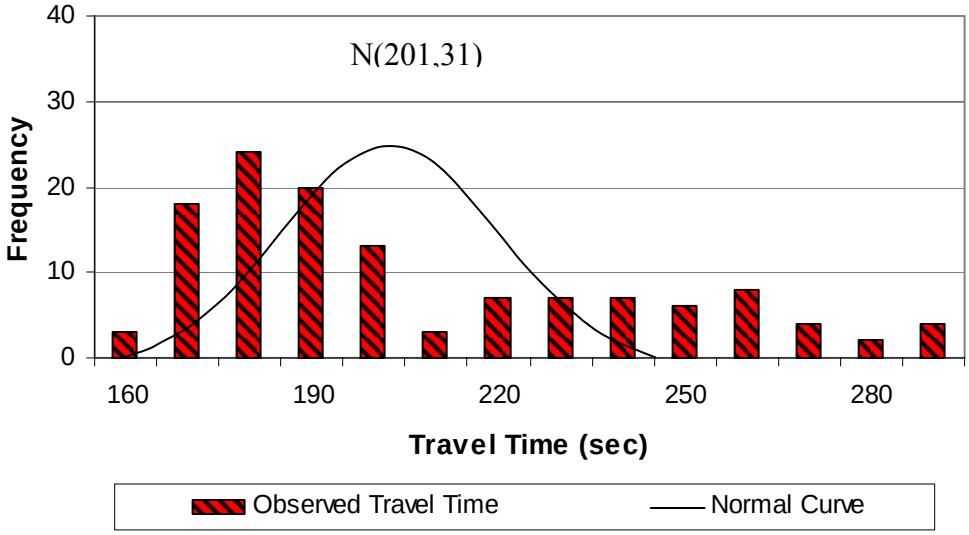

FIGURE 5.5 Histogram of Travel Time for AVI Section 23

5.2 STATISTICALLY BASED CALIBRATION OBJECTIVE FUNCTION

In the preceding section, the distributions of travel times on the Bellaire arterial and I-10 freeway test networks were prepared as target measures in the calibration process. Therefore, the way to best utilize disaggregate data in the calibration of the microscopic traffic simulation model still needs to be determined.

As discussed earlier the use of the aggregated performance measure for the calibration of simulation models may result in an inappropriate parameter set being selected as the "best". To avoid this situation a statistically based approach, which is based on disaggregate form of travel time data, is proposed in this section. Specifically, the "closeness" of the observed travel time distribution to that of the simulated travel time distribution is chosen as the objective function in the calibration process.

5.2.1 Non-Parametric Statistical Test

There are numerous statistical methods for testing whether two samples are drawn from the same population (85). The most popular methods are the student t-test for testing means and the F-test for testing variances. However, its application is questionable for

the calibration of traffic simulation models because its underlying assumptions, such as equal variance and normal distribution, are often violated. This was demonstrated in the figures showing the distributions of observed travel times on the test networks that the data collected in transportation system is likely to violate these assumptions to some degree.

In these situations, non-parametric or distribution-free techniques can be used because they do not require *a priori* assumptions about the distribution of the underlying population. These techniques compute the statistics of the empirical distribution based on the difference in rank or scale and then identify whether the two distributions are identical or not. In this dissertation, the Kolmogorov-Smirnov (KS) test is used to compare the distributions of the observed and simulated travel time distributions.

The Kolmogorov-Smirnov tests can be used to test the null hypothesis that two populations have the same distribution. Let x_1, ..., x_m be the field observations and y_1, ..., y_n be the observations from the microscopic traffic simulation model. The observed empirical distribution function $S(x)$ is computed using Equation 5.1, which represent the fractions of x_1, ..., x_m that are equal to or less than x. In the same manner, the simulated empirical distribution function $S(y)$ is also computed.

$$S(x) = \frac{1}{m}\sum_{i=1}^{m} I\{x_i < x\} \tag{5.1}$$

Where, $I\{x_i < x\}$ returns 1 if $x_i < x$, otherwise it returns 0.

The resulting empirical distribution function $S(x)$ ranks the variable x_i from 1 to m and has the cumulative percentage of the variable such that the cumulative percentage of m^{th} is 100 percent. To see if there is good agreement between $S(x)$ and $S(y)$, the following hypotheses are tested.

$$H_0 \quad : \quad S(x) = S(y) \qquad \textit{for all } x \tag{5.2}$$

$$H_1 \quad : \quad S(x) \neq S(y) \qquad \textit{for at least one value of } x \tag{5.3}$$

For each rank, the cumulative percentage in $S(x)$ is subtracted from the cumulative percentage in $S(y)$. The Kolmogorov-Smirnov test statistic (D) is the largest absolute difference in cumulative percentages for any given ordinal rank, as defined in Equation 5.4. The KS test is shown graphically in Figure 5.6. Both the simulated and empirical distributions are shown as well as the KS test statistic (D).

$$D_{\max} \quad = \quad \max\left|S(x) - S(y)\right| \tag{5.4}$$

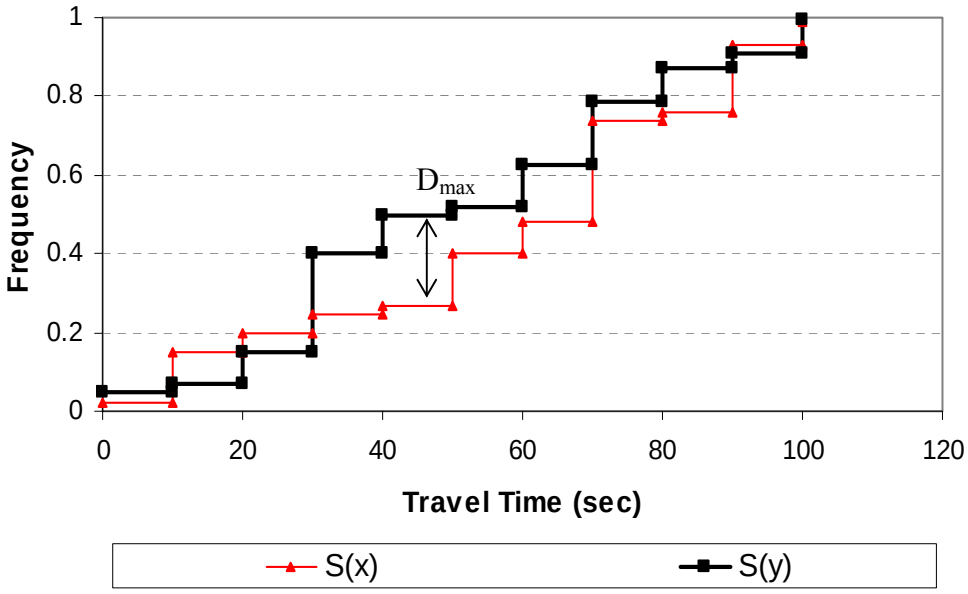

FIGURE 5.6 Kolmogorov-Smirnov Test

The computed value of D_{max} is compared to a table of critical values corresponding to a predefined level of significance. The null hypothesis H_0 is rejected if the test statistic D_{max} exceeds the critical value obtained from a KS table which is found in most statistics text books (85, 86). Note that there are a limited number of entries in these tables with respect to level of significance and number of samples. Consequently, the approximate *p*-value is computed based on the functions shown in Equations 5.5 through 5.7 rather than an interpolation of the KS table (87).

$$P(D) = Q_{KS}\left((\sqrt{N_e} + 0.12 + 0.11/\sqrt{N_e}) \times D\right) \quad (5.5)$$

$$N_e = \frac{N_{obs} N_{sim}}{N_{obs} + N_{sim}} \quad (5.6)$$

$$Q_{KS}(x) = 2\sum_{i=1}^{\infty} (-1)^{i-1} e^{-2i^2x^2} \quad (5.7)$$

$P(D)$ = *p*-value of the KS statistic D ;

N_e = effective number of data points ;

N_{obs}, N_{sim} = number of data points in the simulated and observed distributions, respectively ; and

$Q_{KS}(x)$ = monotonic function for computing *p*-value.

5.2.2 Benefits of a Statistically Based Calibration Objective Function

The purpose of an error measure is to provide an informative and clear summary of the selected performance measures. Sometimes, existing error measures are regarded as insufficient although they are widely used. Furthermore, an error measure should be reliable and resistant to outliers.

Several benefits can be identified for the use of a statistically based objective function based on a disaggregate data for the calibration of the microscopic traffic

simulation model. Firstly, the most prominent of them is the ability to define and quantify "closeness" using a statistical technique. A statistical technique does not mask information by taking into account the observed data in the form of a distribution and offers the potential to improve the calibration results. Secondly, a statistically based objective function is easy to understand and simple to interpret, because it is based on one of the widely understood statistical techniques. In addition, while a statistically based objective function centers around the Kolmogorov-Smirnov test in this dissertation, different statistical techniques can be applicable as well. Finally, the robustness of a statistically based objective function increases if datasets in multiple time-space measurement points are available. While the existing objective functions are based on average of errors in the selected performance measure, a statistically based objective function attempts to ensure that the distributions are satisfied at every time-space measurement points. The use of more disaggregated data, namely temporal, spatial, and combined spatial and temporal, helps capture the necessary complexity in the calibration of microscopic traffic simulation model. For example, it may be difficult for simulated errors to be distributed equally along the network. Therefore, the use of the travel time for each AVI link may increase the calibration accuracy instead of travel time for the full extent of the corridor.

5.3 ANALYSIS OF CALIBRATION RESULTS

5.3.1 Calibration Results for the Bellaire Arterial Test Network

The proposed statistical approach and calibration technique was applied to the Bellaire arterial test network. A total of 128 statistically valid parameter sets were identified in the calibration process and a subset of them are provided in Table 5.5. The definitions of the VISSIM parameters are provided in Section 3.5.1. Also shown are *p*-values for the KS test as well as the travel time MAER. The examples are shown in descending order with respect to *p*-values for the KS test. The complete results may be found in Appendix C.

Most of the acceptable parameter sets have a relatively low travel time mean absolute error ratio (MAER), which ranges from 0.007 (0.7 percent) to 0.07 (7 percent). Only 11 of 128 acceptable parameter sets have travel time MAER above 0.07 (7 percent).

It is important to note that the default parameter set results in a travel time MAER of 0.215 (21.5 percent), indicating that the travel times obtained from an un-calibrated model would have an approximately 21 percent error. More importantly, the travel time distribution obtained using the default parameter set fails to pass the KS distribution test, which illustrates the importance of calibrating the microscopic traffic simulation model prior to the model application.

TABLE 5.5 Subset of Statistically Valid Parameter Sets for the Bellaire Arterial Test Network

No	Calibrated Parameter*						KS Test	MAER**
	P1	P2	P3	P4	P5	P6	*p*-value	
1	3	140	1	5	5	80	0.854	0.023
2	4	100	3	4	3	100	0.779	0.032
3	3	210	3	5	1	130	0.779	0.057
4	1	90	1	6	4	280	0.696	0.057
5	4	130	1	5	5	80	0.312	0.007
6	4	190	2	5	3	90	0.256	0.012
7	3	350	3	5	2	140	0.208	0.013
8	2	240	3	5	2	260	0.132	0.015
9	3	80	2	5	4	270	0.132	0.045
10	4	90	2	5	4	100	0.104	0.100
Default	2	250	2	2	3	200	0.000	0.215

* see Section 3.5.1

** Mean absolute error ration (MAER), see Section 2.2.2

Figure 5.7 shows the cumulative distributions of the observed travel times and two simulated travel times obtained using the statistically "valid" and "invalid" parameter sets, respectively. Both the valid and invalid parameter sets have the same travel time MAER but different *p*-values. The cumulative distribution function (CDF) for the statistically valid parameter set closely follows the CDF of the observed travel times. Overall, the differences in between the CDF's of the statistically valid parameter set and the observed data are negligible. In contrast, the CDF derived from the statistically invalid parameter set shows large deviations from the CDF of the observed data for a wide range of x values. The statistically based calibration objective function gave superior results to that of the non-statistically based approach in terms of matching the CDF of the observed data.

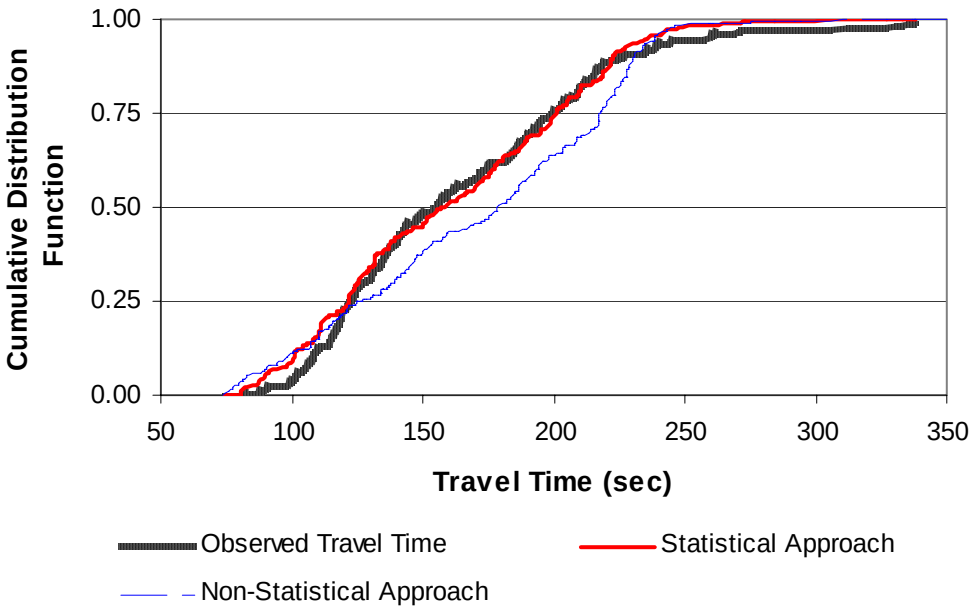

FIGURE 5.7 Cumulative Distribution of Simulated Travel Times for the Bellaire Arterial Test Network

The above result is more clearly supported in Figures 5.8 and 5.9 which show histograms of the two simulated travel times used for generating Figure 5.7. While both distributions have a travel time MAER of 0.01 (1 percent), it can be seen that the shapes of two distributions are considerably different.

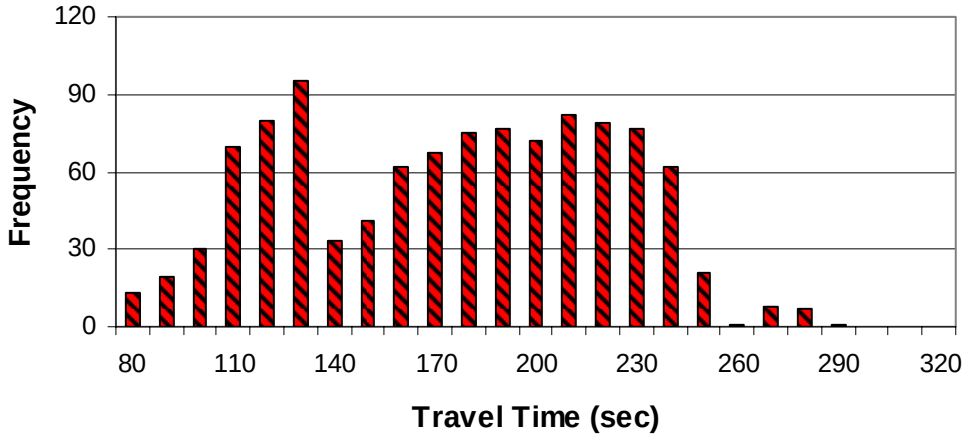

FIGURE 5.8 Histogram of Simulated Travel Time for the Bellaire Arterial Test Network (1% MAER – Rejected)

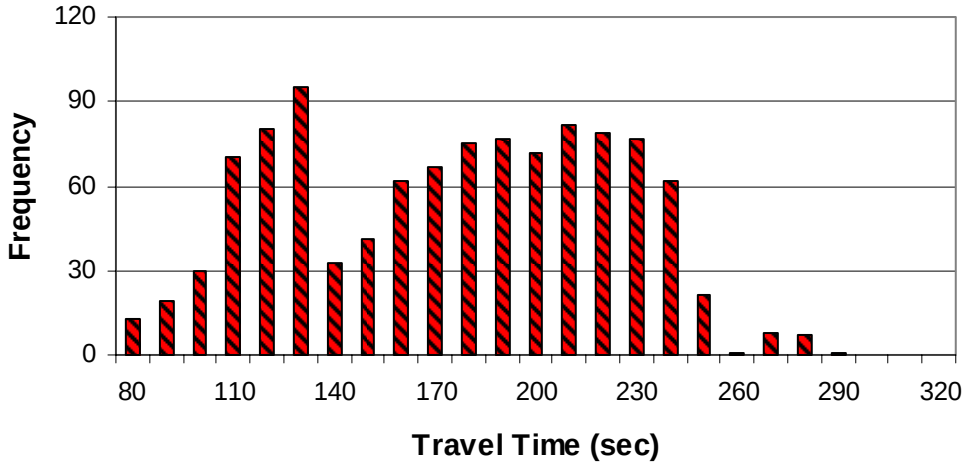

FIGURE 5.9 Histogram of Simulated Travel Time for the Bellaire Arterial Test Network (1% MAER - Accepted)

The travel time for the statistically valid parameter set has a bimodal distribution similar to the observed travel time shown in Section 5.1.2. This result supports the hypothesis of this dissertation that simply using travel time MAER as the sole metric for identifying the best parameter set could lead to erroneous calibration results – it is much better to consider the distribution of travel times when calibrating the microscopic traffic simulation model.

The travel time MAER is plotted in Figure 5.10 as a function of the corresponding *p*-value obtained from the KS test. The parameter sets that are circled (lower left corner) have relatively low MAER but fail to pass the KS test. The statistically based objective function proposed in this chapter performs in such a manner that all the parameter sets within the circle are never selected.

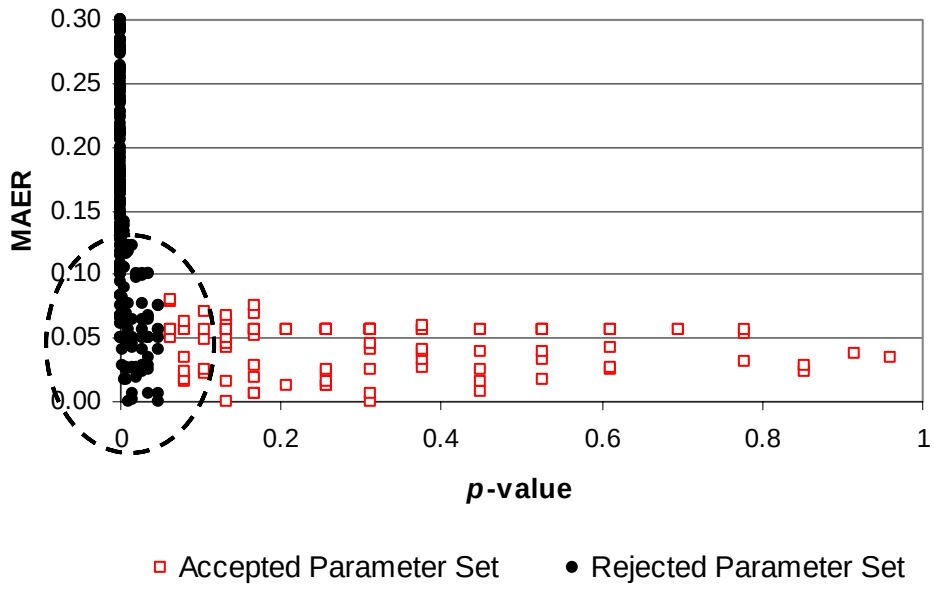

FIGURE 5.10 Relationship between MAER and *p*-value from KS Test on the Bellaire Arterial Test Network

5.3.2 Calibration Results for the I-10 Freeway Test Network

The travel time MAER and *p*-value are tabulated in Table 5.6 Also provided are the averages of the MAER and *p*-value for all three AVI links. The results show that there is no case where the distribution of the simulated travel time passes the KS test. The *p*-values for all three AVI links are, with the exception of a few cases, zero indicates that there is strong evidence against the null hypothesis.

The resulting travel time MAER varies for each AVI link. The minimum travel time MAER is 0.108 (10 percent) for AVI link 01, 0.031 (3 percent) for AVI link 12, and 0.307 (30 percent) for AVI link 23. It can be concluded that in terms of both travel time MAER and *p*-value, the calibration process does not provide comparable results. These results illustrate the necessity of calibrating other inputs to the microscopic traffic simulation as well as behavior parameters. The methodology for calibrating OD demand and behavior parameters will be discussed in detail in the next chapter.

TABLE 5.6 Travel Time MAER and *p*-value for All Three AVI Sections

No	MAER				*p*-value*			
	AVI 01	AVI 12	AVI 23	Ave.	AVI 01	AVI 12	AVI 23	Ave.
1	0.108	0.031	0.360	0.166	0.000	0.007	0.000	0.002
2	0.114	0.019	0.379	0.171	0.000	0.007	0.000	0.002
3	0.108	0.010	0.400	0.173	0.000	0.081	0.000	0.027
4	0.105	0.083	0.351	0.179	0.000	0.000	0.000	0.000
5	0.121	0.153	0.417	0.231	0.000	0.000	0.000	0.000
6	0.073	0.301	0.352	0.242	0.000	0.000	0.000	0.000
7	0.059	0.387	0.307	0.251	0.000	0.000	0.000	0.000
8	0.127	0.229	0.422	0.260	0.000	0.000	0.000	0.000
9	0.128	0.255	0.417	0.266	0.000	0.000	0.000	0.000
10	0.135	0.320	0.432	0.296	0.000	0.000	0.000	0.000

* *p*_value from the Kolmogorov-Smirnov test

In contrast to the results on the Bellaire arterial test network, the results indicate that it is more difficult to identify the parameter set which produces satisfactory results at every measurement point. To further investigate the risk of identifying the "best" parameter set based on aggregated performance measures, it is assumed in this section that the observed travel time only for AVI link 01 is available. Therefore, the calibration process target is to replicate the observed traffic conditions only for AVI link 01.

A subset of parameter sets identified in the calibration process is found in Table 5.7. Also shown is the *p*-value from the KS test as well as the travel time MAER. The calibration process successfully identifies a number of statistically "valid" parameter sets. Overall, most of the acceptable parameter sets have a very low travel time MAER, which is in the range from 0.000 (0.0 percent) to 0.011 (1 percent).

TABLE 5.7 Subset of Statistically Valid Parameter Sets for AVI Section 01

No	Calibrated Parameter*											K-S *p*-value	MAER
	P1	P2	P3	P4	P5	P6	P7	P8	P9	P10	P11		
1	-4.5	100	-3.9	350	1.6	0.95	2	-7	-0.15	0.15	13	0.761	0.000
2	-4.5	100	-3.5	350	1.6	0.95	2	-7	-0.15	0.15	13	0.656	0.000
3	-5.5	280	-4.7	430	1.6	0.90	5	-7	-0.40	0.40	13	0.449	0.010
4	-4.5	300	-3.5	410	1.3	0.90	3	-7	-0.35	0.35	14	0.144	0.005
5	-6.5	220	-5.9	270	1.3	0.90	3	-5	-0.40	0.40	8	0.283	0.004
6	-4.5	220	-3.5	370	1.6	0.95	3	-6	-0.15	0.15	13	0.249	0.004
7	-4.5	300	-4.1	410	1.1	0.95	3	-9	-0.35	0.35	9	0.166	0.005
8	-6.0	300	-5.4	270	1.3	0.95	4	-5	-0.20	0.20	11	0.106	0.009
9	-4.5	300	-4.1	410	1.2	0.95	3	-9	-0.35	0.35	9	0.077	0.016
10	-3.5	180	-3.3	270	1.6	0.85	2	-9	-0.25	0.30	10	0.055	0.011
D**	-4.0	200	-3.0	200	1.5	0.90	4	-8	-0.35	0.35	11	0.000	0.201

* see Section 3.5.2
** D: VISSIM default parameter

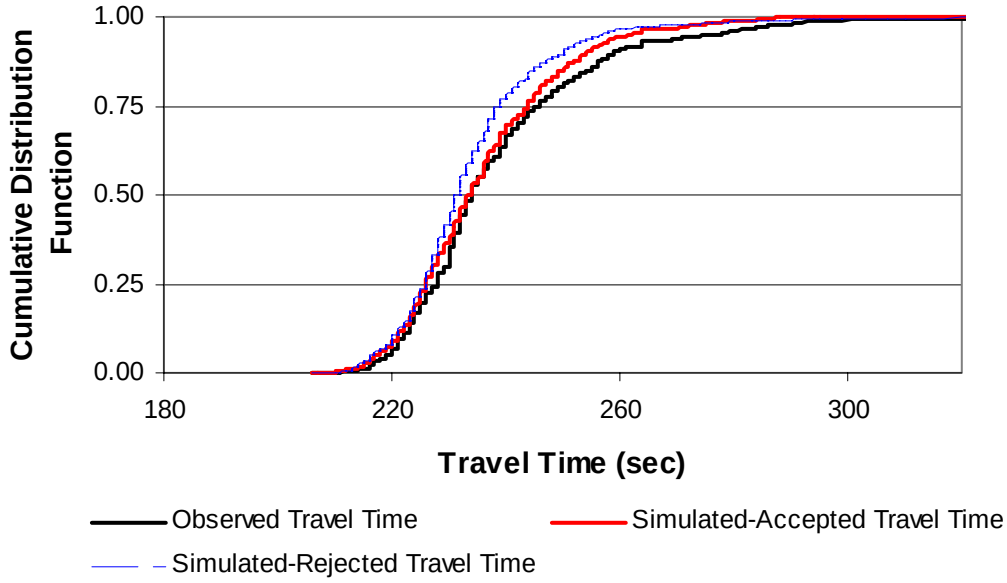

FIGURE 5.11 Cumulative Distribution of Simulated Travel Times for the I-10 Freeway Test Network

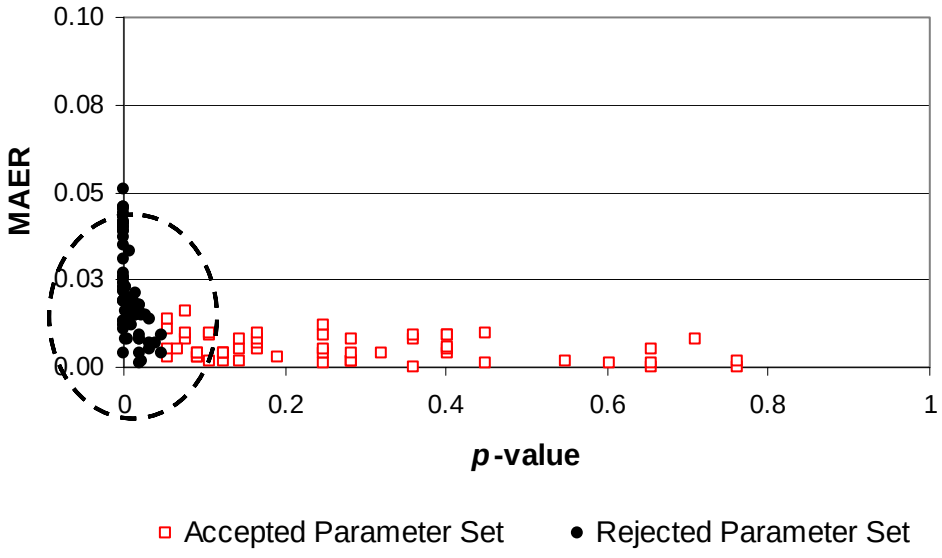

FIGURE 5.12 Relationship between MAER and *p*-value from KS Test for the I-10 Freeway Test Network

The cumulative distributions of two different travel time sets are plotted in Figure 5.11. While both distributions have a travel time MAER of 0.01 (1 percent), the accepted distribution has a *p*-value of 0.249 and the rejected distribution has a *p*-value of 0. It can be seen in Figure 5.11 that the accepted-simulated travel times slightly better trace the observed travel times in that there is a smaller maximum difference between the simulated and observed distributions. This is further supported in Figure 5.12 where the travel time MAER and corresponding *p*-value are plotted.

5.4 PARAMETER SET SELECTION

There may be numerous parameter sets, or none, that match the observed data because the calibration process is statistically based. When a fairly large number of acceptable or "statistically valid" parameter sets are identified, a selection technique for identifying the "best" parameter set among the valid solutions is required. In this section, alternative selection techniques are applied to "statistically valid" parameter sets on the Bellaire arterial test network.

5.4.1 Highest *p*-value and Lowest MAER

Intuitively, the parameter set with the lowest MAER might be selected because it would represent the parameter set that provides the closest measure of central tendency while still providing a statistically valid distribution. Alternatively, the parameter with the highest *p*-value could be selected as the one that most closely represents the observed distribution. Essentially, there is no statistical difference between parameter sets that pass the statistical test. However, descriptive expressions can be used to indicate the strength of the evidence. The parameters with different *p*-values can be interpreted using one of "no evidence", "weak evidence", or "strong evidence". Therefore, it seems reasonable to select parameters with the highest *p*-value as the one with the highest probability that the null hypothesis is true.

These selection techniques are applied to the same parameter sets as provided in Table 5.5. The shaded blocks denote the parameter sets with the highest *p*-value and lowest travel time MAER in Table 5.8.

TABLE 5.8 Parameter Set with Highest *p*-value or Lowest MAER for the Bellaire Arterial Test Network

No	Calibrated Parameter						KS Test	MAER
	P1	P2	P3	P4	P5	P6	*p*-value	
1	3	140	1	5	5	80	0.854	0.023
2	4	100	3	4	3	100	0.779	0.032
3	3	210	3	5	1	130	0.779	0.057
4	1	90	1	6	4	280	0.696	0.057
5	4	130	1	5	5	80	0.312	0.007
6	4	190	2	5	3	90	0.256	0.012
7	3	350	3	5	2	140	0.208	0.013
8	2	240	3	5	2	260	0.132	0.015
9	3	80	2	5	4	270	0.132	0.045
10	4	90	2	5	4	100	0.104	0.100
Default	2	250	2	2	3	200	0.000	0.215

5.4.2 Saturation Flow Rate

The saturation flow rate is one of key components for computing performance measures (LOS) at a signalized intersection. The Highway Capacity Manual (HCM) provides the methodology to adjust the saturation flow rate for a wide range of operational configurations, including geometric and traffic conditions. The saturation flow rate for the Bellaire arterial test network was computed according to Equation 5.8 and was identified as 1606 pc/hr/ln (88).

$$s = s_0 N f_w f_{HV} f_g f_p f_{bb} f_a f_{LU} f_{RT} f_{Lpb} f_{Rpb} \quad (5.8)$$

s = adjusted saturation flow rate (pc/hr/ln) ;

s_0 = base saturation flow rate (1900 pc/hr/ln) ;

N = number of lanes in lane group ; and

$f_{...}$ = adjustment factor for lane width, heavy vehicle, grade, parking activity, bus stop, area type, left turn, right turn, and pedestrian, respectively.

In VISSIM, the saturation flow rate cannot be specified externally by the user. Therefore, the user is responsible for obtaining a reliable saturation flow rate by selecting parameter sets based on site-specific conditions. For comparison with the saturation flow rate from HCM, the saturation flow rates for the "statistically valid" parameter sets were estimated using the VISSIM output. Besides the identified parameters, there are many parameters that affect the saturation flow rate in VISSIM such as the number of lanes, traffic composition, etc. The following parameter settings were used to estimate the saturation flow rate from the VISSIM model (11):

- Traffic volumes were set large enough to as many vehicles as possible discharge during green time.
- Saturation flow rate was measured for through-traffic at the stop line on two lanes over 60 minutes.
- Fixed time signal control was selected. Operating parameters associated with fixed time signal control was assumed (90 seconds cycle, 40 seconds green, 3 seconds amber, 2 seconds all red).
- Driver's desired speed was assumed to be on the range from 57 km/h (35 mph) to 68 km/h (42mph).
- Traffic composition was assumed to consist of only passenger cars.

The saturation flow rates obtained from the VISSIM results are provided in Table 5.9. The last column lists the saturation flow rates for the same parameter sets as provided in Table 5.5, where the shaded block denotes the parameter sets with the least difference from the saturation flow rate from HCM. If driver behavior parameters are appropriately calibrated, the estimated saturation flow rates for the statistically valid parameter sets may be close to that obtained from the HCM. As shown in Figure 5.13, the estimated saturation flow rates scatter around the line representing the base value of 1606 pc/hr/ln from the HCM.

TABLE 5.9 Saturation Flow Rate for Statistically Valid Parameter Sets for the Bellaire Arterial Test Network

No	Calibrated Parameter						KS Test	MAER	Saturation
	P1	P2	P3	P4	P5	P6	p-value		Flow Rate
1	3	140	1	5	5	80	0.854	0.023	1564
2	4	100	3	4	3	100	0.779	0.032	1717
3	3	210	3	5	1	130	0.779	0.057	1580
4	1	90	1	6	4	280	0.696	0.057	1616
5	4	130	1	5	5	80	0.312	0.007	1681
6	4	190	2	5	3	90	0.256	0.012	1634
7	3	350	3	5	2	140	0.208	0.013	1654
8	2	240	3	5	2	260	0.132	0.015	1650
9	3	80	2	5	4	270	0.132	0.045	1566
10	4	90	2	5	4	100	0.104	0.100	1579
D*	2	250	2	2	3	200	0.000	0.215	2180

* D: VISSIM default parameter

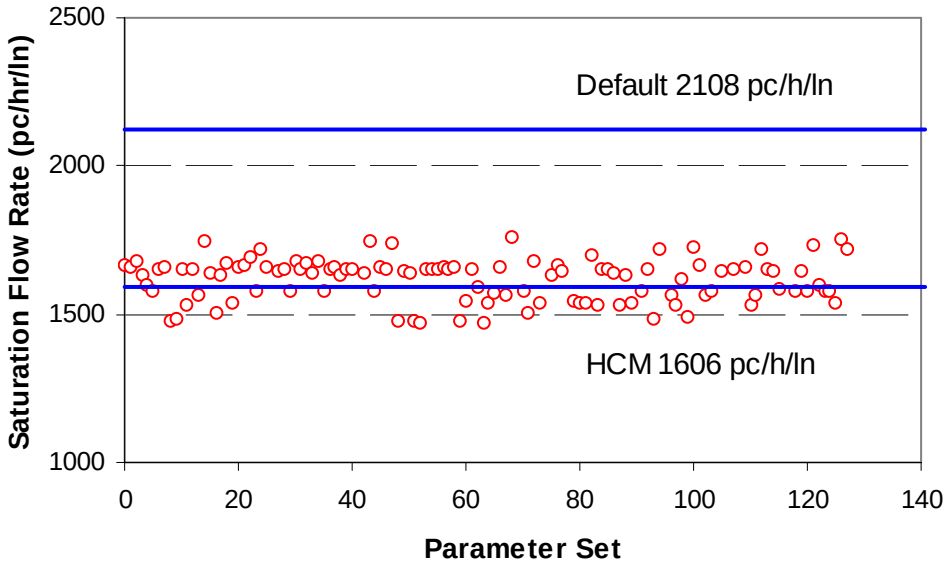

FIGURE 5.13 Saturation Flow Rate for Statistically Valid Parameter Sets for the Bellaire Arterial Test Network

In addition to the identification of the parameter set with the least difference, the estimated saturation flow rates were used to further validate the one sample *t*-test was conducted. Basically this test checks whether the mean of the estimated saturation flow rates is statistically different from the base value of 1606 pc/hr/ln. The null hypothesis and the alternative hypothesis are shown in Equations 5.9 and 5.10, respectively. The test statistic utilized for this analysis is provided in Equation 5.11.

$$H_0 \quad : \quad \mu = 1606 \tag{5.9}$$

$$H_1 \quad : \quad \mu \neq 1606 \tag{5.10}$$

$$t \quad = \quad \frac{\bar{x} - 1606}{s/\sqrt{n}} \tag{5.11}$$

The results of this analysis are summarized in Table 5.10. The test results show that the mean difference is not significant, indicating that there is no evidence against the null hypothesis H_0. This is a further indication that the calibrated parameter sets were selected appropriately. It is also important to note that on the Bellaire arterial test network the default parameter set results in a saturation flow rate of 2180 pc/hr/ln which is approximately 36.2 percent higher than recommended by the HCM.

TABLE 5.10 *t*-test Results of Equality of Saturation Flow Rates

Test Value (1606)	Average	Standard Deviation	Significance	95 % Confidence Interval	
				Lower	Upper
	1617	71	0.089	1604	1629

5.4.3 Least Difference from Default Parameters

According to PTV America, "continuous measurements of different traffic conditions on highways and urban streets are required to model the traffic in a realistic way, which is done at the University of Karlsruhe" (89). PTV America also indicates that they have collected the field data to calibrate/validate parameters in many VISSIM models. Therefore, if updated on the continuous basis, the default parameters can be considered as representative of the current acceptable driving behavior characteristics. Therefore, it is a reasonable selection criterion to select the parameter set, from the set of statistically valid parameters, which is "closest" to the default parameter set. This is because the calibration process potentially identifies the parameter set that are not within acceptable range because it solely aims to replicate the observed conditions. For example, one parameter set might model drivers as exceeding the speed limit. While it might give appropriate results if it is known drivers do not do this then another parameter set with similar statistics might be preferred.

The differences for each of the parameters are aggregated into a composite index. However, some errors may be in place because the scale and sign for the difference are different. To resolve this problem, the absolute value of the difference is first computed and then this value is normalized such that the normalized scale ranges from zero to one. Thereafter, the composite index is computed as the weighted sum of normalized absolute difference, as shown in Equation 5.12. The weights can be determined by the analyst through simple ranking approach or sensitivity analysis on effect of each parameter on the simulation results.

$$I_c = \frac{1}{n}\sum_{i=1}^{n}\alpha_i \frac{\left|P_{default,i} - P_i\right|}{Pd_{i,\max}} \qquad (5.12)$$

I_c = composite index ;

n = number of parameters ;

α_i = weight of i^{th} parameter ;

$P_{default,i}$ = default value of i^{th} parameter ;

P_i = calibrated value of i^{th} parameter ; and

$Pd_{i,\max}$ = maximum difference between i^{th} calibrated and default parameters.

The resulting composite indices are provided in Table 5.11, where the weights for each of the parameters are assumed to be equal. A smaller value of the composite index indicates the parameter set is closer to the default parameter set. Case eight is the best, followed by case six and then case nine. In general, higher composite indices are observed for the parameter set with larger difference in the parameters P_2 (Look ahead distance) and P_6 (Lane change distance).

TABLE 5.11 Statistically Valid Parameter Set with the Least Difference from Default Parameter Set for the Bellaire Arterial Test Network

No	Calibrated Parameter						Composite Index
	P1	P2	P3	P4	P5	P6	
1	3	140	1	5	5	80	0.82
2	4	100	3	4	3	100	0.70
3	3	210	3	5	1	130	0.68
4	1	90	1	6	4	280	0.77
5	4	130	1	5	5	80	0.91
6	4	190	2	5	3	90	0.50
7	3	350	3	5	2	140	0.64
8	2	240	3	5	2	260	0.47
9	3	80	2	5	4	270	0.56
10	4	90	2	5	4	100	0.67
D*	2	250	2	2	3	200	0.00

D*: VISSIM default parameter

5.5 CONCLUDING REMARKS

There are numerous advantages of the proposed non-parametric calibration approach. First, it provides a statistically based approach that goes beyond simply identifying a parameter set that is closest to one simple metric. Simple metrics such as MAER are not robust enough to identify parameter sets that mimic the actual travel time distribution. Second, there is the capacity for additional analysis for the candidate parameter sets. Therefore, the analyst can bring their own knowledge to identifying the most appropriate of the candidate parameter sets. The highest *p*-value or lowest MAER, saturation flow rate, and least difference from default parameters can be used as a secondary objective. In addition, while not done in this dissertation it would be a relatively easy extension to incorporate the decision making into the automatic calibration procedure.

For the Bellaire arterial test network, the proposed calibration procedure was successful in exploring the travel time distributions that are a bimodal mixture of two distributions produced due to the effects of signal progression. The travel time MAER was improved for all the accepted parameter sets as compared to the default values. In contrast, the proposed calibration procedure did not provide a similar travel time distribution to the observed travel time distribution for the I-10 freeway test network. That is while aggregate values such as the MAER were acceptable, the distribution of travel times could not be replicated. It was hypothesized that this occurred because the estimated demand, as defined by the OD matrix, was not correct. A methodology for calibrating the microscopic traffic simulation model and estimating the OD matrix simultaneously will be examined in Chapter VI.

CHAPTER VI

SIMULTANEOUS CALIBRATION OF A TRAFFIC SIMULATION MODEL AND OD MATRIX

In Chapter V, a methodology that uses a statistically based objective function for calibrating the microscopic traffic simulation model was presented. However, the results from the application of this methodology in the I-10 freeway test network showed that under certain situations the approach can not identify an appropriate parameter set that can replicate the distribution of the observed travel time data. It was hypothesized that this occurred because the OD estimate was not valid. Therefore, in this chapter, the methodology is further refined to addresses this issue.

The conventional research on the calibration of microscopic traffic simulation model has focused on the parameters associated with car-following and lane-changing behaviors and their impacts on overall calibration performance. Generally, this research has regarded the OD matrix as a fixed input which remains unchanged during the calibration process. Consequently, the OD estimation has been considered as a preliminary step rather than as a stage that can be included in the calibration process.

Although there is an extensive body of literature on the calibration of microscopic traffic simulation models, there is little information in the literature on how the OD estimation can be included in the calibration process. Recent studies suggested that more precise calibration results can be achieved when the OD matrix is considered as a parameter being calibrated. For example, Kim (27) revealed that the OD matrix has a profound impact on the simulation results and, further, the OD matrix can be calibrated as part of the process. However, Kim's study has limited its application only to the CORSIM model based on a simple gravity model. The study was designed to illustrate the problem rather than provide a viable solution. Consequently, the methodology used in Kim's study is not readily transferable to other simulation models. Another example of the methodology that jointly calibrates a simulation model and the OD matrix can be

found in the study of Darda et al. (39, 40). In their work, the steady-state travel time obtained from the simulation model was used in order to generate the assignment matrix that is a crucial element in the OD estimation, especially on the network with multiple routes. Because a rich set of the observed travel time data was absent, Darda et al. used the stimulated travel time as the alternative. Therefore, their methodology mainly focused on building a time-dependent assignment matrix rather than enhancing the OD estimator in a direct way. Moreover, in order to simulate the travel time, Darda et al. used a seed OD matrix estimated at planning level and coarsely estimated parameters related to behavior and route choice, as the initial values. The use of initial values in their study may raise some concerns on whether the simulation model yields reasonable travel time estimates on the network with a high level of congestion since simulation outputs vary considerably with congestions.

In this chapter, a methodology in which the OD matrix and driver behavior parameters are calibrated simultaneously is developed and presented using a bi-level approach. To formulate the relationship between travel time data and the OD matrix, the observed travel times are incorporated into a Kalman filter OD estimator. This methodology provides a mean to model interdependent relationships between driver behavior parameters, OD matrix, and simulation results (travel time).

In subsection 6.1, the estimation of the initial OD matrix based on AVI data is described. In subsection 6.2, a description of the proposed methodology is provided. Also, the assumptions and issues related to the proposed methodology are discussed. Finally, the concluding remarks for Chapter VI are presented in subsection 6.3.

6.1 ESTIMATING AN INITIAL OD MATRIX

In this section, the methodology employed to estimate the initial OD matrix is presented. The main framework for the methodology is adapted from the research performed by Dixon (1). Based on various information extracted from AVI data, the OD estimator is formulated.

The use of AVI data helps to resolve the difficulties inherent to the OD estimators based on the observed link volumes. First, AVI data provides relatively accurate information on a trip progression. To obtain a reliable link choice proportion, the information on the trip progression on a link by link basis is very critical. In addition, it is more important on a long freeway corridor where the route travel time is relatively longer than the OD estimation time-increment. Therefore, by using AVI data, it is possible to estimate accurate link choice proportions based on direct observation without relying on any assumptions to approximate trip progression. Second, AVI data can be used as a good source of historical information. Consequently, the reliable inputs to the Kalman filter, such as historical OD matrix, initial OD variance covariance matrix, and measurement error variance covariance matrix, can be obtained because these kinds of inputs are based on the information sampled from AVI data.

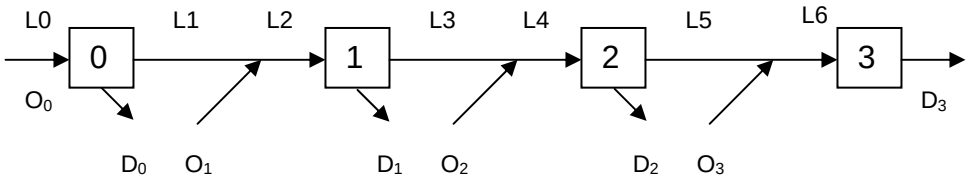

AVI Station	0	~	3
Origin	O0	~	O3
Destination	D0	~	D3
Link	L0	~	L6

FIGURE 6.1 I-10 Freeway AVI System

The I-10 AVI system used to formulate OD estimator for the initial OD matrix is shown in Figure 6.1. The system is comprised of 4 AVI stations and 7 AVI links. Since AVI stations function as origins and destinations there are 10 AVI OD pairs in total. In this model, the last AVI link $L6$ and OD pair from 3 to 3 are excluded from the analysis because all vehicles departing from origin 3 are, by definition, traveling to AVI station 3.

6.1.1 Mathematical Model

The constrained Kalman filter is adopted because 1) it has been widely used for OD estimation; 2) additional measurement data can also be integrated into the estimation framework through augmentation techniques; and 3) its discrete stochastic linear structure is suitable for estimating time-dependant OD patterns (90, 91). In this dissertation, the OD split proportions, instead of OD flows, are used because OD split proportions can be sampled directly from AVI data. The definitions of the variables used in formulating the Kalman filter OD estimator are shown as follows.

$b(t)$ = column vector whose elements are $b_{ij}(t)$, OD split proportions entering the network from origin *i* to destination *j* during interval *t* ;

$v(t)$ = column vector whose elements are $v_l(t)$, number of link traffic volumes passing link *l* during time interval *t* ;

$O(t)$ = diagonal matrix whose elements are $o_i(t)$, number of vehicles entering the network from origin *i* during interval *t* ;

$L^d(t)$ = link choice proportion matrix whose elements are $L_{ij}^{ld}(t)$, the fraction of vehicles that enter network during interval *d* from origin *i* to destination *j* and use link *l* during time interval *t* ;

$H_v(t)$ = linear link volume connection matrix which is the product of $L^t(t)O(t)$;

$R_v(t)$ = diagonal variance covariance matrix whose elements are measurement noise of link volume during time interval *t* ;

$Q(t)$ = diagonal variance covariance matrix whose elements are transition noise during time interval t ;

$P(t)$ = error variance covariance matrix whose elements are $E[\varepsilon_{bij}\varepsilon_{bij}^{T}]$; and

$K_v(t)$ = Kalman gain matrix for link volume measurements for time interval *t.*

By definition the observed link volumes contain information on the OD split proportions. Equation 6.1 shows that the observed link volumes $v(t)$ can be related to the OD split proportions $b(t)$ through a link choice proportion matrix $L^d(t)$. In addition, the formulation assumes that the link volumes at time interval *t* are not a function of the OD split proportions at time interval *t*. The flows departing at time interval *t-1, …, t-M* may have an influence on the link volumes at time interval *t*.

$$v_t = v(t) = \sum_{k=t-M}^{t} L^k(t)\, O(k)\, b(k) + \varepsilon_v(t) \qquad (6.1)$$

M = maximum number of time intervals required for vehicles to travel from origin i to link l ; and

$\varepsilon_v(t)$ = error matrix of link volumes $v(t)$.

The Kalman filter model used in Dixon's study is shown in Equations 6.2 through 6.6. This model can be used to estimate the initial OD split proportions based on the link volumes. Note that in this dissertation the link volumes used are the AVI link volumes. To model an autoregressive process which captures temporal dependency between the OD estimates, it is assumed that the OD split proportions $b(t-1)$ at time interval *t-1* are the best estimates for the OD split proportions $b(t)$ at time interval *t*.

Through analyzing the link choice proportion matrices $L^d(t)$ for the I-10 freeway test network, it was found that the travel times for most vehicles did not exceed the OD estimation time-increment (thirty minutes). Therefore, as can be seen in Equations 6.1

and 6.5, the maximum number of time intervals *M* to be considered is set to 1. In other words, fractions of vehicles departing at time interval *t-1* pass the link *l* at time interval *t.* It should be also noted that the observed OD split proportions $b^{obs}(t-1)$ is used in Equation 6.5. The substitution of the observed OD split proportions instead of the estimated OD split proportions increases the accuracy of OD estimation process.

$$b^{-}(t) = b(t-1) + \varepsilon(t) \quad (6.2)$$

$$P^{-}(t) = P(t-1) + Q(t) \quad (6.3)$$

$$K_v(t) = P^{-}(t)H_v(t)\left(H_v(t)^T P^{-}(t)H_v(t) + R_v(t)\right)^{-1} \quad (6.4)$$

$$b(t) = b^{-}(t) + K_v(t)\left(v(t) - H_v(t)b^{-}(t) - H_v(t-1)b^{obs}(t-1)\right) \quad (6.5)$$

$$P(t) = \left(I - K_v(t)H_v(t)\right)P^{-}(t) \quad (6.6)$$

6.1.2 Treatment of Constraints

In order to ensure that the OD estimates obtained from Equations 6.2 through 6.6 satisfy implicit transportation system operating conditions, two constraints (e.g. non-negativity and equality constraints) are used in the Kalman filter OD estimator. Several researchers have pointed out the need to enforce the non-negativity and equality constraints. Bell et al. enforced the non-negativity constraint using the Lagrange multiplier (92). Van der Zijpp also modeled the equality constraint as a perfect observation (93). These approaches require relatively complicated computations such as a matrix inversion or the identification of a convergent Lagrange multiplier. Alternatively, Nihan et al. proposed an alternative approach, the truncation and normalization process to enforce these constraints (94). This approach is selected in this dissertation because it is simple and easy to be written into the program designed to handle the Kalman filter algorithm.

Non-negativity constraints ensure that the estimated OD split proportions are non-negative. In the Kalman filter formulation, the non-negativity constraint is achieved

by adding the correction matrix *r(t)* into the measurement equation, as shown in Equations 6.7 through 6.9. Note that "super minus" sign is used to denote the estimates for the OD split proportions at time interval *t* given knowledge of the process prior to time interval *t*.

$$b_{ij}(t) \geq 0 \tag{6.7}$$

$$r_i(t) = \min_{ci<0}\left(\frac{b^{-}_{ij}(t)}{-c_i(t)}\right) \tag{6.8}$$

$$b(t) = b^{-}(t) + r(t)K(t)\left(v(t) - H_v(t)b^{-}(t) - H_v(t)b^{obs}(t-1)\right) \tag{6.9}$$

Given that the link volume measurements at time interval *t* have been obtained, the correction amount is determined as the product of the Kalman gain matrix and the difference between the observed and estimated link volumes. Therefore, if $b^{-}(t)$ is equal to or greater than zero, adding the correction matrix could prevent the estimated OD split proportions $b(t)$ at time interval *t* from violating the non-negativity constraint. Let $C(t)$ be the second right hand component of Equation 6.5 and $c_i(t)$ be the *i*th element of $C(t)$. If the correction matrix $r(t)$ is computed such that Equation 6.8 is satisfied, the estimated OD split proportions are guaranteed to meet the non-negativity constraint. As a result, the correction matrix is added in front of the Kalman gain matrix, as shown in Equation 6.9.

Equality constraints ensure that the total number of vehicles entering the system is equal to the total number of exiting vehicles. The application of the equality constraint is simpler than that of the non-negativity. The enforcement of this constraint involves the step of normalizing the OD split proportions from origin *i* to all destinations, as shown in Equation 6.11.

$$\sum_j b_{ij}(t) = 1 \tag{6.10}$$

$$b_{ij} = \frac{b_{ij}}{\sum_j b_{ij}} \tag{6.11}$$

If the non-negativity constraint is not applied first, the OD split proportions with negative values may result which is problematic. Therefore, the non-negativity constraint is applied first and then the equality constraint is applied.

6.1.3 Error Variance Covariance Matrix

The Kalman filter OD estimator, as defined in this dissertation, requires prior knowledge of several inputs including the variance covariance matrix of the initial OD split proportions, the measurement error variance covariance matrix, and the transition error variance covariance matrix. However, these are theoretically unknown unless we have perfect information on the system being modeled. Therefore, these matrices were generated based on empirical observations.

In this dissertation, reliable estimates could be derived from AVI data, while OD estimators based on only the observed link volumes often assume default matrix as a starting point. For example, if the first time interval is from 5:00 AM to 5:30 AM, the OD split proportions obtained from the AVI data between 4:30 AM and 5:00 AM can be used as the best estimates of the OD split proportions $b(0)$ for the first time interval. In the same manner, the $P(0)$ is computed based on the historical data regarding the OD split proportions for time interval 4:30 AM~5:00 AM.

As shown in Equations 6.12 through 6.15, the transition error variance covariance matrix $Q(t)$ and measurement error variance covariance matrix $R_v(t)$ are also computed based on the historical variance covariance matrices. Note that it is assumed that the $Q(t)$ and $R_v(t)$ possess diagonal elements only. This means that this

simplification allows the estimation of these matrices from the historical variance covariance matrices.

$$\varepsilon_b(t) = b(t+1) - b(t) \quad (6.12)$$

$$Q(t) = E(\varepsilon_b \ \varepsilon_b^T) \quad (6.13)$$

$$\varepsilon_v(t) = v(t) - \sum_{k=t-M}^{t} H_v(t)\, b(k) \quad (6.14)$$

$$R(t) = E(\varepsilon_v \ \varepsilon_v^T) \quad (6.15)$$

$\varepsilon_b(t), \varepsilon_v(t)$ = state (OD) and measurement (link volume) noises, respectively ; and

$b(k)$ = OD split proportions during interval *k*.

6.2 INCORPORATING TRAVEL TIME INFORMATION INTO OD ESTIMATOR

As was shown in Chapter V, the calibration of only the driver behavior parameters did not yield satisfactory results for the I-10 freeway test network. In this section, the initial OD matrix, which is assumed to be true in Phase 1, is considered as an additional parameter that can be calibrated.

In order to calibrate the OD matrix, the observed travel time information is used as an additional measurement. Basically, the method explicitly considers how changes in the OD split proportions are reflected in the simulated travel times. It is hypothesized that the inclusion of travel time information into the OD estimator allows the simulation model to better replicate the observed conditions. This would be particularly true for highly dynamic networks where changes in traffic patterns would not be immediately identified using traffic detectors (72).

6.2.1 Mathematical Model

To incorporate travel times information into the Kalman filter OD estimator the relationship between the OD split proportions and travel times needs to be identified first. However, this relationship is very complicated and it would be difficult to write a closed form solution. Therefore, in this dissertation, this relationship is captured from the simulation results and incorporated into the OD estimator using the Extended Kalman filter (EKF) approach. Basically the EKF is designed to approximate the true solution using a linearization approach (4, 5, 6). The definitions of the additional variables used in formulating the EKF are shown as follows.

$TT(t)$ = column vector whose elements are, $tt_i(t)$, travel time obtained from AVI data during interval t ;

$H_{TT}(t)$ = travel time connection matrix ; and

$K_{TT}(t)$ = Kalman gain matrix for travel time measurements for time interval t.

The mathematical model of the EKF is similar to that of the KF model. The difference between these two models is that the travel time information is incorporated into the measurement equation through an augmentation technique. The measurement equation of the EKF defines the relationships between OD split proportions and travel times as well as between OD split proportions and link volumes. Similar to the measurement equation of link volumes, the travel times at time interval t are assumed to be a function of the OD split proportions at time interval t and t-1. In other words, the travel times at current time interval are influenced by the vehicles departing at both previous and current time intervals. If a freeway is long or congested, this assumption becomes reasonable. Therefore, Equations 6.1 and 6.5 are rewritten as Equations 6.16 and 6.17, respectively.

$$\begin{bmatrix} v(t) \\ TT(t) \end{bmatrix} = \begin{bmatrix} H_v(t) \\ H_{TT}(t) \end{bmatrix} b(t) + \begin{bmatrix} H_v(t-1) \\ H_{TT}(t-1) \end{bmatrix} b(t-1) + \begin{bmatrix} \varepsilon_v(t) \\ \varepsilon_{TT}(t) \end{bmatrix} \quad (6.16)$$

$$b(t) = b^{-}(t) + K(t)\left(\begin{bmatrix} v(t) \\ TT(t) \end{bmatrix} - \begin{bmatrix} H_v(t) \\ H_{TT}(t) \end{bmatrix} b^{-}(t) - \begin{bmatrix} H_v(t-1) \\ H_{TT}(t-1) \end{bmatrix} b^{obs}(t-1) \right) \quad (6.17)$$

Unlike other detection techniques (e.g. inductive loop detector) that provide only estimates of link travel times, travel times for OD pairs as well as link travel times can be sampled from AVI data. In this dissertation, in order to evaluate the effects of including two different types of travel time information on the calibration precision, two OD estimators are proposed and these are shown in Figure 6.2. The first EKF, denoted as EKF_LTT, incorporates the travel times between AVI stations into the measurement equation. The second EKF, denoted as EKF_ODTT, uses the travel time between each OD pair. As shown in Figure 6-1, there are 4 AVI stations in the I-10 freeway test network. Therefore, there are three travel time measurements for the EKF_LTT and six travel time measurements for the EKF_ODTT.

$$\text{TT(t)} = \begin{bmatrix} \text{TT (AVI 0~1)} \\ \text{TT (AVI 1~2)} \\ \text{TT (AVI 2~3)} \end{bmatrix} \qquad \text{TT(t)} = \begin{bmatrix} \text{TT (OD 0~1)} \\ \text{TT (OD 0~2)} \\ \text{TT (OD 0~3)} \\ \text{TT (OD 1~2)} \\ \text{TT (OD 1~3)} \\ \text{TT (OD 2~3)} \end{bmatrix}$$

EKF_LTT EKF_ODTT

FIGURE 6.2 Observed Travel Time Matrices (EKF_LTT and EKF_ODTT)

6.2.2 Criteria for Evaluating Average Travel Time

The Extended Kalman filter approach is, by definition, recursive in nature. As new measurements are obtained, the EKF "corrects" the estimates projected from the previous time interval. In this dissertation, the new measurements correspond to the average travel times between AVI stations and OD pairs. In other words, the disaggregate characteristics of travel times can not be taken into account in the Kalman filter OD estimator.

The average travel time can be easily obtained from the VISSIM output file by simply defining the travel time sections corresponding to the AVI stations. In Phase 1, the disaggregate travel times are used to compare the observed and simulated distribution. If there is no parameter set that produces statistically valid simulation results, the calibration process continues in Phase 2, where the average travel times are incorporated into the Kalman filter measurement equation to calibrate the OD split proportions. It is important to note that the simulated average travel times vary significantly depending on the driver behavior parameters identified in Phase 1. Therefore, appropriate criteria for selecting driver behavior parameters in Phase 1 should be carefully decided. The selected driver behavior parameters are used as a base case in Phase 2 in order to obtain the simulated average travel times as well as their partial derivatives with respect to the OD split proportions as outlined in the next subsection.

A list of the AVI sections and OD pairs is provided in Table 6.1 that influence the average travel times if their OD split proportions are changed. For example, all vehicles departing from AVI station 0 pass through AVI section 01 to reach their destinations. The only exception is the OD flow from AVI station 0 to AVI station 0. Therefore, the number of vehicles on AVI section 01 may not change noticeably even though the OD split proportions for those with AVI station 0 as their origin are changed. As a result, the average travel time for AVI sections 01 may not change appreciably even though the split proportions are changed.

TABLE 6.1 OD Pairs Excluded along Network by AVI Section

AVI Section	AVI Station		OD Pairs
	From	To	
AVI 01	0	1	● AVI Station 0 → 0
AVI 12	1	2	● AVI Station 0 → 0, AVI Station 0 → 1 ● AVI Station 1 → Station 1
AVI 23	2	3	● AVI Station 0 → 0, AVI Station 0 → 1, AVI Station 0 → 2 ● AVI Station 1 → 1, AVI Station 1 → 2 ● AVI Station 2 → 2

Intuitively, for links which are located downstream of the first AVI station, the number of OD pairs that may influence the average link travel time increases. In the I-10 freeway test network, the travel time for AVI section 01 is probably the least susceptible to change. Therefore, higher confidence should be placed on the observed travel time for AVI section 01. To model this concept a weight term α_i is introduced into the MAER formula, as shown in Equation 6.18.

$$MAER_{ATT} = \frac{1}{N}\sum_{i=1}^{N}\alpha_i MAER_i = \frac{1}{N}\sum_{i=1}^{N}\alpha_i \frac{\left|TT_i^O - TT_i^S\right|}{TT_i^O} \quad (6.18)$$

N = number of AVI sections ;

TT_i^O = observed average travel time on AVI section i ;

TT_i^S = simulated average travel time on AVI section i ; and

α_i = weight given to AVI section i.

6.2.3 Travel Time Connection Matrix

There are two "roles" of the travel time connection matrix in the Kalman filter. First, according to the Equation 6.17, it is used to estimate the average travel times for the AVI sections with the estimated OD split proportions. Second, it is also used to derive the partial derivative matrix that is used to compute the Kalman gain matrix $K_{TT}(t)$.

By definition, a partial derivative represents the slope in a particular direction. In the Kalman filter OD estimator, the partial derivative signifies the slope in the solution space of possible OD split proportions. However, because it is difficult to describe the travel time connection matrix in the form of analytical functions, a derivative matrix cannot be obtained by differentiating the travel time connection matrix. Therefore, in this dissertation, a derivative matrix is estimated from the simulation outputs. Because this information is not available directly from the VISSIM output, the following procedure is employed to estimate the derivative matrix.

- Step 1: Select as a base case the simulation output that gives the smallest $MAER_{ATT}$ in Phase 1.
- Step 2: Determine the change Δ in OD split proportion.
- Step 3: Increase OD split proportion by Δ and run the VISSIM with the increased OD split proportion.
- Step 4: Compute the differences in the average travel times between the base case and new simulation output.
- Step 5: Compute the rate of change by dividing the differences by Δ.
- Step 6: Repeat Step 3 to Step 5 for each OD pair and time intervals to be considered.

To obtain reliable results from the above procedure, the amount of change in the OD split proportion allowed during the iteration should be controlled. From a practical perspective, too small an amount may not yield reasonable partial derivatives of travel

times when applied to microscopic traffic simulation models. This occurs because travel times are stochastic in nature and their outputs depend on the random numbers assigned to behavior characteristics. For example, if it was decided that a link travel time was too low the natural solution would be to assign more traffic to that link. However, if only a few vehicles were added to this link, this might not yield the desired effect because of the stochastic nature of the microscopic traffic simulation model. This would be particularly true on networks with nearly free-flow traffic conditions because the link travel time is insensitive to the increase of volumes. Therefore, the estimate of the change in the OD split proportion should be small enough to give an accurate slope for given OD split proportions and large enough to control this stochasticity issue. In this dissertation, the sensitivity analysis was carried out using values of 0.02, 0.03, 0.05 and 0.07 and a value of 0.05 was identified as the optimal amount.

Figure 6.3 shows the structure of the derivative matrix for the EKF_LTT. This 18×3 dimensional matrix contains the partial derivative of the travel time with respect to the OD split proportions. In the case of the EKF_ODTT, the dimension is changed to 18×6 because there are six travel time measurements.

$$G(t) = \left[\begin{array}{ccc|ccc} \frac{\partial TT_1(t)}{\partial OD_0(t)} & \cdots & \frac{\partial TT_1(t)}{\partial OD_8(t)} & \frac{\partial TT_1(t)}{\partial OD_0(t-1)} & \cdots & \frac{\partial TT_1(t)}{\partial OD_8(t-1)} \\ \frac{\partial TT_2(t)}{\partial OD_0(t)} & \cdots & \frac{\partial TT_2(t)}{\partial OD_8(t)} & \frac{\partial TT_2(t)}{\partial OD_0(t-1)} & \cdots & \frac{\partial TT_2(t)}{\partial OD_8(t-1)} \\ \frac{\partial TT_3(t)}{\partial OD_0(t)} & \cdots & \frac{\partial TT_3(t)}{\partial OD_8(t)} & \frac{\partial TT_3(t)}{\partial OD_0(t-1)} & \cdots & \frac{\partial TT_3(t)}{\partial OD_8(t-1)} \end{array}\right]$$

FIGURE 6.3 Derivative Matrix of Travel Time Connection Matrix

Because one simulation run constitutes one column vector, the number of the observed travel times in the measurement equation has no influence on the computational time. The number of simulation runs required increases with the number of OD pairs and the number of time intervals to be considered. Consequently, this approach can be a burden on the network with a large number of OD pairs and time intervals to be considered. In this case, however, it makes the proposed approach more feasible to simplify a network by grouping the set of origins and destinations to correspond to the AVI stations in the system.

6.3 CONCLUDING REMARKS

This section outlined methodologies for calibrating the OD matrix as well as estimating the initial OD matrix based on the information derived from AVI data. The estimation of the initial OD matrix was formulated using the constrained Kalman filter (KF) model based on AVI link volumes. The error variance covariance matrices are assumed to be known *a priori* in the Kalman filer model. However, these matrices are not readily available and then were estimated from the AVI historical dataset.

In general, the relationship between the OD matrix and travel time data can not be written in a deterministic form because it may vary both spatially and temporally. Therefore, the Extended Kalman filter (EKF) model, which can handle nonlinear state dynamics and nonlinear measurement equations, was selected to relate the estimation of the OD matrix to travel time measurements. In the formulation, the travel time data were incorporated into the measurement equation using an augmentation technique. Therefore, these travel time data were used to calibrate the OD matrix with the AVI link volumes. It was hypothesized in this section that the inclusion of travel time data in the calibration of the OD matrix results in the improved calibration precision. In this section two OD estimators were proposed, one of which is based on the AVI link travel time and the other of which is based on the AVI OD travel time. The results of these models for the I-10 freeway test network will be presented in Chapter VII.

CHAPTER VII

ANALYSIS OF BI-LEVEL CALIBRATION RESULTS

In the preceding chapter, a new methodology for calibrating the OD matrix was proposed, which incorporated the travel time information and the AVI link volumes into the OD estimators. The objective of this chapter is to verify the performances of the bi-level calibration process. In addition to the I-10 freeway test network, a case study network is examined in order to provide a comprehensive sensitivity analysis.

Subsection 7.1 provides the results for the I-10 freeway test network. These results are analyzed to verify the performance and feasibility of the proposed approach. Subsection 7.2 presents the results for the case study network. The focus of analysis is placed in the comparison of the simulated and observed travel time distributions. Finally subsection 7.3 provides concluding remarks and findings.

7.1 CALIBRATION RESULTS FOR THE I-10 FREEWAY TEST NETWORK

To evaluate the effects of including two types of travel time information on the calibration precision, the proposed EKF_LTT (AVI link travel time model) and EKF_ODTT (AVI OD travel time model) algorithms are applied to the I-10 freeway test network.

7.1.1 Average Travel Times for the AVI Sections

The verification of the proposed model was accomplished by comparing the simulated output to the observed data. The primary metric was related to the average travel times between AVI stations. The travel time MAER and average travel times at each iteration for the EKF_LTT algorithm are provided in Table 7.1 and a graphical representation of the average travel times are provided in Figure 7.1.

The results show that the average travel time MAER for AVI section 01 fall within the range of 0.01 and 0.03 for all iterations of the bi-level process. This result would be expected because higher "confidence" is given to the observed travel time for AVI section 01 when identifying the best parameters in Phase 1, as explained in Section 6.2.2.

On the other hand, large differences occur in AVI section 12 and 23 at iteration 0, where the average travel times differ by 20 percent and 27 percent for AVI section 12 and 23, respectively. It is important to note here that the model does not provide similar results to observed conditions, thereby pointing out the necessity of calibrating the OD matrix as well as driver behavior parameters. It was hypothesized in Chapter VI that the addition of travel times into the OD estimator aids in providing comparable results to the observed travel times. The model finally provides the "best" results with respect to the observed travel times after 6 iterations. At this point the travel time MAER is 0.03 or less for all three AVI sections.

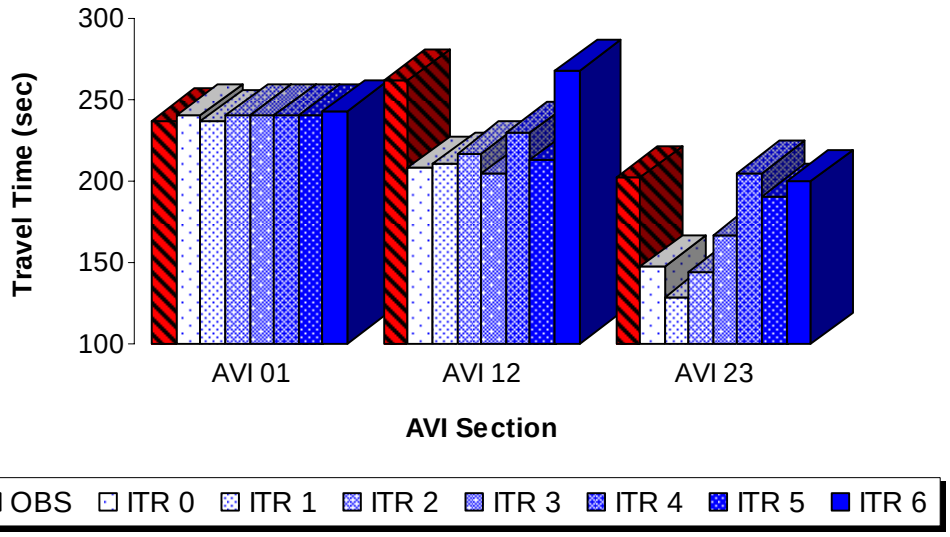

FIGURE 7.1 Average Travel Times from the EKF_LTT Algorithm for the I-10 Freeway Test Network (7:00AM~8:00AM)

The calibration results for the EKF_ODTT algorithm are shown in Figure 7.2. The results indicate that the same trend holds true for the EKF_ODTT algorithm. The EKF_ODTT algorithm provides nearly identical average travel times for AVI section 01. The average travel times for AVI sections 12 and 23 are 7 seconds (3 percent) and 8 seconds (4 percent) lower than those from the EKF_LTT algorithm, respectively. In order to match the observed travel times to within 5 percent for all three sections five iterations of the EKF_ODTT algorithm were required.

It is important to note here that the results for only full peak hour (7:00AM ~ 8:00AM) are presented in Figure 7.1 and 7.2 because of space limitation. The results for thirty minute intervals (6:30AM ~ 8:00AM) for each algorithm are provided in Appendix D. Similar trends for these intervals were identified.

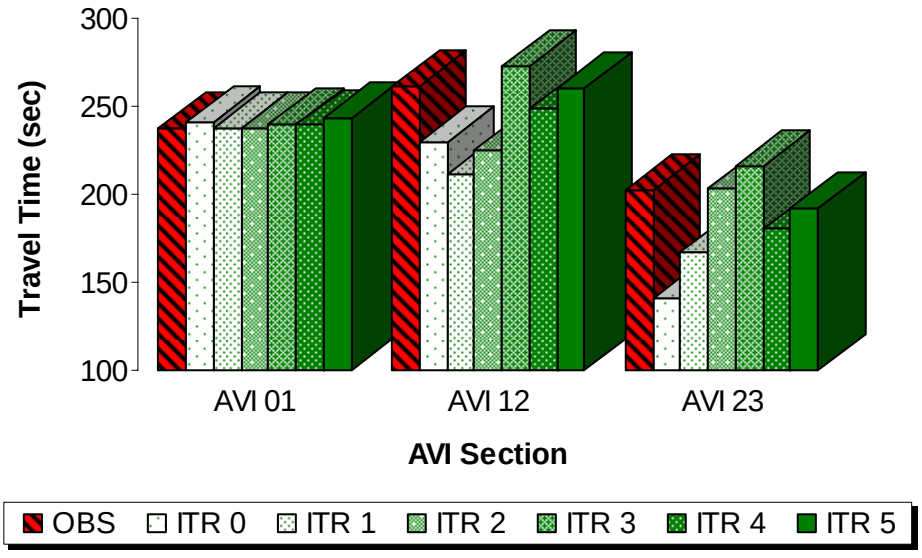

FIGURE 7.2 Average Travel Times from the EKF_ODTT Algorithm for the I-10 Freeway Test Network (7:00AM~8:00AM)

TABLE 7.1 Average Travel Time at Each Iteration for the I-10 Freeway Test Network

Model	AVI Section	Iteration							OBS	MAER
		0	1	2	3	4	5	6		
EKF_LTT	AVI 01	240	237	241	241	241	241	243	237	0.023
	AVI 12	208	211	217	205	230	213	268	262	0.023
	AVI 23	148	129	145	167	205	191	200	202	0.014
EKF_ODTT	AVI 01	241	238	238	240	239	243	-	237	0.024
	AVI 12	230	211	225	273	249	260	-	262	0.006
	AVI 23	140	167	203	216	180	193	-	202	0.046

There are three key findings associated with the above analyses. First, it was expected that the EKF_LTT algorithm would have closer results to the observed conditions than the EKF_ODTT algorithm. Because the former algorithm utilizes three travel time sets for AVI sections as additional measurements. In contrast the latter algorithm attempts to replicate the observed travel times for each AVI section using six OD travel time sets. However, both the EKF_LTT and EKF_ODTT algorithms provide close results in terms of average travel time MAER for each AVI sections. The second is that the inclusion of travel times improves the travel time MAER. The iterative process ensures that the proposed models keep on responding appropriately to the difference between the observed and simulated conditions until the pre-defined stopping criteria (five percent of the observed average travel time) is met. Finally, it can be seen that the two algorithms converge to the observed conditions in different ways. The EKF_LTT algorithm firstly provides a satisfactory result for AVI section 23 and sequentially identifies a comparable result for AVI section 12. In contrast, the EKF_ODTT algorithm closely resembles the observed average travel time for both AVI sections 12 and 23 at the same time and then makes minor adjustments to reduce the difference. This

difference may occur because driver behavior parameters identified in phase 1 are not identical due to the stochastic nature of Genetic Algorithm.

TABLE 7.2 Driver Behavior Parameters Identified at Each Iteration for the I-10 Freeway Test Network

Model	ITR	Calibrated Parameter										
		P1	P2	P3	P4	P5	P6	P7	P8	P9	P10	P11
EKF LTT	0	-4.5	300	-4.1	410	1.3	1.00	3	-9	-0.30	0.30	15
	1	-4.5	220	-4.1	370	1.6	0.85	3	-6	-0.15	0.15	7
	2	-4.5	100	-3.9	370	1.6	0.95	2	-7	-0.15	0.15	9
	3	-4.5	200	-4.1	370	1.6	0.85	3	-6	-0.15	0.15	7
	4	-4.5	220	-4.1	370	1.6	0.85	3	-6	-0.15	0.15	7
	5	-3.5	180	-3.1	310	1.3	0.90	2	-10	-0.35	0.35	9
	6	-4.5	180	-4.1	430	1.5	0.95	2	-9	-0.25	0.25	7
EKF ODTT	0	-5.0	140	-4.6	270	1.3	1.00	3	-7	-0.15	0.15	13
	1	-4.5	300	-4.1	410	1.3	1.00	3	-9	-0.30	0.30	11
	2	-4.5	300	-4.1	410	1.3	1.00	3	-9	-0.30	0.30	11
	3	-6.5	220	-6.5	270	1.3	1.00	4	-9	-0.20	0.20	15
	4	-5.0	140	-4.6	270	1.3	1.00	3	-7	-0.15	0.15	13
	5	-6.5	260	-6.5	270	1.3	1.00	4	-9	-0.20	0.20	8
Default		-4.0	200	-3.0	200	1.5	0.9	4.0	-8	-0.35	0.35	11

Table 7.2 lists the driver behavior parameters that are identified in Phase 1, where it can be seen that different parameters are identified for each model and iteration. The calibrated values of parameter 6 (P6) from both models, which is the key parameter that determines the desired safety distance in the car-following mode, are slightly larger than the default value. This implies that a larger space headway between vehicles is identified for the calibrated models. On the other hand, the calibrated values of the

maximum deceleration rates (P1 and P3) result in a more aggressive reaction of drivers in the case of necessary lane changes. However, the impact of one parameter on overall driver behavior can not be considered separately but interpreted in conjunction with other parameters.

It is important to note at this point that the calibration of OD matrix is performed while the parameters identified in Phase 1 remain unchanged. At iteration 0, both models face the same traffic states for the given initial OD matrix. However, as the bi-level process continues, different parameters are likely to be identified based on the individual operational rules of the Genetic Algorithm. As a result, the simulated traffic conditions may change from one iteration to the next. Additionally, an estimate of the partial derivative matrix of the travel time connection matrix depends on simulated traffic conditions derived from Phase 1. Therefore, different amount of changes in the OD matrix is made. In turn, the EKF_LTT and EKF_ODTT algorithms face different intermediate traffic stages at each iteration.

To better illustrate the overall results, the travel time MAER were plotted as a function of iteration number. It is important to note that two types of MAER are used in Figure 7.3. One is the MAER for all three AVI sections while the other is for only AVI sections 12 and 23. The latter one shows a better representation in reduction of MAER because travel time MAER for AVI section 01 ranges within 3 percent of the observed conditions across all iterations.

In general, the travel time MAER decreases as the iteration number increases. However, the EKF_LTT algorithm a shows slight increase in MAER at iterations 1 and 5, while the EKF_ODTT algorithm shows consistent decreases in MAER. Note that the bi-level approach does not guarantee lower MAER values at each iteration. The results also indicate that for the EKF_ODTT algorithm, the travel time MAER decreases at an increasing rate at the beginning of the iterations and is relatively flat after iteration 2. The decrease in travel time MAER may be attributed to the increase in trips passing through AVI sections 12 and 23, as a result of the calibrated OD matrix. This topic is discussed in more detail later in this chapter.

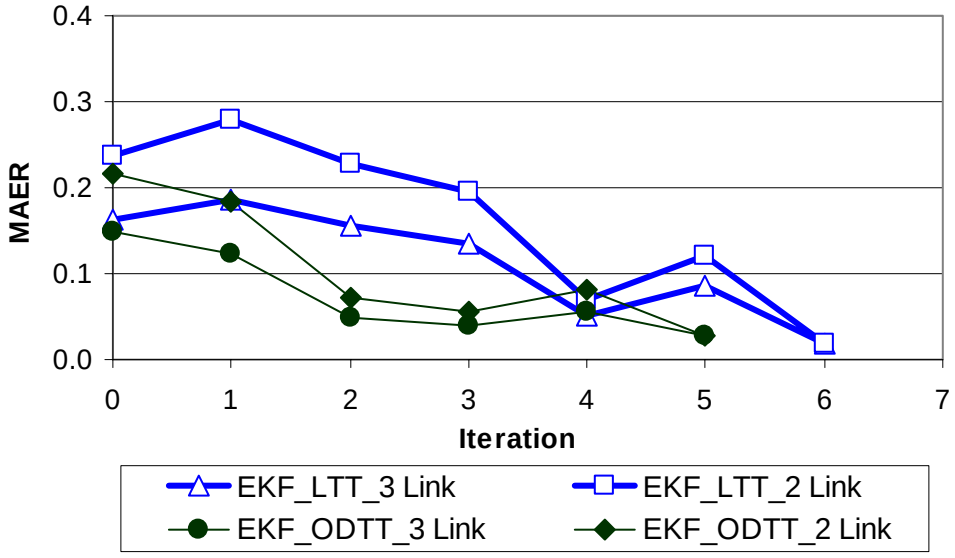

FIGURE 7.3 Average Travel Time MAER at Each Iteration for the I-10 Freeway Test Network

7.1.2 Average Travel Times for OD Pairs

The average travel times for all six OD pairs for the full peak hour (7:00AM ~ 8:00AM) for the last iteration are provided in Figure 7.4. It should be noted that similar results were obtained for the two thirty minute periods on either side of the peak hour. These results were not provided in this section but may be found in Appendix D.

The results indicate that both the EKF_LTT and EKF_ODTT algorithms provide nearly identical results to the observed conditions. That is, the use of either travel time set improved the results. It is found that the average OD travel time MAER decreases from 0.16 to 0.02 for the EKF_LTT algorithm and decreases from 0.14 to 0.01 for the EKF_ODTT algorithm. This is an interesting result because it raises the possibility that the EKF_LTT algorithm provides comparable results with great accuracy in terms of average OD travel times. This is important because the algorithm only utilizes travel times from the AVI sections.

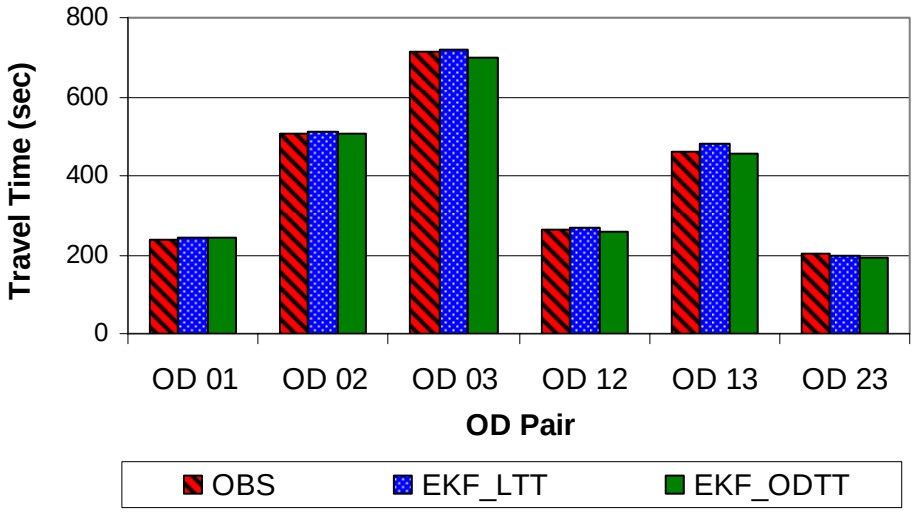

FIGURE 7.4 Average Travel Times for OD Pairs for the I-10 Freeway Test Network (7:00AM~8:00AM)

7.1.3 Calibrated OD Matrix

In order to gain some insights into the effect of the OD matrix on average travel times for the AVI sections an analysis of the calibrated OD estimates was conducted. It was found that at iteration 0, the simulated travel times for AVI sections 12 and 23 were 27 and 20 percent lower than the observed travel times for the EKF_LTT algorithm, respectively, and 12 and 30 percent lower for the EKF_ODTT algorithm, respectively. A t-test was conducted on the means to check if the average travel times are significantly different. The test results show that the mean differences for AVI sections 12 and 23 are statistically significant at the 95% level of testing. In other words, for this network the calibration of the OD matrix is necessary to replicate observed conditions.

The OD matrices for two intervals of thirty minutes (7:00AM ~ 7:30AM, 7:30AM ~ 8:00AM) obtained at each iteration are tabulated in Tables 7.3 and 7.4. In addition the differences between the initial and the calibrated OD matrices are also found. Table 7.3 contains the results for the EKF_LTT algorithm, while Table 7.4

provides the results for the EKF_ODTT algorithm. The results for initialization time period (6:30AM~7:00AM) is provided in Appendix D. The initial and calibrated OD matrices for the final iteration are shown in Figures 7.5 and 7.6, respectively. These figures show how changes in OD matrix are reflected in the link volume on AVI sections 12 and 23. For example, it can be seen that among the OD pairs that have origin 0, the split proportions for OD pairs 02 and 03 increase as the number of iteration increase. Therefore, there is a corresponding increase in trips passing through AVI sections 12 and 23. This, in turn, leads to increases in travel times for the same sections. Note that it may not be appropriate to explain travel time increase simply based on increased trip numbers because of the complex relationship between the two parameters. However, it can be expected that the increases in volume of OD pairs 02 and 03 have a positive influence on the increase in travel time for these sections, taking into account that vehicles entering the network from origin 0 (main-lane) is much larger than ones from other entries (on-ramps). As was shown in Chapter V it was impossible to calibrate travel times without adjusting the OD volumes.

Some points need to be addressed regarding the results from the EKF_LTT and EKF_ODTT algorithms. First, the two models provide different calibrated OD matrices. It is well known that the OD estimator based on link volumes can be formulated as an underdetermined linear equation and its solution cannot be uniquely identified because there could be a number of combinations that meet link volume constraint. In the same manner, the calibrated OD matrix can be considered as one of many solutions that reflect travel times and link volumes equally well. Therefore, it is possible to obtain different OD matrices from the EKF_LTT and EKF_ODTT algorithms.

Second, it is reasonable to take into account the number of vehicles departing from each origin when interpreting the calibrated OD matrix. Note that in this dissertation the OD matrix does not represent OD flows but OD split proportions. For example, even though the smallest difference between the initial and calibrated matrices occurs in OD pairs with origin 0, this change may primarily influence the network

performance because the number of vehicles entering the network is much larger than from other entries.

The last point is about deviations of the calibrated OD matrix from the initial OD matrix. In this dissertation, the "closeness" is defined as a sum of the weighted absolute values of the differences between the each element of the initial and calibrated OD matrices relative to the total number of vehicles entering system. Equation 7.1 is used to quantify the "closeness" between the initial and calibrated OD matrices. It can be seen in Figure 7.5 that the EKF_ODTT algorithm tends to provide a calibrated OD matrix that is "closer" to the initial OD matrix, compared to the results from the EKF_LTT algorithm. The closeness measures of the EKF_LTT and EKF_ODTT algorithms for the first thirty minute period were 0.52 and 0.14, respectively. In other words, the EFK_ODTT algorithm provides the calibrated OD matrix that is more than three times closer to the initial OD matrix for the given time period. It can be concluded, therefore, that the EKF_ODTT performs better in that it includes travel time information as additional measurements while retaining the information related to the link volumes.

$$CM_t = \frac{1}{n}\sum_{i=1}^{n}\frac{v_{kt}\left|od_{it}^{ini} - od_{it}^{cal}\right|}{Tv_t} \qquad (7.1)$$

CM_t = closeness measure for time interval t ;

n = number of OD pairs ;

v_{kt} = number of vehicles entering from AVI station k at time interval t (veh) ;

Tv_t = total number of vehicles entering system at time t (veh) ;

od_{it}^{ini} = initial OD split proportion of OD pair i at time interval t ; and

od_{it}^{cal} = calibrated OD split proportion of OD pair i at time interval t.

On the other hand, Figure 7.6 shows that differences between the initial and calibrated OD matrices are relatively closer for both algorithms. The closeness measures for the second time period were 0.10 and 0.11, respectively.

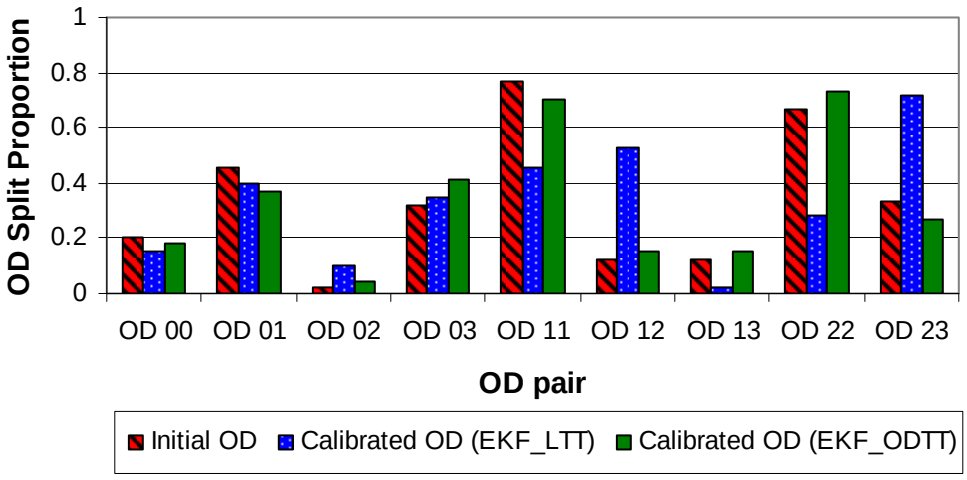

FIGURE 7.5 Calibrated OD Split Proportion from the EKF_LTT and EKF_ODTT Algorithm for the I-10 Freeway Test Network (7:00AM~7:30AM)

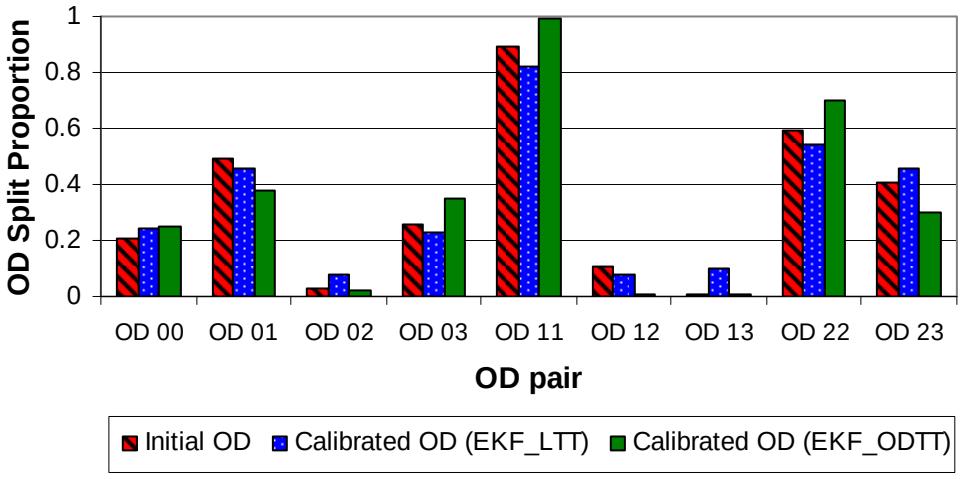

FIGURE 7.6 Calibrated OD Split Proportion from the EKF_LTT and EKF_ODTT Algorithm for the I-10 Freeway Test Network (7:30AM~8:00AM)

TABLE 7.3 Initial and Calibrated OD Split Proportions at Each Iteration from the EKF_LTT Algorithm for the I-10 Freeway Test Network

Time Interval	OD Pair	0 (Initial)	1	2	3	4	5	6	Diff*
7:00~7:30	00	0.20	0.18	0.17	0.15	0.16	0.17	0.15	-0.05
	01	0.46	0.58	0.54	0.43	0.42	0.41	0.40	-0.06
	02	0.02	0.08	0.11	0.10	0.03	0.09	0.10	0.08
	03	0.32	0.16	0.18	0.32	0.39	0.34	0.35	0.03
	11	0.77	0.69	0.59	0.60	0.50	0.47	0.46	-0.31
	12	0.12	0.28	0.41	0.40	0.50	0.53	0.53	0.41
	13	0.12	0.03	0.00	0.00	0.00	0.00	0.02	-0.10
	22	0.67	0.57	0.42	0.40	0.40	0.36	0.28	-0.39
	23	0.33	0.43	0.58	0.60	0.60	0.64	0.72	0.39
7:30~8:00	00	0.21	0.25	0.28	0.28	0.24	0.19	0.24	0.03
	01	0.49	0.47	0.34	0.36	0.41	0.47	0.46	-0.03
	02	0.03	0.05	0.06	0.04	0.03	0.06	0.08	0.05
	03	0.26	0.23	0.32	0.32	0.31	0.28	0.23	-0.03
	11	0.89	0.79	0.86	0.83	0.81	0.83	0.82	-0.07
	12	0.11	0.21	0.14	0.16	0.18	0.11	0.08	-0.03
	13	0.01	0.00	0.00	0.01	0.01	0.06	0.10	0.09
	22	0.59	0.50	0.56	0.57	0.52	0.54	0.54	-0.05
	23	0.41	0.50	0.44	0.43	0.48	0.46	0.46	0.05

* Difference between the initial and final OD split proportions

TABLE 7.4 Initial and Calibrated OD Split Proportions at Each Iteration from the EKF_ODTT Algorithm for the I-10 Freeway Test Network

Time Interval	OD Pair	0 (Initial)	1	2	3	4	5	Diff*
	00	0.20	0.20	0.24	0.24	0.21	0.20	0.00
	01	0.46	0.46	0.37	0.33	0.40	0.38	-0.08
	02	0.02	0.02	0.02	0.02	0.01	0.03	0.01
	03	0.32	0.32	0.37	0.41	0.38	0.39	0.07
7:00~7:30	11	0.77	0.77	0.76	0.73	0.73	0.68	-0.09
	12	0.12	0.12	0.19	0.21	0.16	0.18	0.06
	13	0.12	0.12	0.04	0.06	0.11	0.15	0.03
	22	0.67	0.67	0.64	0.59	0.65	0.71	0.04
	23	0.33	0.33	0.36	0.41	0.35	0.29	-0.04
	00	0.21	0.21	0.23	0.21	0.22	0.25	0.04
	01	0.49	0.49	0.47	0.48	0.47	0.45	-0.04
	02	0.03	0.03	0.03	0.02	0.01	0.00	-0.03
	03	0.26	0.26	0.27	0.29	0.30	0.30	0.04
7:30~8:00	11	0.89	0.89	0.91	0.94	0.93	0.92	0.03
	12	0.11	0.11	0.05	0.05	0.05	0.05	-0.06
	13	0.00	0.00	0.04	0.01	0.02	0.03	0.03
	22	0.59	0.59	0.65	0.63	0.64	0.66	0.07
	23	0.41	0.41	0.35	0.37	0.36	0.34	-0.07

* Difference between the initial and final OD split proportions

7.1.4 Travel Time Distribution

In order to analyze the relationship between travel times and the calibrated OD matrix the travel time histograms from the EKF_LTT algorithm for AVI sections 01, 12, and 23 were plotted in Figures 7.7, 7.8, and 7.9, respectively. The travel time histograms from the EKF_ODTT algorithm are provided in Figures 7.10 through 7.12. Also shown are *p*-values for the Kolmogorov-Smirnov statistical test as well as the travel time MAER. Note that each of these figures is composed of two graphs a and b. Graph a shows the travel time distribution for iteration 0 (e.g. calibration without OD estimation) while graph b shows the travel time distribution for the final iteration.

Even though the equalities of the observed and simulated travel time distributions for all three AVI sections are not supported at a 95 percent confidence level, the results clearly illustrate that both models provide closer results to the observed travel time distributions. For AVI section 01, no improvements are made. However, the travel time distributions for AVI sections 12 and 23, which are somewhat skewed to left at iteration 0, shift to right and closely follow the observed distributions after the final iteration. The results also demonstrate that the EKF_ODTT algorithm shows slightly superior results to the EKF_LTT, particularly for AVI section 23. These results are more clearly demonstrated in the cumulative distribution functions of simulated travel times, as shown in Figures 7.13 through 7.15.

From a graphical comparison, there seem no significant differences between the EKF_LTT and EKF_ODTT algorithms. To determine whether or not both algorithms produce the same travel time distributions, the Kolmogorov-Smirnov statistical test was conducted. The test statistics and significance level from the KS test are found in Table 7.5. As indicated in Table 7.5, the travel time distribution for AVI section 12 is statistically identical while the equalities of the travel time distributions for AVI sections 01 and 23 are not supported at a 95 percent confidence level.

TABLE 7.5 Equality Test of Travel Time Distributions from the EKF_LTT and EKF_ODTT Algorithms for the I-10 Freeway Test Network

	Kolmogorov-Smirnov Test	
	Statistics	Significance
AVI section 01	0.144	0.031
AVI section 12	0.131	0.361*
AVI section 23	0.217	0.007

* We do not reject, at the 95 percent (0.05) level, the hypothesis that the distributions are identical.

A subset of the results of the statistical test (KS test) for the travel time distributions obtained after the final iteration is provided in Table 7.6. Also are presented *p*-values and the travel time MAER in Table 7.6. Most of the travel time MAER values are within 6 percent or less of the observed travel times while *p*-values are close to zero. It can be also seen that there is no case where a statistically based objective functions for more than one AVI sections are satisfied, even though the average travel time MAER are significantly improved.

It is hypothesized that results may be mainly due to the fact that the inputs to the VISSIM microscopic traffic simulation model were compiled based on the data collected for multiple days. From a practical point of view, it is rarely possible to collect a complete dataset, including traffic counts on the main lanes and ramps, over a large network without a significant amount of effort and cost

TABLE 7.6 Subset of Travel Time MAER and *p*-value for the EKF_LTT Algorithm for the I-10 Freeway Test Network

	Case	MAER			*p*-value		
		AVI 01	AVI 12	AVI 23	AVI 01	AVI 12	AVI 23
EKF_LTT	1	0.031	0.081	0.026	0.003	0.000	0.000
	2	0.016	0.064	0.071	0.006	0.000	0.000
	3	0.032	0.034	0.090	0.000	0.004	0.000
	4	0.059	0.042	0.016	0.000	0.016	0.000
	5	0.023	0.023	0.014	0.000	0.090	0.000
EKF_ODTT	1	0.062	0.027	0.094	0.000	0.013	0.000
	2	0.015	0.053	0.033	0.000	0.003	0.002
	3	0.025	0.005	0.052	0.000	0.000	0.020
	4	0.027	0.113	0.009	0.000	0.000	0.342
	5	0.054	0.054	0.040	0.000	0.000	0.027

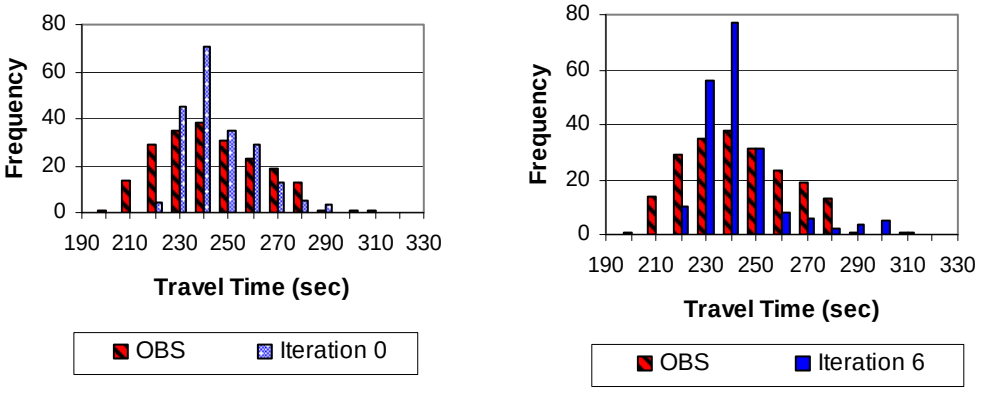

(a) MAER: 0.012 *p*-value: 0.000 (b) MAER: 0.032 *p*-value: 0.000

FIGURE 7.7 Histogram of Travel Time for AVI Section 01 of the I-10 Freeway Test Network (EKF_LTT Algorithm)

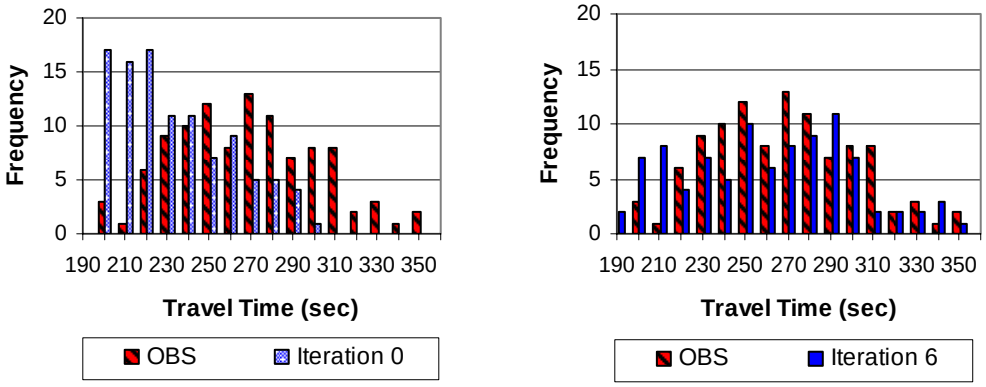

(a) MAER: 0.204 *p*-value: 0.000 (b) MAER: 0.034 *p*-value: 0.004

FIGURE 7.8 Histogram of Travel Time for AVI Section 12 of the I-10 Freeway Test Network (EKF_LTT Algorithm)

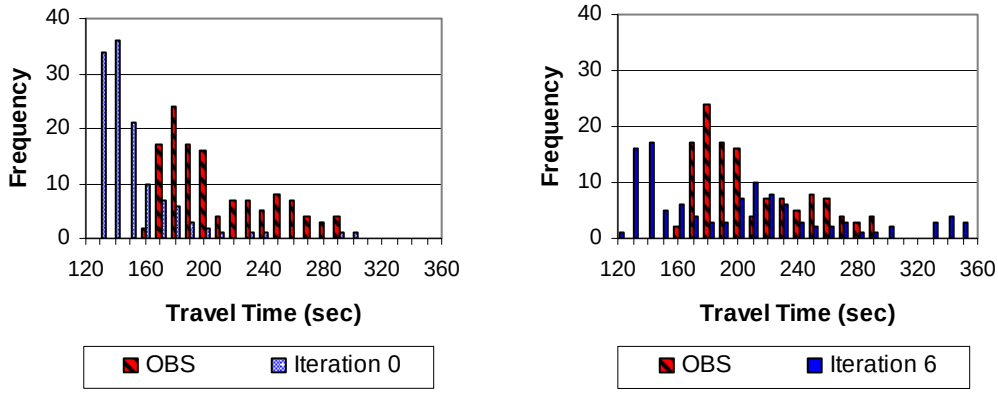

(a) MAER: 0.271 *p*-value: 0.000 (b) MAER: 0.090 *p*-value: 0.000

FIGURE 7.9 Histogram of Travel Time for AVI Section 23 of the I-10 Freeway Test Network (EKF_LTT Algorithm)

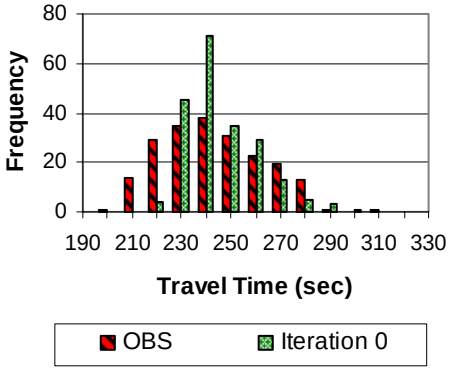

(a) MAER: 0.016 *p*-value: 0.000

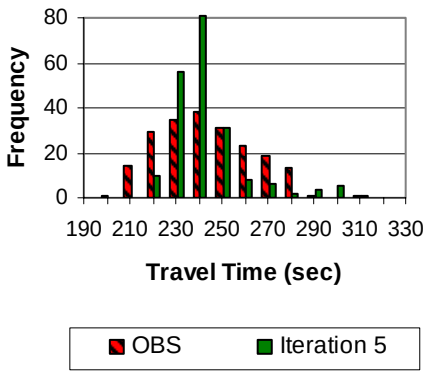

(b) MAER: 0.015 *p*-value: 0.000

FIGURE 7.10 Histogram of Travel Time for AVI Section 01 of the I-10 Freeway Test Network (EKF_ODTT Algorithm)

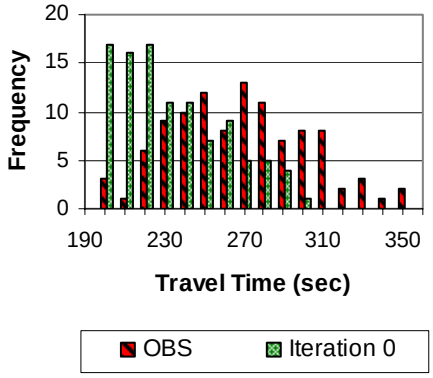

(a) MAER: 0.124 *p*-value: 0.000

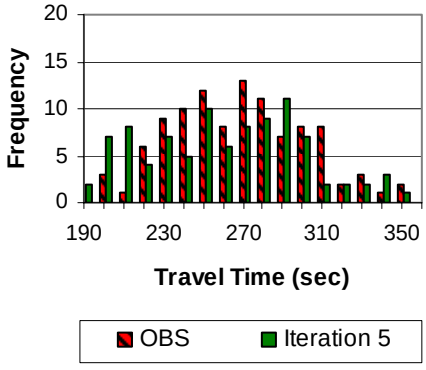

(b) MAER: 0.053 *p*-value: 0.003

FIGURE 7.11 Histogram of Travel Time for AVI Section 12 of the I-10 Freeway Test Network (EKF_ODTT Algorithm)

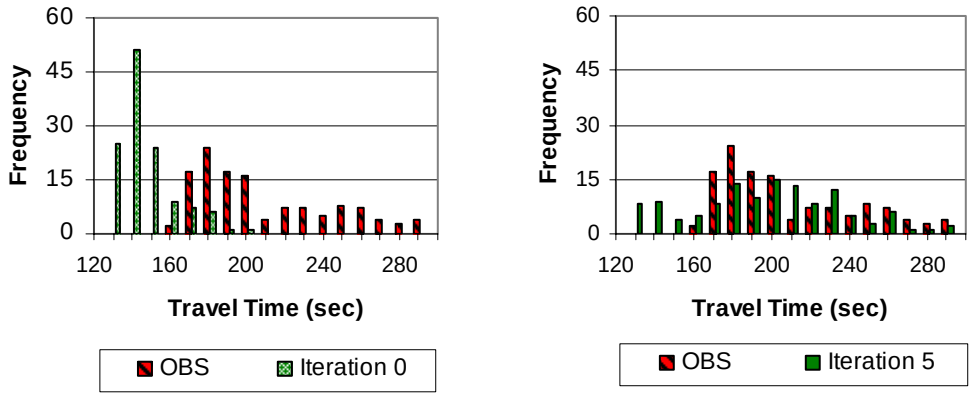

(a) MAER: 0.307 *p*-value: 0.000 (b) MAER: 0.033 *p*-value: 0.002

FIGURE 7.12 Histogram of Travel Time for AVI Section 23 of the I-10 Freeway Test Network (EKF_ODTT Algorithm)

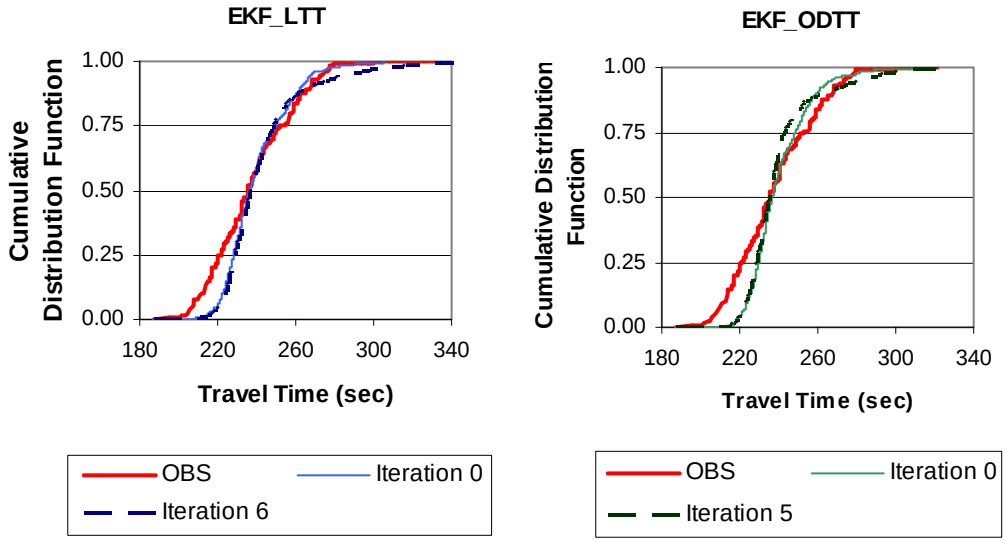

FIGURE 7.13 Travel Time Cumulative Distribution Function for AVI Section 01 of the I-10 Freeway Test Network

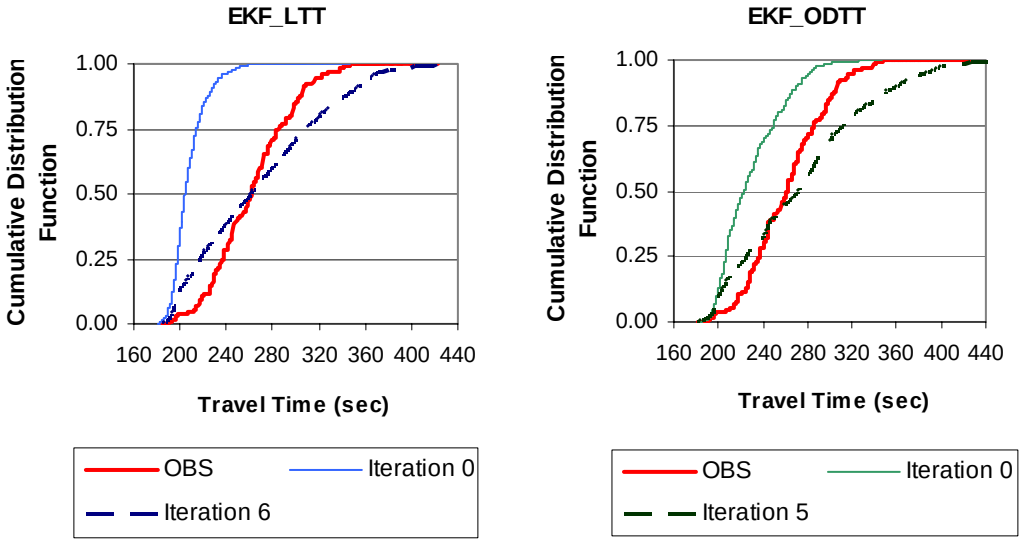

FIGURE 7.14 Travel Time Cumulative Distribution Function for AVI Section 12 of the I-10 Freeway Test Network

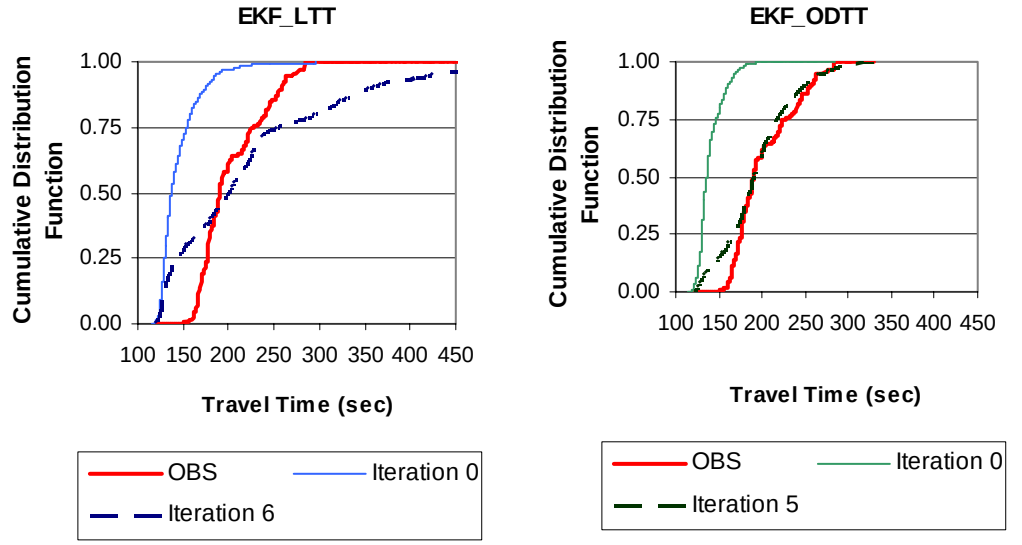

FIGURE 7.15 Travel Time Cumulative Distribution Function for AVI Section 23 of the I-10 Freeway Test Network

7.2 CALIBRATION RESULTS FOR THE CASE STUDY NETWORK

In Section 7.1, the calibration results for the I-10 freeway test network were presented. To verify the performances of the proposed models, these results were compared with the observed conditions. The analysis of results indicates that both models provide better results in terms of average travel times. However, while it was possible to replicate the travel time distribution on one AVI section, it was not possible to obtain the statistically valid calibration results for all three AVI sections. It was hypothesized that this occurred because travel demand data were compiled based on the data collected for multiple days.

Therefore, in this section, a simulation case study was designed to verify the performance of the proposed models using disaggregated data. The focus is the distribution of individual travel time that is used as a performance measure in a statistically based objective function. In summary, the performance of the approach will be analyzed using perfect, albeit simulated, data.

7.2.1 Preparing the Case Study Data

Figure 7.16 depicts the research framework of the case study. The first step consists of preparation of the network supply and "true" traveler demand data. To reduce the effort on network coding and manipulation of the automated calibration program (Perl program), most of network data are obtained from the information regarding the I-10 freeway test network. The case study network has the same geometries such as lane connectivity, number of lanes, length of network, and number of ramps, and sensor locations (AVI stations) as the I-10 freeway test network does. Therefore, the number of OD pairs and travel time data set are exactly same as that in the I-10 freeway test network. However, as stated in Chapter III, a severe blockage was found in the right-most lane for the I-10 freeway test network when congestion occurs. To avoid this situation, the length of auxiliary lane is increased at the location where a vehicle can not often make a lane change necessary to stay on its route due to the extremely short length of the auxiliary lane.

The "true" OD matrix is selected such that free-flow and congested states can be generated along the case study network. This OD matrix will be used as a "target" OD matrix in the comparison with the calibrated OD matrix. In addition, other information associated with the estimation of the OD matrix, such as the error variance covariance matrices, are defined *a priori*. In this step, the time-varying input volumes at all entries including main-lane and on-ramps are also defined. The volumes are chosen to be large enough to generate congested traffic conditions in conjunction with the selected OD matrix.

The second step is to run the VISSIM simulation with the "true" OD matrix. This step is to check whether the VISSIM model performs in an intended manner. In particular, if the blockage in the right-most lane causes incorrect vehicular movements, the proportions of partial route decision, which is used to keep fractions of vehicles out of the right-most lane, were adjusted so as to eliminate such potential problem in the next simulation run.

The third step consists of compiling average link travel times, travel time distributions, and the statistics of simulated traffic conditions from the VISSIM output files. These travel time data are used in further analysis as "target" measures being replicated through the bi-level calibration process.

The purpose of the forth step is to generate the "starting" OD matrix by introducing bias in the "true" OD matrix. Given the biased OD matrix, the bi-level calibration process begins to calibrate driver behavior parameters in Phase 1. It should be noted that more attention should be paid in selecting the amount of bias to introduce. In other words, if the "starting" simulated traffic condition is similar to that with the "true" OD matrix, the "true" traffic condition can be replicated by calibrating only driver behavior parameters. Therefore, the selected bias should be large enough to necessitate the bi-level calibration process so that the performance of the proposed models can be evaluated.

The fifth step is to run the VISSIM simulation and to check whether the selected bias is sufficient. After deciding appropriate bias, the bi-level calibration process begins to calibrate the "starting" (biased) OD matrix and driver behavior parameters.

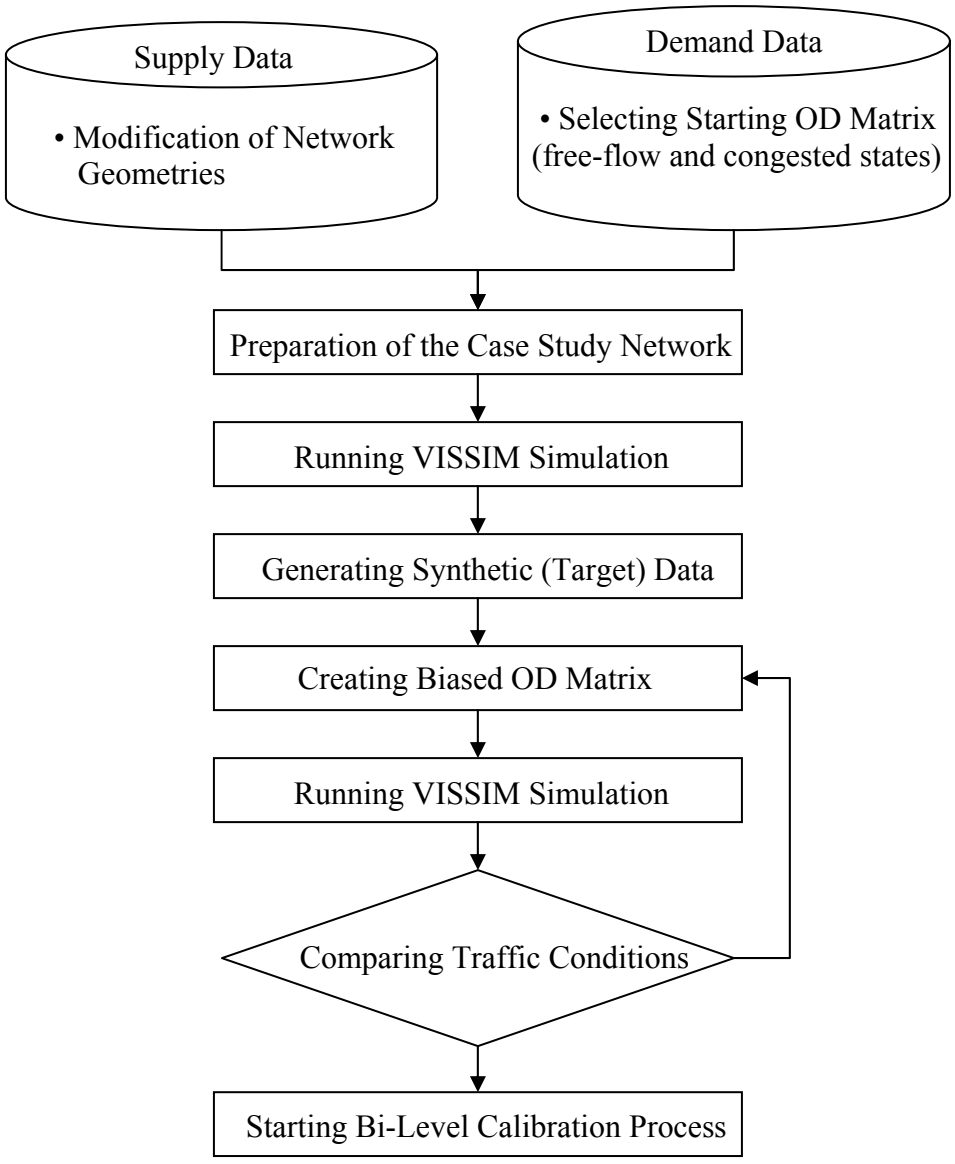

FIGURE 7.16 Research Framework of the Case Study

To introduce bias, the "true" OD matrix was changed for all three thirty minute time intervals including the initialization time period (6:30AM~7:30AM) and the peak hour (7:00AM~8:00AM). Note that fractions of vehicles departing at the initialization time period transverse along the case study network during the peak hour. As can be seen in Table 7.7, the "starting" OD matrix has higher OD split proportions for OD pairs that depart from origin 0 and 1 and head to destination 3. To reach their destination, the vehicles associated with the "starting" OD matrix have to pass though the entire case study network. Therefore, it is expected that the level of congestion on AVI sections 12 and 23 will increase. However, as stated in Section 6.2.2, the number of vehicles on AVI section 01 may not change noticeably.

The statistics, including the average travel time, the standard deviation, maximum, minimum, and link travel speed associated with the "true" and "starting" OD matrix are summarized in Table 7.8. Note that for the I-10 freeway test network the traffic conditions shift from non-congested at iteration 0 to congested conditions at the final iteration.

TABLE 7.7 True and Starting OD Matrices for Case Study

Time Interval	OD Pair	True	Starting (Biased)
6:30 AM ~ 7:00 AM	00	0.1	0.1
	01	0.4	0.3
	02	0.2	0.15
	03	0.3	0.45
7:00 AM ~7:30 AM	11	0.4	0.3
	12	0.3	0.25
7:30 AM ~8:00 AM	13	0.3	0.45
	22	0.4	0.4
	23	0.6	0.6

In contrast, for the case study network, the shift from congested to non-congested traffic conditions is to be achieved under the bi-level calibration framework. As found in Table 7.8, the average travel times for AVI sections 12 and 23, given the "true" OD matrix, are 213 and 134 seconds, respectively, and these values are changed to 322 and 272 seconds after the bias was introduced. The graphical representations of travel time distributions for all AVI sections for the "true" and "starting" OD matrix are presented in Figures 7.17 through 7.19, respectively.

TABLE 7.8 Summary Statistics of True and Starting Traffic Conditions for the Case Study Network

		AVI 01	AVI 12	AVI 23
True OD Matrix	Average (sec)	264.3	213.4	134.0
	Standard Deviation (sec)	37.0	30.9	7.0
	Minimum (sec)	206	178	117
	Maximum (sec)	363	319	166
	Link Speed (km/h)	88.6	92.6	93.1
Starting OD Matrix	Average (sec)	264.2	322.7	272.2
	Standard Deviation (sec)	36.9	70.1	36.7
	Minimum (sec)	206	188	207
	Maximum (sec)	363	498	363
	Link Speed (km/h)	88.6	61.6	45.7

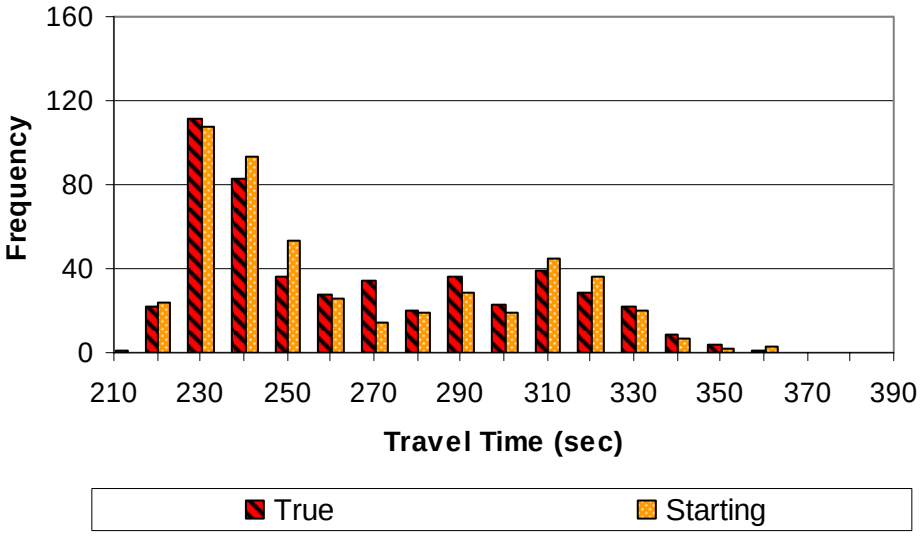

FIGURE 7.17 Histogram of True and Starting Travel Time on AVI Section 01 for the Case Study Network

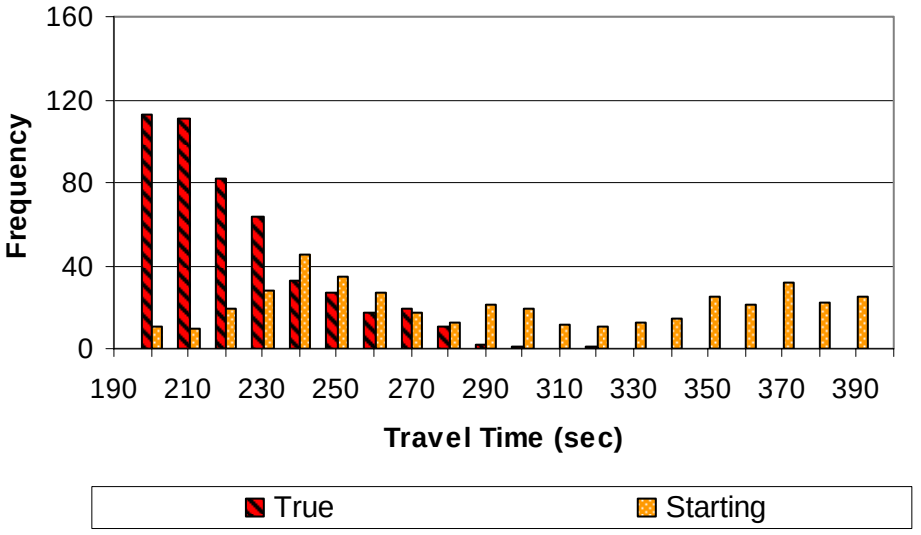

FIGURE 7.18 Histogram of True and Starting Travel Time on AVI Section 12 for the Case Study Network

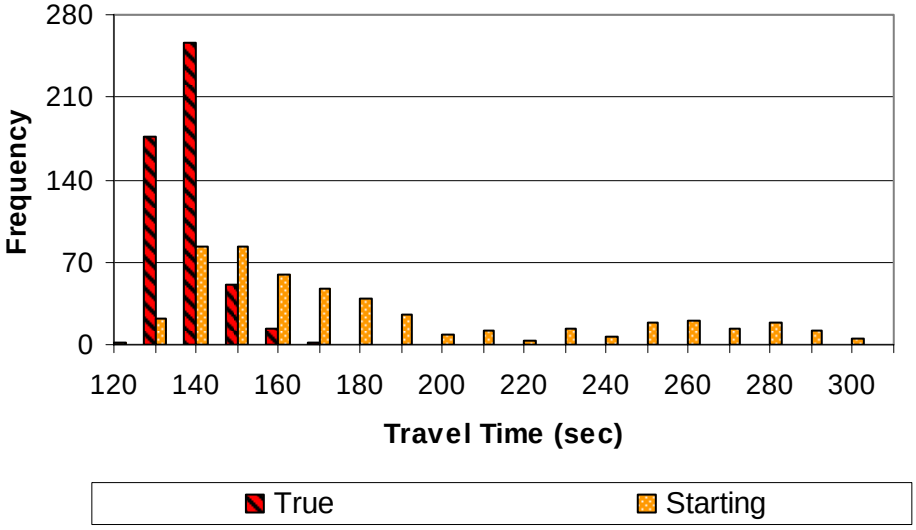

FIGURE 7.19 Histogram of True and Starting Travel Time on AVI Section 23 for the Case Study Network

7.2.2 Average Travel Times for the AVI Sections

The travel time MAER and average travel times at each iteration for the EKF_LTT and EKF_ODTT algorithms are provided in Table 7.9. It may be seen that both models provide similar results to the target traffic conditions. The EKF_LTT algorithm provides the average travel time MAER results less than 0.01 (1 percent) for all 3 AVI sections, while the EKF_ODTT algorithm shows MAER less than 0.03 (3 percent). Large differences occur at iteration 0 for AVI sections 12 and 23, where the average travel times differ by 44 percent and 73 percent for the EKF_LTT algorithm, and by 65 percent and 7 percent for the EKF_ODTT algorithm, respectively. However, these differences largely disappear after 3 and 2 iterations for the EKF_LTT and EKF_ODTT algorithms, respectively. The calibration results for the full peak hour (7:00AM ~ 8:00AM) are shown in Figures 7.20 and 7.21 because of space limitation. The results for thirty minute disaggregate time intervals (6:30AM ~ 8:00AM) are provided in Appendix E. Similar trends for these intervals were identified.

TABLE 7.9 Average Travel Time at Each Iteration for the Case Study Network

Model	AVI Section	Iteration				True	MAER
		0	1	2	3		
EKF_LTT	AVI 01	261	261	260	263	264	0.003
	AVI 12	307	319	220	215	213	0.007
	AVI 23	232	155	146	135	134	0.011
EKF_ODTT	AVI 01	261	261	261	-	264	0.010
	AVI 12	352	230	220	-	213	0.031
	AVI 23	143	137	135	-	134	0.010

Because of the nature of this case study the "true" VISSIM parameter set is known *a priori*. Consequently the parameter set identified from the bi-level process can be compared directly to the "true" parameter set. Table 7.10 lists the driver behavior parameter set that are identified in phase 1 at each iteration as well as the "true" parameter set. It should be noted that the effect of each parameter on the VISSIM output can not be evaluated in isolation which make it difficult to interpret the calibrated parameter set. However, it may be seen that the calibrated parameters are not markedly different from the "true" parameters for either algorithm.

TABLE 7.10 Driver Behavior Parameters Identified at Each Iteration for the Case Study Network

Model	ITR	Parameter										
		P0	P1	P2	P3	P4	P5	P6	P7	P8	P9	P10
EKF_LTT	0	-4.0	240	-3.0	370	1.2	0.75	6	-10	-0.15	0.15	13
	1	-4.5	140	-4.5	370	1.0	0.85	5	-7	-0.15	0.15	13
	2	-4.5	140	-4.5	330	1.0	0.85	5	-7	-0.15	0.15	13
	3	-4.0	140	-3.0	310	1.5	0.70	5	-9	-0.15	0.15	16
EKF_ODTT	0	-5.0	240	-4.6	310	1.6	0.90	2	-10	-0.25	0.25	15
	1	-4.5	260	-5.0	310	1.5	0.85	4	-8	-0.30	0.30	9
	2	-5.0	260	-5.0	290	1.5	0.90	2	-8	-0.25	0.25	10
True Parameters		-5.0	250	-4.5	350	1.5	0.85	4	-8	-0.35	0.35	11

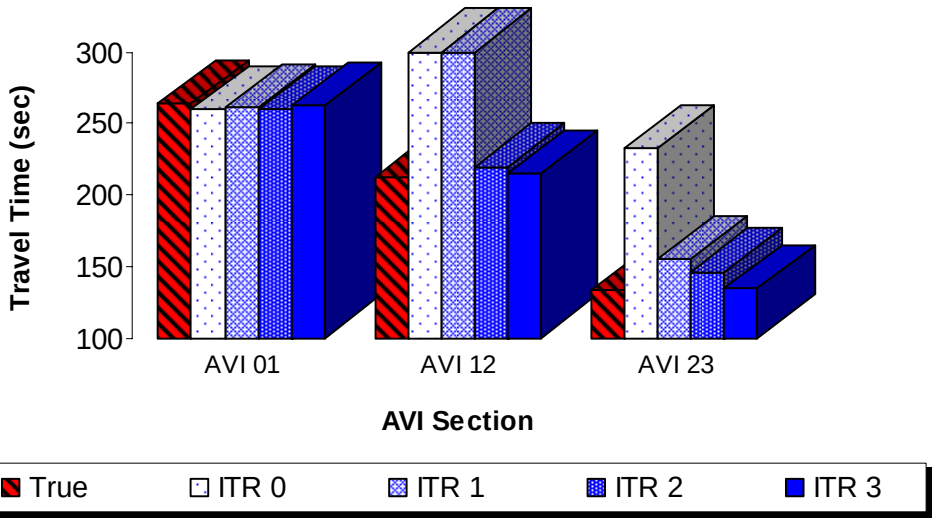

FIGURE 7.20 Average Travel Times from the EKF_LTT Algorithm for the Case Study Network (7:00AM~8:00AM)

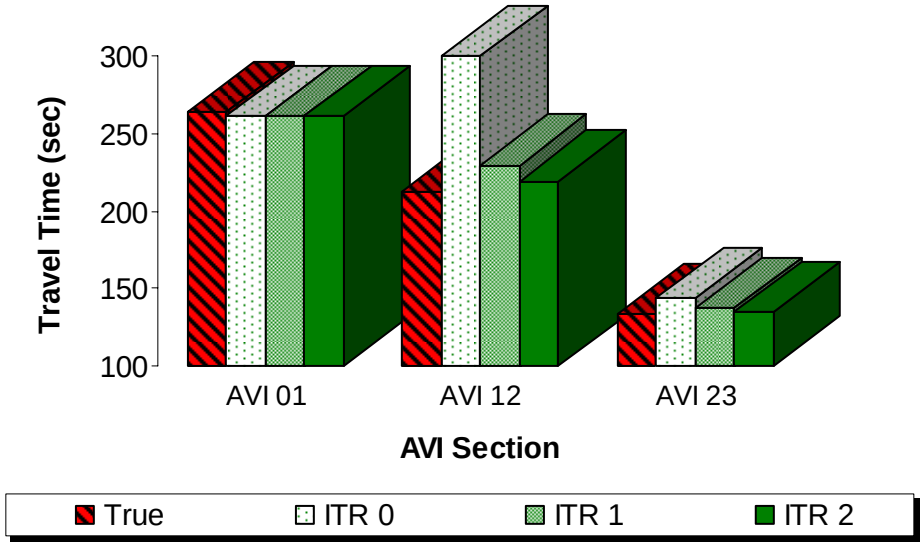

FIGURE 7.21 Average Travel Times from the EKF_ODTT Algorithm for the Case Study Network (7:00AM~8:00AM)

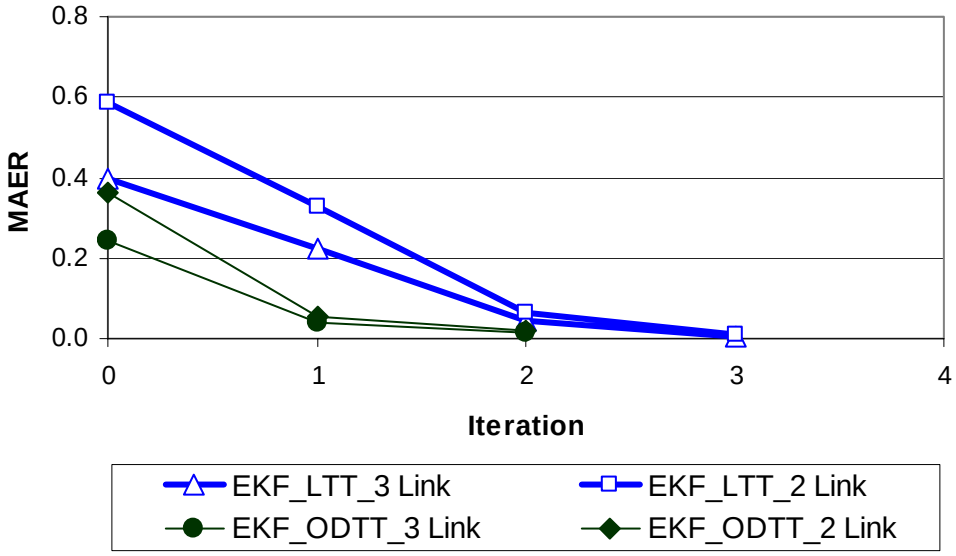

FIGURE 7.22 Average Travel Time MAER at Each Iteration for the Case Study Network

To better illustrate the overall results, the travel time MAER were plotted against iteration number for each of EKF_LTT and EKF_ODTT algorithms, as shown in Figure 7.22. In general, the travel time MAER decreases as the number of iterations increase and this decease is at a decreasing rate. While slight increases in MAER were observed during iterations at the I-10 freeway test network, both models provide consistent decreases in MAER.

7.2.3 Average Travel Times for OD Pairs

The average OD travel times for the full peak hour (7:00AM ~ 8:00AM) for the last iteration are shown in Figure 7.23. Similar results are obtained for the thirty minutes on either side of the peak hour and are not shown in this section. However, they are provided in Appendix E. Similar to the results for the I-10 freeway test network, both models provide closer results to the target travel times. The average OD travel times for the EKF_LTT and EKF_ODTT algorithms are within 1 percent and 2 percent of the "true" travel times, respectively.

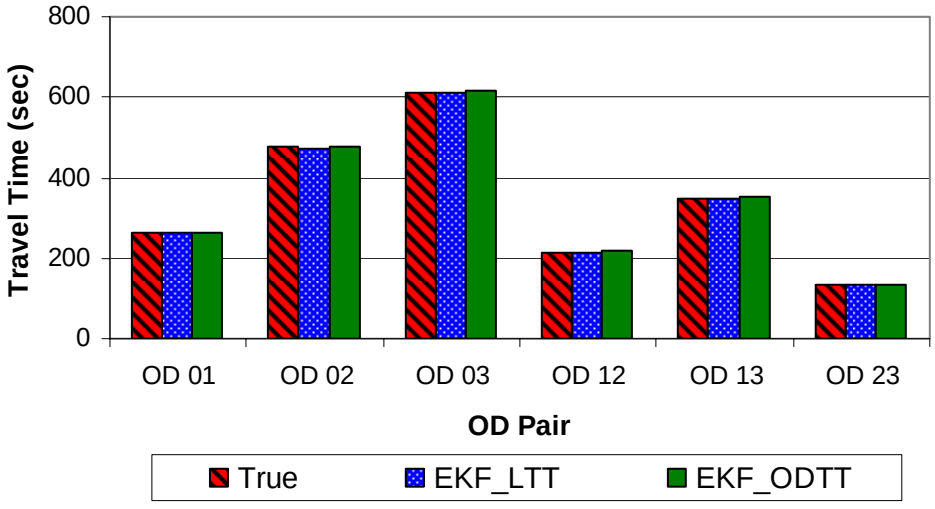

FIGURE 7.23 Average Travel Times for OD Pairs for the Case Study Network (7:00AM~8:00AM)

7.2.4 Calibrated OD Matrix

The OD matrices for two time periods (7:00AM ~ 7:30AM and 7:30AM ~ 8:00AM) for each iteration are tabulated in Tables 7.11 and 7.12. The results for the initialization time period (6:30AM~7:00AM) is provided in Appendix E. It can be seen that there are small differences between the starting and calibrated OD matrices for the initialization time period. After the final iteration, the starting OD matrix is not markedly changed. This would be expected because the case study network is under free-flow traffic conditions for the given time period.

The true, starting, and calibrated OD matrices after the final iteration are shown in Figures 7.24 and 7.25. In these figures, the first column bar indicates the "true" OD split proportions. The second indicates the "starting" OD split proportions. The third and forth indicate the calibrated OD split proportions for the EKF_LTT and EKF_ODTT algorithms, respectively.

Three key findings may be specified from the results. First, it can be seen in Figures 7.24 and 7.25 that the EKF_LTT and EKF_ODTT algorithms provide different calibrated OD matrices. Similar to the reasons for the I-10 freeway test network, the differences between the two models is because they can identify just one of the many potential OD matrices that reflect travel times and link volumes equally well. Second, the "closeness" of the calibrated matrices to the "true" matrix was quantified using Equation 7.1. The closeness measures for the EKF_LTT and EKF_ODTT algorithms were 0.25 and 0.08 for the first thirty minute period, respectively and 0.23 and 0.11 for the second period, respectively. Unlike the results for the I-10 freeway test network, the EKF_ODTT performs better in that it provide a calibrated OD matrix that is "closer" to the true OD matrix for the both time periods.

Finally, the results indicate that both models can adequately replicate the "true" traffic conditions even though the calibrated OD matrices are not identical to the "true" OD matrices, as shown in Figures 7.26 through 7.31 in the following section. It is hypothesized that this occurs because the bi-level process keep searching the best parameters as well as calibrating an OD matrix until the difference between true and

simulated travel times falls within an acceptable range. Therefore, on the case study network where the shift from congested to less congested traffic conditions needs to be made, more aggressive behavior parameters are likely to be identified in order to reduce a certain portion of this difference.

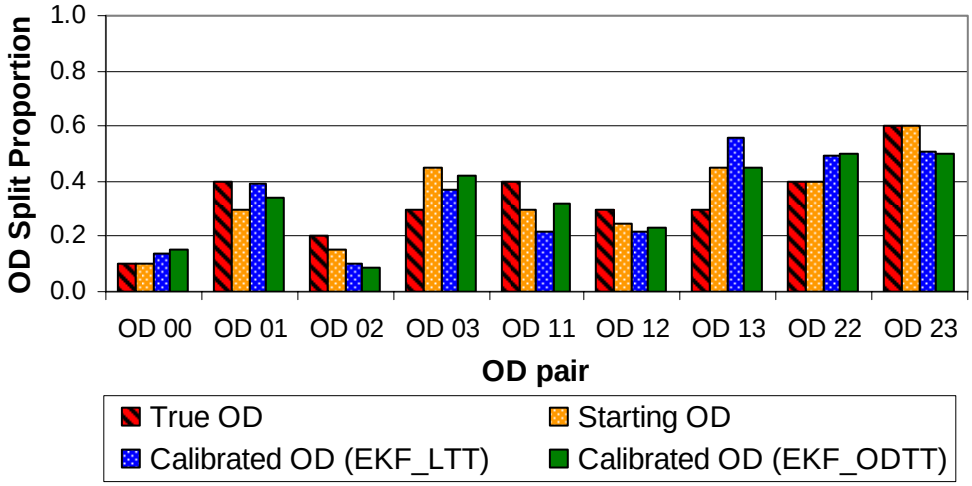

FIGURE 7.24 Calibrated OD Split Proportion for the Case Study Network (7:00AM~7:30AM)

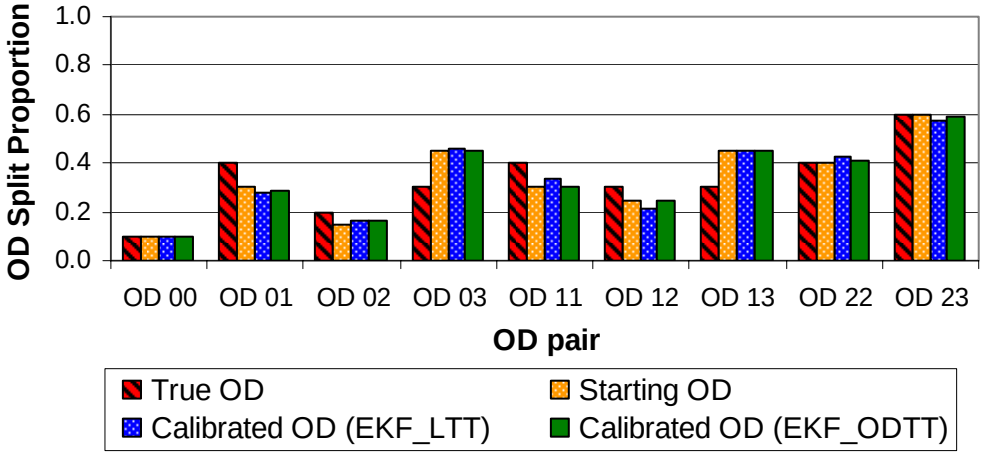

FIGURE 7.25 Calibrated OD Split Proportion for the Case Study Network (7:30AM~8:00AM)

TABLE 7.11 True, Starting, and Calibrated OD Split Proportions at Each Iteration from the EKF_LTT Algorithm for the Case Study Network

Time Interval	OD Pair	True	Starting	1	2	3	Diff*
7:00~7:30	00	0.10	0.10	0.11	0.13	0.14	0.04
	01	0.40	0.30	0.31	0.39	0.39	-0.01
	02	0.20	0.15	0.14	0.10	0.10	-0.10
	03	0.30	0.45	0.43	0.38	0.37	0.07
	11	0.40	0.30	0.30	0.21	0.22	-0.18
	12	0.30	0.25	0.21	0.23	0.22	-0.08
	13	0.30	0.45	0.49	0.56	0.56	0.26
	22	0.40	0.40	0.46	0.49	0.49	0.09
	23	0.60	0.60	0.54	0.51	0.51	-0.09
7:30~8:00	00	0.10	0.10	0.10	0.10	0.10	0.00
	01	0.40	0.30	0.30	0.28	0.28	-0.12
	02	0.20	0.15	0.15	0.16	0.16	-0.04
	03	0.30	0.45	0.45	0.46	0.46	0.16
	11	0.40	0.30	0.30	0.34	0.34	-0.06
	12	0.30	0.25	0.25	0.22	0.21	-0.09
	13	0.30	0.45	0.45	0.45	0.45	0.15
	22	0.40	0.40	0.40	0.42	0.43	0.03
	23	0.60	0.60	0.60	0.58	0.57	-0.03

* Difference between the true and final OD split proportions

TABLE 7.12 True, Starting, and Calibrated OD Split Proportions at Each Iteration from the EKF_ODTT Algorithm for the Case Study Network

Time Interval	OD Pair	True	Starting	1	2	Diff*
7:00~7:30	00	0.10	0.10	0.11	0.12	0.02
	01	0.40	0.30	0.44	0.43	0.03
	02	0.20	0.15	0.07	0.07	-0.13
	03	0.30	0.45	0.38	0.37	0.07
	11	0.40	0.30	0.15	0.15	-0.25
	12	0.30	0.25	0.35	0.34	0.04
	13	0.30	0.45	0.50	0.51	0.21
	22	0.40	0.40	0.41	0.44	0.04
	23	0.60	0.60	0.59	0.56	-0.04
7:30~8:00	00	0.10	0.10	0.10	0.10	0.00
	01	0.40	0.30	0.31	0.31	-0.09
	02	0.20	0.15	0.15	0.14	-0.06
	03	0.30	0.45	0.45	0.45	0.15
	11	0.40	0.30	0.30	0.30	-0.10
	12	0.30	0.25	0.23	0.22	-0.08
	13	0.30	0.45	0.47	0.48	0.18
	22	0.40	0.40	0.44	0.46	0.06
	23	0.60	0.60	0.56	0.54	-0.06

* Difference between the true and final OD split proportions

7.2.5 Travel Time Distribution

The travel time histograms from the EKF_LTT algorithm for AVI sections 01, 12, and 23 were plotted in Figures 7.26, 7.27, and 7.28, respectively. Also shown are *p*-values for the Kolmogorov-Smirnov statistical test as well as the travel time MAER. As before two graphs are shown in each figure. Graph a (left hand side) shows the true and simulated travel time distributions for the EKF_LTT algorithm while graph b shows the results for the EKF_ODTT algorithm after the final iteration.

The results clearly illustrate that both models provide nearly identical results to the true travel time distributions. For all three AVI sections, the *p*-values are 0.066, 0.191, and 0.051 for the EKF_LTT algorithm, respectively and the *p*-values are 0.124, 0.077, and 0.091 for the EKF_ODTT algorithm, respectively. Therefore, the equalities of the true and simulated travel time distributions for all three AVI sections are supported at a 95 percent confidence level.

It may be seen that a marked improvements for AVI sections 12 and 23 are achieved as compared to the starting traffic conditions that were shown in Figures 7.17 through 7.19. These results are further supported by the cumulative distribution functions for AVI sections 12 and 23 that are shown in Figures 7.30 and 7.31. The cumulative fractions of the "starting" traffic conditions, which are strictly less than those of the true at iteration 0, closely match the cumulative fractions of the true traffic conditions after the final iteration. From these figures, other information on the true and starting travel time can be derived. It can be seen from that the travel time data for the starting traffic conditions span much a wider and higher range of values at iteration 0. This implies that the simulated travel times have higher means and variance. However, after the final iteration, the cumulative fractions converge to those of the true travel times.

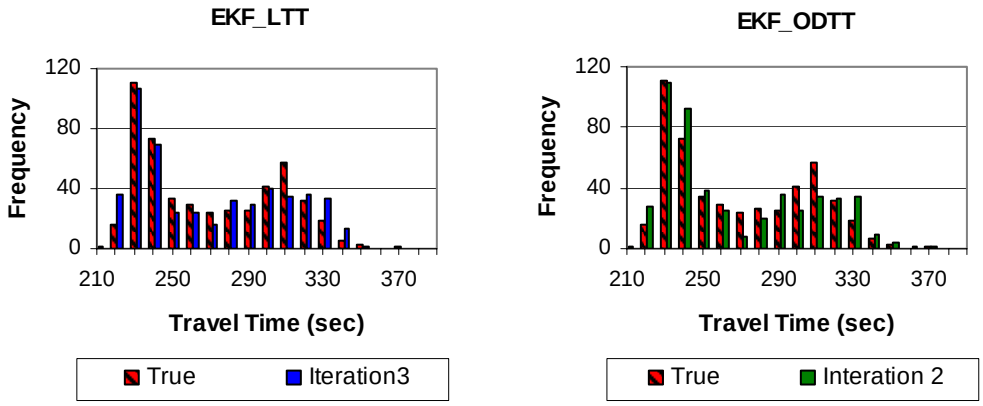

(a) MAER: 0.003 *p*-value: 0.066 (b) MAER: 0.014 *p*-value: 0.124

FIGURE 7.26 Histogram of Travel Time for AVI Section 01 of the Case Study Network

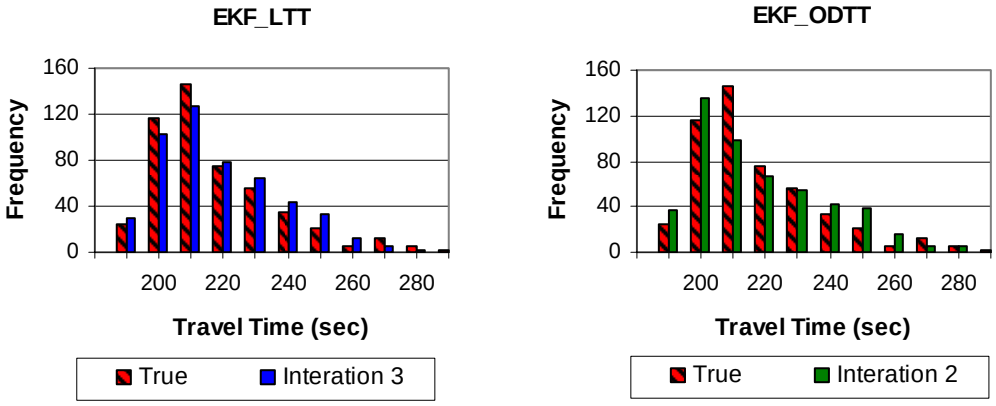

(a) MAER: 0.007 *p*-value: 0.191 (b) MAER: 0.072 *p*-value: 0.077

FIGURE 7.27 Histogram of Travel Time for AVI Section 12 of the Case Study Network

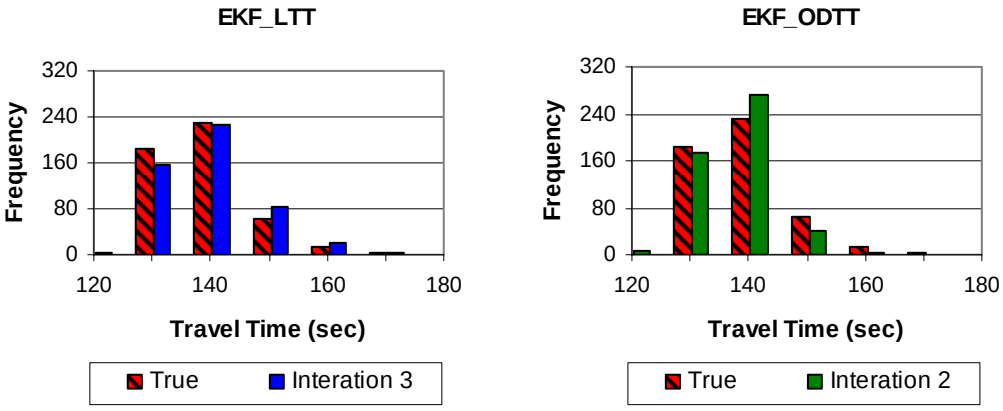

(a) MAER: 0.011 *p*-value: 0.051 (b) MAER: 0.020 *p*-value: 0.091

FIGURE 7.28 Histogram of Travel Time for AVI Section 23 of the Case Study Network

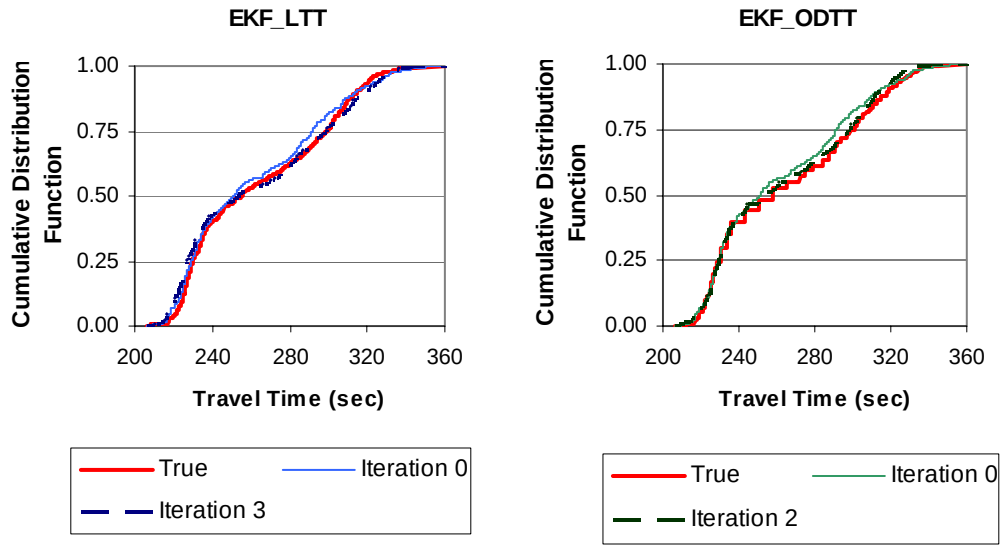

FIGURE 7.29 Travel Time Cumulative Distribution Function for AVI Section 01 of the Case Study Network

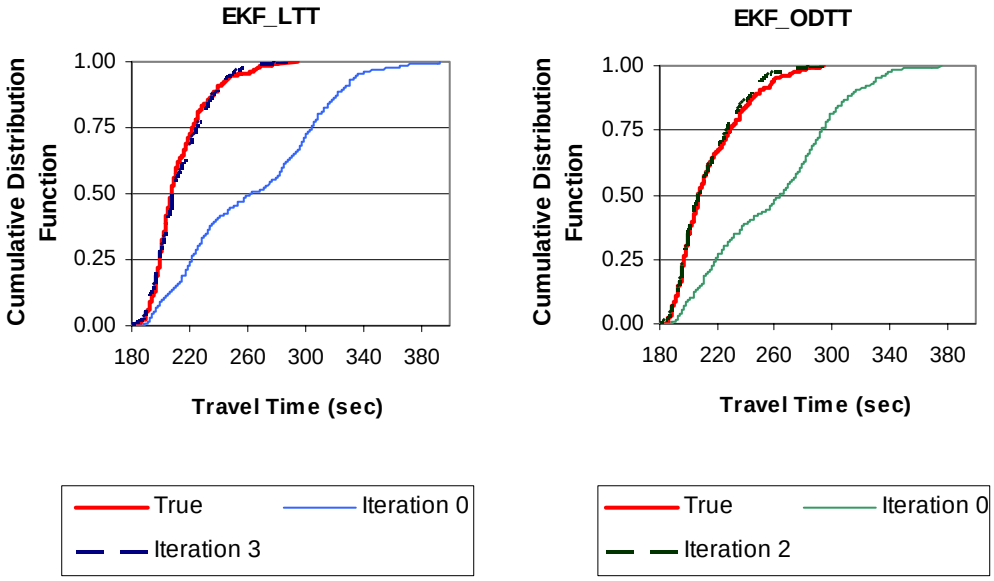

FIGURE 7.30 Travel Time Cumulative Distribution Function for AVI Section 12 of the Case Study Network

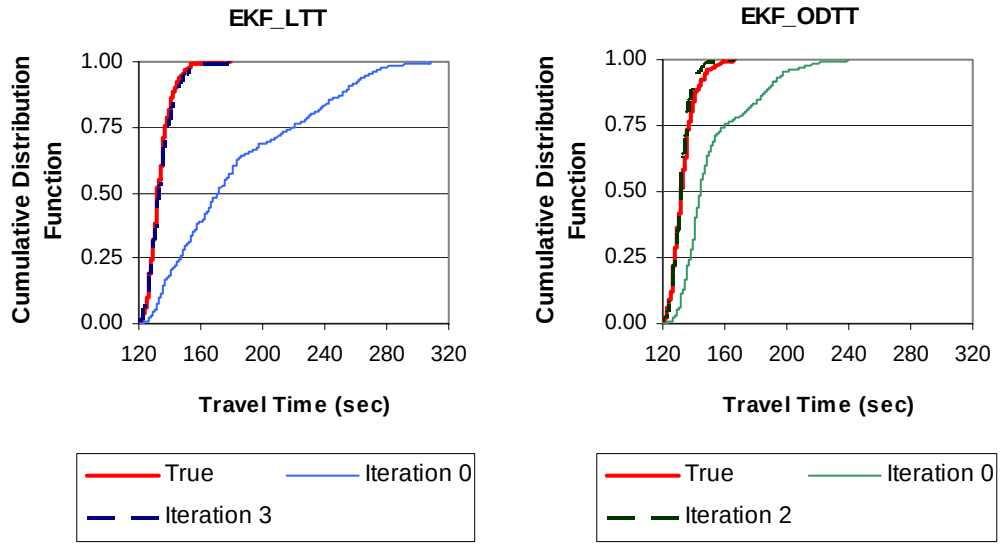

FIGURE 7.31 Travel Time Cumulative Distribution Function for AVI Section 23 of the Case Study Network

7.3 CONCLUDING REMARKS

In this chapter, the two bi-level calibration algorithms (EKF_LTT and EKF_ODTT) proposed in Chapter VI were applied to the I-10 freeway test network in order to evaluate their abilities to replicate observed traffic conditions. The simulated outputs were compared to the observed data. They included: 1) average travel time for the AVI section; 2) average travel time for each OD pair; 3) initial and calibrated OD matrix; and 4) individual travel time distribution.

The results clearly indicated that neither algorithm could replicate the observed conditions by only calibrating the driver behavior parameter set. By adopting the bi-level calibration process, both models provided nearly identical results after several iterations, in terms of average travel times for the AVI sections as well as for the OD pairs.

The analysis of the calibrated OD matrix provided some insights into the effects of changes in OD matrix on average travel times. The results showed that the OD matrix was adjusted such that travel times for AVI sections 12 and 23 were increased, where a shift from less congested to congested traffic conditions needed to be made.

Although there were some improvements in individual travel time distributions as a result of calibrating the OD matrix using the bi-level approach, no case was found that provides statistically valid travel time distributions for all three AVI sections. It was hypothesized that this was because the simulation input data were compiled from the dataset collected for multiple days. Consequently, a simulation case study was conducted where all the underlying information was assumed to be known *a priori*. The bi-level approaches were run using synthetic "true" data, and a calibrated OD matrix and parameter set were obtained. These were then compared to the true values.

The results of the case study demonstrated that both models provided nearly identical results to the "true" traffic conditions. More importantly it was found that the simulated travel time distributions were statistically equivalent to the "true" distributions for all three AVI sections.

CHAPTER VIII

SUMMARY AND CONCLUSIONS

8.1 SUMMARY

The problem statement of this dissertation identified three main needs: 1) the need to incorporate disaggregate ITS data into the calibration of microscopic traffic simulation models; 2) the need to adopt a statistically based calibration objective function to account for disaggregate data; 3) the need to perform simultaneous calibration of driver behavior parameters and the OD matrix. A summary of how these needs is addressed in this dissertation and the conclusions are provided in the following subsections.

8.1.1 Incorporating Disaggregate ITS Data into the Calibration of Microscopic Traffic Simulation Models

With the recent widespread deployment of intelligent transportation system (ITS) there is an abundance of data on traffic systems. Even though ITS data have been utilized to some extent in the calibration of microscopic traffic simulation models, most effort has focused on improving the quality of the calibration based on aggregate form of ITS data rather than disaggregate data. It was hypothesized that the use of disaggregate data in the calibration improves the ability of the model to replicate reality because all parts of disaggregate data have specific qualities which represent stochastic attributes of observed traffic conditions. In this dissertation, travel times in the form of a distribution derived from Automatic Vehicle Identification (AVI) data were used as performance measures to be replicated, as opposed to simple measures of central tendency such as the mean. They are not only key features associated with existing traffic conditions but also are of critical interest of most drivers.

Even though AVI data has been increasingly used as a main source of travel time data, there is a chance that the AVI data contains errors. Consequently, the data needs to be filtered out to ensure that a suspected observation is removed for use in the calibration of microscopic traffic simulation models. The purpose of Chapter IV was to evaluate the existing AVI travel time filtering algorithms and to develop a filtering algorithm to account for the sudden onset of congestion during peak hours. The existing filtering algorithms included: 1) simple moving average; 2) simple moving average plus median; 3) TranStar TMC algorithm; and 4) TransGuide TMC algorithm. To evaluate the existing filtering algorithms, travel time data were derived from the AVI dataset collected along the I-10 freeway corridor in Houston, Texas. To overcome the deficits found in the evaluation of the existing filtering algorithm, a better algorithm was proposed such that underlying increasing or decreasing trends in AVI travel time observations can be traced better.

8.1.2 Adopting a Statistically Based Calibration Objective Function to Account for Disaggregate Data

In the calibration of microscopic traffic simulation models, the indicators that measure how well the simulation model is performing have been computed based on an average of travel time or volume counts on a specific link. However, these types of indicators can not sufficiently address certain aspects of observed traffic conditions. Therefore, in order to accurately replicate the dynamics of observed traffic conditions, a methodology for incorporating disaggregate data in the calibration of microscopic traffic simulation models needs to be developed. In this dissertation, a statistically based approach, which is based on a more disaggregate form of the observed travel time, was proposed in Chapter V. This approach was used to identify the best model parameter set by comparing the observed travel time distribution with the simulated travel time distribution. Specifically, the “consistency” between the observed and simulated travel time distributions was chosen as the objective function in the calibration process.

A statistically based approach was applied to one arterial (Bellaire Boulevard) and one freeway (I-10 freeway) test networks located to west of downtown in Houston, Texas. When the traffic conditions have large variability and a highly non-normal distribution, the use of parametric statistical test is questionable because they are based on some assumptions such as normality. It was found that the distributions of observed travel times on the two test networks violated these assumptions to some extent. Therefore, a non-parametric or distribution-free statistical approach was used because it does not require *a priori* assumptions about the distribution of the underlying population. In this dissertation, the Kolmogorov-Smirnov (KS) test was selected to check whether the observed and simulated data have the same travel time distribution. Not only was the resulting *p*-value from the KS test used to identify best model parameter set, it was also used in an automated calibration methodology, where the Genetic Algorithm (GA) operates on the principle of natural selection and genetics.

Several advantages were identified for the use of a statistically based calibration objective function as a performance indicator. They included: 1) it defines what the "consistency" means; 2) it provides insight of how the "consistency" is quantified; 3) it provides a performance indicator that is easy to understand and simple to interpret; and 4) the robustness of a statistically based objective function increases if datasets in multiple time-space measurement points are available.

8.1.3 Calibrating Driver Behavior Parameters and the OD Matrix Simultaneously

The interdependent relationship between travel demands and driver behavior parameters has not been taken into account in the calibration of microscopic traffic simulation models. The estimation of the OD matrix has been considered as a preliminary step to obtain the fixed travel demands that are used as inputs to microscopic traffic simulation models, rather than as variables to be adjusted in the calibration process. However, under certain situations, it is not possible to identify an appropriate parameter set that can replicate reality by only calibrating driver behavior parameters.

A methodology in which the OD matrix and driver behavior parameters are calibrated simultaneously using a bi-level approach was presented in Chapter III. In a bi-level approach, driver behavior parameters and the OD matrix are calibrated iteratively. The upper phase seeks to minimize the difference between observed and simulated traffic conditions by adjusting driver behavior parameters, while the OD matrix is calibrated in the lower phase. To accomplish this purpose, detailed mathematical models were established in Chapter VI.

It was hypothesized that inclusion of travel time information into the calibration of the OD matrix makes the simulation model replicate the observed traffic conditions better. To accomplish this purpose, the complex relationship between travel time data and the OD matrix should be identified first. However, it is difficult to write a closed form solution. Therefore, in this dissertation the Extended Kalman Filter algorithm (EKF) that can handle nonlinear system based on a linear approximation was selected to formulate this relationship. In addition, the issues relating to the estimation of the OD matrix were discussed. They included: 1) the estimation of the initial OD matrix using the Kalman filter algorithm; 2) the enforcement of non-negativity and equality constraints; 3) the estimation of error variance covariance matrices using a historical AVI dataset; and 4) the estimation of the derivative matrix of travel time connection matrix in the EKF formulation.

The proposed method was applied to the I-10 freeway test network, where to evaluate the effects of including two types of the travel time data (AVI link travel time and AVI OD travel time) on the calibration accuracy the results were analyzed with respect to four different categories; 1) the average AVI section travel time; 2) the average OD travel time; 3) the calibrated OD matrix; and 4) the travel time distribution.

8.2 CONCLUSIONS

This dissertation resulted in a number of findings. The following are the more important conclusion and findings:

- The existing AVI travel time filtering algorithms did not trace underlying trends of increasing and decreasing travel times and result in the subsequent observation removed from the valid travel time data set.
- A better method was proposed such that 1) it can represent underlying trends of travel time observations; 2) it can respond better when sudden changes in traffic conditions; and 3) it can reduce the chance of excluding valid travel time observations falsely.
- The non-parametric statistical calibration objective function successfully explored the observed travel time distribution on the Bellaire arterial test network. In addition to the reduction in travel time MAER (21 percent) compared to default values, the calibration results indicated that the statistically based approach gave much superior results to those of simple metrics. Simple metrics are not robust enough to identify parameters that replicate the actual travel time distribution.
- The non-parametric statistical approach identified a large number of statistically valid parameter set. Therefore, the analyst can bring their own knowledge for additional analysis to identify the best parameter set among the candidate parameter sets.
- The application results of the statistical approach on the I-10 freeway test network indicated that it is not possible to identify an appropriate parameter set that can mimic the travel time distributions for entire AVI links by only calibrating driver behavior parameters.
- The bi-level calibration results demonstrated that the marked improvement can be achieved by calibrating the OD matrix and driver behavior parameters simultaneously. Specifically, both models (EKF_LTT and EKF_ODTT

algorithms) provided the average AVI section travel times and the average OD travel times nearly identical to the observed data after several iterations. Even though it was not possible to replicate statistically valid travel time distributions for entire AVI sections, there were also noticeable improvements in travel time distributions.

- The results of the case study, where all information were assumed to be known, indicated that both models provides the travel time distribution that are statistically equivalent to the true distributions.

8.3 FUTURE RESEARCH

Even though this dissertation contributes to the literature on the calibration of microscopic traffic simulation models in several way, there are a number of topics for the future research:

- Removing outliers from AVI data is an important task to obtain reliable AVI travel time data. A model that responds to sudden onset of congestion was proposed in order to filter out AVI data in the first step of the research. However, the model was applied to AVI data from five weekdays. Future studies should be performed to verify the performance of the model with a larger amount of AVI data and under various traffic conditions. In addition, further research on a robust indicator that accurately captures changes in traffic conditions is required.
- In this dissertation, the Kolmogorov-Smirnov test was selected as a statistical test to check whether the simulated and observed travel time distributions are statistically identical or not. More research regarding the use of different statistical tests are necessary.
- The bi-level calibration process was applied to the freeway network with four AVI stations. Future studies can check the performance of the bi-level calibration approach with longer freeway networks. In addition, it is recommended that the bi-level calibration be applied to an arterial network.

- In this dissertation the application of the bi-level calibration process was limited to the congested network. It is recommended that further research be performed at a variety of congestion levels.
- The maximum and minimum allowable values of the selected driver behavior parameters were based on engineering judgment in this dissertation. These values determined the parameter space to be searched in the Genetic Algorithm. To reduce computational challenge, future studies concerning the selection of allowable ranges should be performed.

REFERENCES

1. Dixon, M. *Incorporating of Advanced Vehicle Identification Data into the Synthetic OD Estimation Process*. Ph.D. dissertation, Texas A&M University, College Station, 2000.
2. Bureau of Public Roads. *Traffic Assignment Manual*. U.S. Department of Commerce, Urban Planning Division, Washington D.C., 1964.
3. Spiess, H. Conical Volume Density Functions. *Transportation Science*, Vol. 24, No. 2, 1990, pp. 153-158.
4. Chui, C. K. *Kalman Filtering: With Real-Time Applications*. Springer, New York, 1999.
5. Welch, G. and G. Bishop. *An Introduction to the Kalman Filter*. TR 95-041, 2004. [http://www.cs.unc.edu/~welch]
6. Welch, G. and G. Bishop. *An Introduction to the Kalman Filter*. ACM SIGGRAPH, 2001.
7. Gartner, N. H., C. J. Messer, and A. K. Rathi. *Traffic Flow Theory*. Oak Ridge National Laboratory, Oak Ridge, TN, 1997.
8. Diekmann, J. K. A *Modeling for Evaluation Network Impacts of Operational-Level Transportation Projects*. M.S. thesis, Virginia Polytechnic Institute and State University, Blacksburg, VA, 2000.
9. Druitt, S. An Introduction to Microsimulation. *Traffic Engineering and Control*, Vol. 39, No. 9, September 1998, pp. 480–483.
10. Choa, F., and R. Milam. *Recommended Guidelines for the Calibration and Validation of Traffic Simulation Models*. Fehr and Peers Transportation Consultants.
    http://www.fehrandpeers.com/Papers/Guidlines_traff_simulation.pdf. Accessed January, 2006.
11. *VISSIM User Manual–version 4.00*. PTV Planung Transport Verkehr AG, Karlsruhe, Germany, 2004.

12. Bloomberg, L., and J. Dale. Comparison of VISSIM and CORSIM Traffic Simulation Models on a Congested Network. In *Transportation Research Record 1727*, Transportation Research Board, National Research Council, Washington, D.C., 2000, pp. 25-60.
13. Wiedemann, R. *Simulation des Verkehrsflusses*. Schriftenreihe des Instituts für Verkehrswesen, Heft 8, Universität (TU), Karlsruhe, Germany, 1974.
14. Wiedemann, R. Modeling of RTI-Elements on multi-lane roads. In *Advanced Telematics in Road Transport* (edited by the Commission of the European Community, DG XIII), Brussels, 1991.
15. Schulze, T, and T. Fliess. Urban Traffic Simulation with Psycho-Physical Vehicle-Following Models. *Proceedings of the 1997 Winter Simulation Conference*, Atlanta, GA 1997, pp. 1222-1228.
16. Fritzsche, H. A model for traffic simulation. *Traffic Engineering and Control*, Vol. 35, No. 5, 1994. pp. 317-321.
17. *CORSIM User's Guide*. FHWA, U.S. Department of Transportation, Washington, D.C., 2001.
18. Wicks, D. A., and E. B. Lieberman. *Development and Testing of INTRAS, a Microscopic Freeway Simulation Model Vol. 1 Program Design, Parameter Calibration and Freeway Dynamics Component Development*. Report FHWA/RD-80/106. FHWA, U.S. Department of Transportation, Washington, DC, 1980.
19. Aycin, M. F., and R. F. Benekohal. Comparison of Car-Following Models for Simulation. In *Transportation Research Record 1678*, Transportation Research Board, National Research Council, Washington, D.C., 1999, pp. 116–127.
20. Halati, A., H. Lieu, and S. Walker. CORSIM-Corridor Traffic Simulation Model. In *Traffic Congestion and Traffic Safety in the 21st Century: Challenges, Innovations, and Opportunities*, American Society of Civil Engineers (ASCE), Chicago, IL, 1997, pp. 570–576.

21. Skabardonis, A. Simulation of Freeway Weaving Areas. In *Transportation Research Record 1802*, Transportation Research Board, National Research Council, Washington, D.C., 2002, pp. 115–124.

22. Rakha, H., and B. Crowther. Comparison of Greenshields, Pipes, and Van Aerde Car-Following and Traffic Stream Models. In *Transportation Research Record 1802*, Transportation Research Board, National Research Council, Washington, D.C., 2002, pp. 248–262.

23. Fox, K. A., and R. Liu. Simulation Modelling Applied Road Transport European Scheme Tests. Institute for Transporation Studies at University of Leeds. 1999. http://www.its.leeds.ac.uk/projects/smartest/finrep.PDF. Accessed December, 2005.

24. Chundury S., and B. Wolshon. Evaluation of CORSIM Car-Following Model by Using Global Positioning System Field Data. In *Transportation Research Record* 1710, Transportation Research Board, National Research Council, Washington, D.C., 2000, pp. 114-121.

25. Fellendorf, M., and P. Vortisch. Validataion of the Microscopic Traffic Flow Model VISSIM in Different Real-World Situations. In *Transportation Research Board 80th Annual Meeting Compendium of Papers* (CD-ROM), Transportation Research Board, National Research Council, Washington, D.C., 2001.

26. Gartner, N. H., C. J. Messer, and A. K. Rathi. *Traffic Flow Theory*. Oak Ridge National Laboratory, Oak Ridge, TN, 1997.

27. Kim, K. *Optimization Methodology for the Calibration of Transportation Network Micro-Simulation Models*. Ph.D. dissertation, Texas A&M University, College Station, 2002.

28. Park, B. B., and H. Qi. *Development and Evaluation of a Calibration and Validation Procedure for Microscopic Simulation Models*. Report VTRC 05-CR1, Virginia Transportation Research Council, Charlottesville, VA, 2004.

29. Cheu, R. L., W. W. Recker, and S. G. Ritchie. Calibration of INTRAS for simulation of 30-sec loop detector output. In *Transportation Research Record 1457*, Transportation Research Board, National Research Council, Washington, D.C., 1994, pp. 202-215.

30. Cheu, R. L., X. Jin, K. C. Ng, Y. L. Ng, and D. Srinivasan. Calibration of FREESIM for Singapore Expressway Using Genetic Algorithm. *Journal of Transportation Engineering*, ASCE, December 1998, pp. 526-535.

31. Ma, T. and B. Abdulhai. Genetic Algorithm-Based Optimization Approach and Generic Tool for Calibrating Traffic Microscopic Simulation Parameters. In *Transportation Research Record 1800*, Transportation Research Board, National Research Council, Washington, D.C., 2002, pp. 6–15.

32. Lee, D., X. Yang, and P. Chandrasekar. Parameter Calibration for PARAMICS Using Genetic Algorithm. In *Transportation Research Board 80th Annual Meeting Compendium of Papers* (CD-ROM), Transportation Research Board, National Research Council, Washington, D.C., 2001.

33. Park, B., and J. D. Schneeberger. Microscopic Simulation Model Calibration and Validation: A Case Study of VISSIM for a Coordinated Actuated Signal System. In *Transportation Research Board 81^{s} Annual Meeting Compendium of Papers* (CD-ROM), Transportation Research Board, National Research Council, Washington, D.C., 2002.

34. Rakha, H., M. Van Aerde, L. Bloomberg, and X. Huang. Construction and Calibration of a Large-Scale Microsimulation Model of the Salt Lake Area. In *Transportation Research Record* 1644, Transportation Research Board, National Research Council, Washington, D.C., 1998, pp. 93-102.

35. Kim, K. and L. R. Rilett. Simplex Based Calibration of Traffic Microsimulation Models Using ITS Data. In *Transportation Research Record* 1855, Transportation Research Board, National Research Council, Washington, D.C., 2003, pp. 80-89.

36. Gomes, G., A. May, and R. Horowitz. A Microsimulation Model of a Congested Freeway Using VISSIM. In *Transportation Research Record* 1876, Transportation Research Board, National Research Council, Washington, D.C., 2004, pp. 71-81.

37. Liu, S. S., and J. D. Fricker. Estimation of a Trip Table and the Theta Parameter in a Stochastic Network. *Transportation Research* A, Vol. 30, No. 4, 1996, pp. 287-305.

38. Yang, H., G. Meng, and M. G. H. Bell. Simultaneous Estimation of the Origin-Destination Matrices and Travel-Cost Coefficient for Congested Networks in a Stochastic User Equilibrium. *Transportation Science*, Vol. 35, No. 2, 2001, pp. 107-123.

39. Ben-Akiva, M. E., D. Darda, M. Jha, H. Koutsopoulos, and T. Toledo. Calibration of Microscopic Traffic Simulation Models with Aggregate Data. In *Transportation Research Record* 1876, Transportation Research Board, National Research Council, Washington, D.C., 2004, pp. 10-19.

40. Darda, D. *Joint Calibration of a Microscopic Traffic Simulator and Estimation of Origin-Destination Flows*, M.S. thesis, Dept. of Civil and Environmental Engineering, Massachusetts Institute of Technology, 2002.

41. Chu, L., H. X. Liu, J. Oh, and W. Recker. A Calibration Procedure for Microscopic Traffic Simulation. In *Transportation Research Board 83rd Annual Meeting Compendium of Papers* (CD-ROM), Transportation Research Board, National Research Council, Washington, D.C., 2004.

42. Armstrong, J. S. and F. Collopy. Error Measures for Generalizing about Forecasting Methods: Empirical Comparisons. *International Journal of Forecasting*, Vol. 8, 1992, 69-80.

43. Armstrong, J. S. *Long-Range Forecasting: From Crystal Ball to Computer*. John Wiley and Sons, New York, 1985.

44. Daigle, G., M. Thomas, and M. Vasudevan. Field Applications of Corsim: I-40 Freeway Design Evaluation, Oklahoma City, OK. In *Proceedings from the 1998 Winter Simulation Conference*, Washington, D.C., 1998, pp. 1161-1168.

45. Horst, R. and P. Pardalos. *Handbook of Global Optimization.* Kluwer Academic Publisher, Boston, 1995.

46. Kurian, M. *Calibration of a Microscopic Traffic Simulator*. M.S. thesis, Massachusetts Institute of Technology, Department of Civil and Environmental Engineering, 2000.

47. Foy, M. D., R. F. Benekohal, and D. E. Goldberg. Signal Timing Determination Using Genetic Algorithms. In *Transportation Research Record* 1365, Transportation Research Board, National Research Council, Washington, D.C., 1992, pp. 108–115.

48. Hadi, M. A., and C. E. Wallace. Hybrid Genetic Algorithm to Optimize Signal Phasing and Timing. In *Transportation Research Record* 1421, Transportation Research Board, National Research Council, Washington, D.C., 1993, pp. 104–112.

49. Abu-Lebdeh, G. and R. F. Benekohal. Development of Traffic Control and Queue Management Procedures for Oversaturated Arterials. In *Transportation Research Record* 1603, Transportation Research Board, National Research Council, Washington, D.C., 1997, pp. 119–127.

50. Park, B., C. J. Messer, and T. Urbanik II. Traffic Signal Optimization Program for Oversaturated Conditions: Genetic Algorithm Approach. In *Transportation Research Record* 1683, Transportation Research Board, National Research Council, Washington, D.C., 1999, pp. 133–142.

51. Park, B., C. J. Messer, and T. Urbanik II. Enhanced Genetic Algorithm for Signal- Timing Optimization of Oversaturated Intersections. In *Transportation Research Record* 1727, Transportation Research Board, National Research Council, Washington, D.C., 2000, pp. 32–41.

52. Abdulhai, B., J. B. Sheu, and W. Recker. *Simulation of ITS on the Irvine Fort Area Using Paramics 1.5 Scalable Microscopic Traffic Simulator: Phase 1: Model Calibration and Validation.* Technical Report, UCB PATH Research Report, 1999.

53. Tom, V. M. and S. Mohan. Transit Route Network Design Using Frequency Coded Genetic Algorithm. *Journal of Transportation Engineering*, Vol. 129, No. 2, 2003, pp. 186–195.

54. Pattnaik, S. B., S. Mohan, and V. M. Tom. Urban Bus Transit Route Network Design Using Genetic Algorithm. *Journal of Transportation Engineering*, Vol. 124, No. 4, 1998, pp. 368–375.

55. Chu, L. and X. Yang. Optimization of the ALINEA Ramp-metering Control Using Genetic Algorithm with Micro-simulation. In *Transportation Research Board 82nd Annual Meeting Compendium of Papers* (CD-ROM), Transportation Research Board, National Research Council, Washington, D.C., 2003.

56. Yin, Y. Genetic-Algorithms-based Approach for Bilevel Programming Models. *Journal of Transportation Engineering*, ASCE, Vol. 126, No. 2, 2000, pp. 115-120.

57. Baek-S, Kim-H, and Lim-Y. Multiple-Vehicle Origin-Destination Matrix Estimation from Traffic Counts Using Genetic Algorithm. *Journal of Transportation Engineering*, Vol. 130, No. 3, 2004, pp. 339-347.

58. Reeves C., and J. Rowe. *Genetic Algorithms: Principles and Perspectives*. Kluwer, Boston, 2002.

59. Saviotti, P. *Applied Evolutionary Economics: New Empirical Methods and Simulation Techniques.* Edward Elgar Publishing, Northampton, MA, 2002.

60. Cremer, M. and Keller, H. A New Class of Dyanamic Methods for the Identification of Origin-Destination Flows. *Transportation Research* B, Vol. 21, No. 2, 1987, pp. 117-132.

61. Van Zuylen, H. J. and L. G. Willumsen. The Most Likely Trip Matrix Estimated from Traffic Counts. *Transportation Research* B, Vol. 14, No. 4, 1980, pp. 281-293.

62. Bell, Michael G. H. Variance and Covariance for Origin-Destination Flows When Estimated by Log-Linear Models. *Transportation Research* B, Vol. 19, No. 6, 1985, pp. 497-507.

63. Cascett, E. and S. Nguyen. A Unified Framework for Estimating or Updating Origin/Destination Matrices from Traffic Counts. *Transportation Research* B, Vol. 22, No. 6, 1988, pp. 437-455.

64. Chen, A., P. Chootinan, W. Recker, and H. M. Zhang. *Development of a Path Flow Estimator for Deriving Steady-State and Time-Dependent Origin-Destination Trip Tables*. Institute of Transportation Studies University of California, Irvine, 2004.

65. Abrahamsson, T. *Estimation of Origin-Destination Matrices Using Traffic Counts–A Literature Survey*. International Institute for Applied Systems Analysis, Austria, 1998.

66. Okutani, I. The Kalman Filtering Approaches in Some Transportation and Traffic Problems. *Proceedings of the 10th International Symposium on Transportation and Traffic Flow*, Elsevier Science, Cambridge, MA, 1987, pp. 397-416.

67. Ashok, K. and M. E. Ben-Akiva. Dynamic Origin-Destination Matrix Estimation and Prediction for Real-Time Traffic Management System. *Proceedings of the 12nd International Symposium on Transportation and Traffic Flow*, Elsevier Science, Berkeley, CA, 1993, pp. 465-484.

68. Van der Zijpp, N. J. and R. Hamerslag. Improved Kalman Filtering Approach for Estimating Origin-Destination Matrices for Freeway Corridors. In *Transportation Research Record* 1443, TRB, National Research Council, Washington, D.C., 1994, pp. 54-63.

69. Debashish B, K. C. Shina, and J. V. Krogmeier. Real-Time Freeway O-D Prediction Algorithm Under ATIS Environment. *Proceedings of the 5th International Conference on Application of Advanced Technologies in Transportation*, Newport Beach, CA, 1998, pp. 147-459.

70. Chang, G. L. and J. Wu. Recursive Estimation of Time-Varying Origin-Destination Flows from Traffic Counts in Freeway Corridors. *Transportation Research* B, Vol. 28, No. 2, 1994, pp. 141-160.

71. Shou-Ren, H., S. M. Madant, J. V. Krogmeier, and S. Peeta. Estimation of Dynamic Assignment Matrices and OD Demands Using Adaptive Kalman Filtering. *ITS Journal*, Vol. 6, 2001, pp. 281-300.

72. Hironori S., T. Nakatsuji, Y. Tanaboriboon, and K. Takahashi. Dynamic Estimation of Origin-Destination Travel Time and Flow on a Long Freeway Corridor. In *Transportation Research Record* 1739, TRB, National Research Council, Washington, DC, 2000, pp. 67-76.

73. Kim, K. and L. R. Rilett. Calibration of Micro-Simulation Supply and Demand Parameters Using a Bi-level Algorithm. *Proceedings of the 7th International Conference on Applications of Advanced Technology in Transportation Conference*, Boston, MA, August 2002, pp 902-909.

74. Kim, W. *An Improved Bus Signal Priority System for Networks with Nearside Bus Stops*. Ph.D. dissertation, Texas A&M University, College Station, 2004.

75. Schultz, G. *Developing a Methodology to Account for Commercial Motor Vehicles Using Microscopic Traffic Simulation Models*. Ph.D. dissertation, Texas A&M University, College Station, 2003.

76. Dion, F., and H. Rakha. Estimating Spatial Travel Times Using Automatic Vehicle Identification Data. In *Transportation Research Board 82nd Annual Meeting Compendium of Papers* (CD-ROM), Transportation Research Board, National Research Council, Washington, D.C., 2003.

77. Jacobson, L. N., N. L. Nihan, and J. D. Bender. Detecting Erroneous Loop Detector Data in a Freeway Traffic Management System. In *Transportation*

Research Record 1287, Transportation Research Board, National Research Council, Washington, D.C., 1990, pp. 151-166.

78. Park, E. S., S. Turner, and C. H. Spiegelman. (2003), Empirical Approaches to Outlier Detection in ITS Data. In *Transportation Research Board 82nd Annual Meeting Compendium of Papers* (CD-ROM), Transportation Research Board, National Research Council, Washington, D.C., 2003.
79. Zietsman, J. *Incorporating Sustainability Performance Measures into the Transportation Planning Process*. Ph.D. dissertation, Texas A&M University, College Station, 2000.
80. Bloomberg, L., and A. D. May. *Simulation Modeling of the Santa Monica Freeway.* California PATH Working Paper, UCB-ITS-PWP-94-14, 1994.
81. Brockfeld, E., R. D. Kühne, and P. Wagner. Calibration and Validation of Microscopic Traffic Flow Models. In *Transportation Research Board 83rd Annual Meeting Compendium of Papers* (CD-ROM), Transportation Research Board, National Research Council, Washington, D.C., 2004.
82. Koplelman, F. S. Prediction with Disaggregate Models: The Aggregation Issue. In *Transportation Research Record* 527, Transportation Research Board, National Research Council, Washington, D.C., 1974, pp. 73-80.
83. Benjamin, J. R., and C. A. Cornell. Probability, Statistics, and Decision for Civil Engineers. McGraw-Hill, New York, 1970.
84. Shultz, G. Developing a Methodology to Account for Commercial Motor Vehicles Using Microscopic Traffic Simulation Models. Texas A&M University, College Station, TX, 2003.
85. Devore, J. L. *Probability and Statistics for Engineering and the Sciences*, 4th Edition, Duxbury Press, Pacific Grove, CA, 1995.
86. O'Connor, P. D. T. *Practical Reliability Engineering*, 4th Edition, John Wiley & Sons Inc., New York, 2002.

87. Press, W. H., S. Teukolsky, W. Vetterling, and B. Flannery. *Numerical Recipes in C: The Art of Scientific Computing.* Cambridge University Press, New York, 2002.

88. *Highway Capacity Manual (HCM)*. TRB, National Research Council, Washington, D.C., 2000.

89. PTV America Inc., VISSIM FAQ, www.english.ptv.de/cgi-bin/traffic/traf_faq.pl, Accessed November, 2005.

90. Ashok, K. *Estimation and Prediction of Time-Dependent Origin-Destination Flows*. Ph.D. dissertation, Massachusetts Institute of Technology, Cambridge, MA, 1996.

91. Brandriss, J. J. *Estimation of Origin-Destination Flows for Dynamic Traffic Assignment*. M.S, thesis, Massachusetts Institute of Technology, Cambridge, MA, 2001.

92. Bell, M. G. H. The Estimation of Origin-Destination Matrices by Constrained Generalized Least Squares. *Transportation Research* B, Vol. 25, No. 1, 1991, pp. 13-22.

93. Van der Zijpp, N. J. and R. Hamerslag. Improved Kalman Filtering Approach for Estimating Origin-Destination Matrices for Freeway Corridors. In *Transportation Research Record* 1443, TRB, National Research Council, Washington, D.C., 1994, pp. 54-63.

94. Nihan, N. L. and G. A. Davis. Recursive Estimation of Origin-Destination Matrix from Input/Output Counts. *Transportation Research* B, Vol. 21, No. 2, 1987, pp. 149-163.

APPENDIX A

PERL AUTOMATED CALIBRATION PROGRAM FOR THE BI-LEVEL APPROACH

The original source code consists of more than 2500 lines. Because of space limitations, the overall structures of Perl program for the bi-level calibration are presented. The focus is placed on describing the tasks that are performed in each sub functions.

```
# Specify user controllable inputs
        number of population ($population)
        number of generation ($generation)
        maximum number of bi-level iteration ($bi)
        probabilities of crossover and mutation($pro_cross, $pro_mutation)
        total number of bits in binary chromosome($bit)
        simulation time interval ($from_time, $to_time)
        number of off-ramp connector($off_ramp)
        number of OD pairs($OD pair)
# Set file names
        input file (*.inp)
        output file (accepted and rejected parameter, p_value and MAER, log file, )
        other files required to run VISSIM (ex. *.ini, *.pua, *.vap)
        observed link travel time file
        observed OD travel time file
        VISSIM output file (*.rsr, *.rsz)

# Open output files and write headings
        print heading (parameters, generation, iteration , p_value, MAER, and etc)

# Define path and directories information
        VISSIM directory "c:/Program Files/PTV_Vision/ViSSIM400/Exe/"
        path “c:\\automated bi level calibration\\”

# Define time varying variables
        Kalman filter variables (observed and estimated split proportion matrix,  link
        choice proportion matrix, origin matrix, traffic count matrix, Kalman ganin
        matrix, and etc)
```

```
# MAIN
{
        sub function: &Read ramp information file;
        sub function: &Read observed link travel time file;
        sub function: &Read observed OD travel time;
        sub function: &Read basic Kalman filter matrix;

        for ($i=$bi;…;…)
        {
            #### GA algorithm ####
            sub function: &Initial; (#generate and test 1st trial candidate chromosomes)
            do
            {
                sub function: &Crossover;
                sub function: &Mutation;
                sub function: &Conversion to real;
                sub function: &VISSIM run;
                sub function: &Statistical test;
                sub function: &Selection;
            } while($generation);

            #### Kalman filter ####
            for ($i=$population;… ;…)
            {
                sub function: &Kalman matrix;
                sub function: &Derivative matrix;
                sub function: &Travel time matrix;
                sub function: &Extended Kalman filter;
            }
            sub function: &Write new OD matrix in VISSIM input file;
        }
}


# sub function &Initial
{
        for ($i=$population;… ;…) { generate binary chromosome; }
        sub function: &Conversion to real;
        sub function: &VISSIM run;
        sub function: &Statistical test;
        sub function: &Selection;
}
```

```
# sub function & Conversion to real
{
        for ($i=$population;…;…)
        {
            convert parameters represented in binary strings to real numbers;
            repeat conversion for all selected parameters;
            compute values of each parameter by taking into account its maximum,
            minimum, and precision;
        }
}


# sub function & VISSIM run
{
        for ($i=$population;…;…)
        {
            open VISSIM *.inp file;
            make new directories for VISSIM run;
            write trial VISSIM behavior parameters in *.inp file;
            run "VISSIM ".$path.$new_dir."\\I10.inp\" -s1" ;
        }
}


# sub function & Statistical test
{
        for ($i=$population;…;…)
        {
            read simulated travel time from *.rsz and *rsr files;
            combine and sort observed and simulated travel times;
            construct simulated CDF;
            construct observed CDF;
            compute Kolmogorov-Smirnov test statistics;
            compute p_value;
            compute MAER;
        }
}
```

```
# sub function & Conversion to real
{
    for ($i=$population;…;…)
    {
        convert parameters represented in binary strings to real numbers;
        repeat conversion for all selected parameters;
        compute values of each parameter by taking into account its maximum,
        minimum, and precision;
    }
}


# sub function & VISSIM run
{
    for ($i=$population;…;…)
    {
        open VISSIM *.inp file;
        make new directories for VISSIM run;
        write trial VISSIM behavior parameters in *.inp file;
        run "VISSIM ".$path.$new_dir."\\I10.inp\" -s1" ;
    }
}


# sub function & Statistical test
{
    for ($i=$population;…;…)
    {
        read simulated travel time from *.rsz and *rsr files;
        combine and sort observed and simulated travel times;
        construct simulated CDF;
        construct observed CDF;
        compute Kolmogorov-Smirnov test statistics;
        compute p_value;
        compute MAER;
    }
}
```

```
# sub function & Selection
{
        for ($i=$population;…;…)
        {
            save trial chromosome information if it pass KS test;
            compute fitness value using p_value;
        }
        compute relative fitness for each accepted chromosomes;
        compute cumulative fitness for all accepted chromosomes;
}


# sub function & Crossover
{
        for ($i=$population/2;…;…)
        {
            choose randomly bit location and bit length for crossover operation;
            select two chromosomes using crossover probability;
            perform crossover operation;
        }
}



# sub function & Mutation
{
        for ($i=$population;…;…)
        {
            choose randomly bit location for mutation operation;
            select one chromosome using mutation probability;
            perform mutation operation;
        }
}
```

sub function & Kalman matrix

```
{
        for ($i=$time_step;…;…)
        {
            create time varying Kalman matrices;
        }
        *observed and estimated split proportion matrix,  link choice proportion matrix,
        origin matrix, traffic count matrix, Kalman ganin matrix, and etc
}
```

sub function & Derivative matrix

```
{
        make new directories for VISSIM run;
        write best behavior parameters in *.inp;
        write OD estimates from previous time step in *.inp;
        run VISSIM;
        obtain simulated travel time(1) ;
        for ($i=$OD pair;…;…)
        {
            make new directories for VISSIM run;
            increase OD matrix by Δ for obtaining partial derivative;
            write OD+ Δ in *.inp;
            run VISSIM;
            obtain simulated travel time(2);
        }
}
```

sub function & Travel time matrix

```
{
        for ($i=$OD pair;…;…)
        {
             compute difference (derivative) between simulated travel times 1 and 2;
        }
        create travel time connection matrix using partial derivative;
        create travel time measurement matrix using observed and travel times 1
}
```

sub function & Extended Kalman filter

{

perform Kalman filter alogorithm based on matrices listed above sub functions;

$$
\begin{aligned}
b^{-}(t) &= b(t-1) \\
P^{-}(t) &= P(t-1) \\
K(t) &= P^{-}(t)H(t)\left(H(t)^{T}P^{-}(t)H(t)+R(t)\right)^{-1} \\
b(t) &= b^{-}(t)+K(t)\begin{pmatrix} v(t) \\ tt(t) \end{pmatrix} - H(t)b^{-}(t) - H(t-1)b^{obs}(t-1) \\
P(t) &= \left(I-K(t)H(t)\right)P^{-}(t)
\end{aligned}
$$

check non-negativity and equality constraints;

}

APPENDIX B

NETWORK SUPPLY AND DEMAND DATA

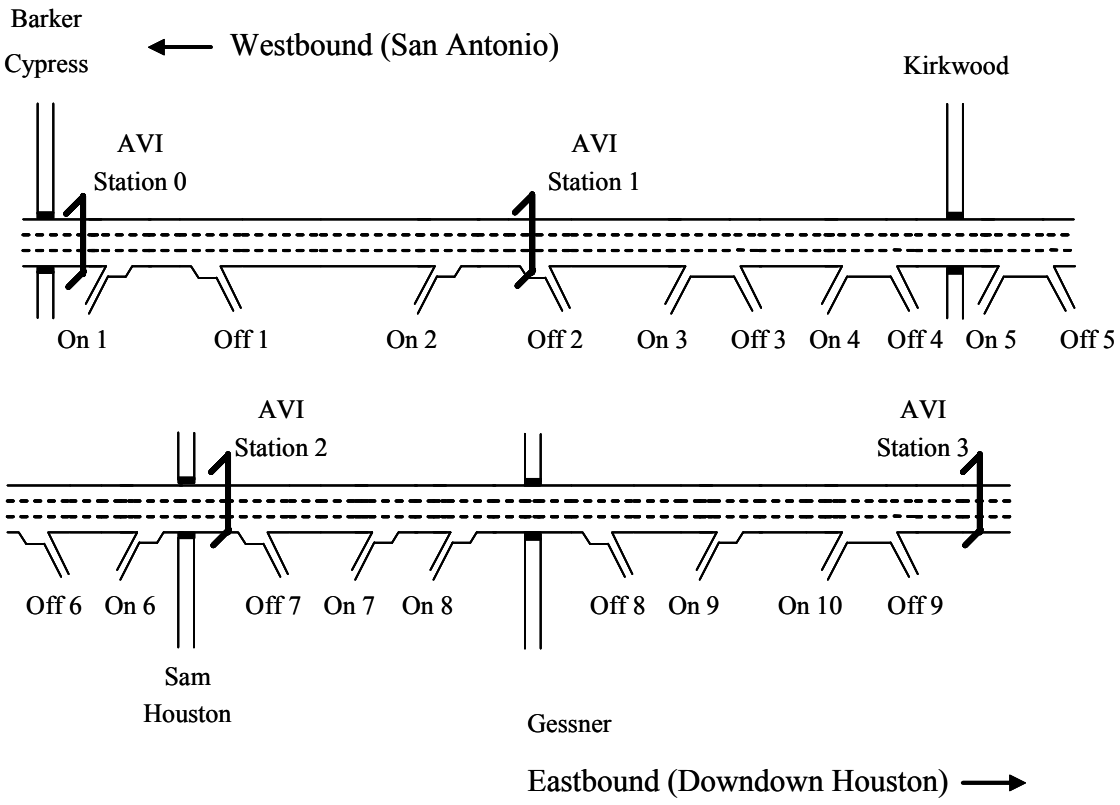

FIGURE B.1 Detailed Layout of the I-10 Freeway Test Network in Houston

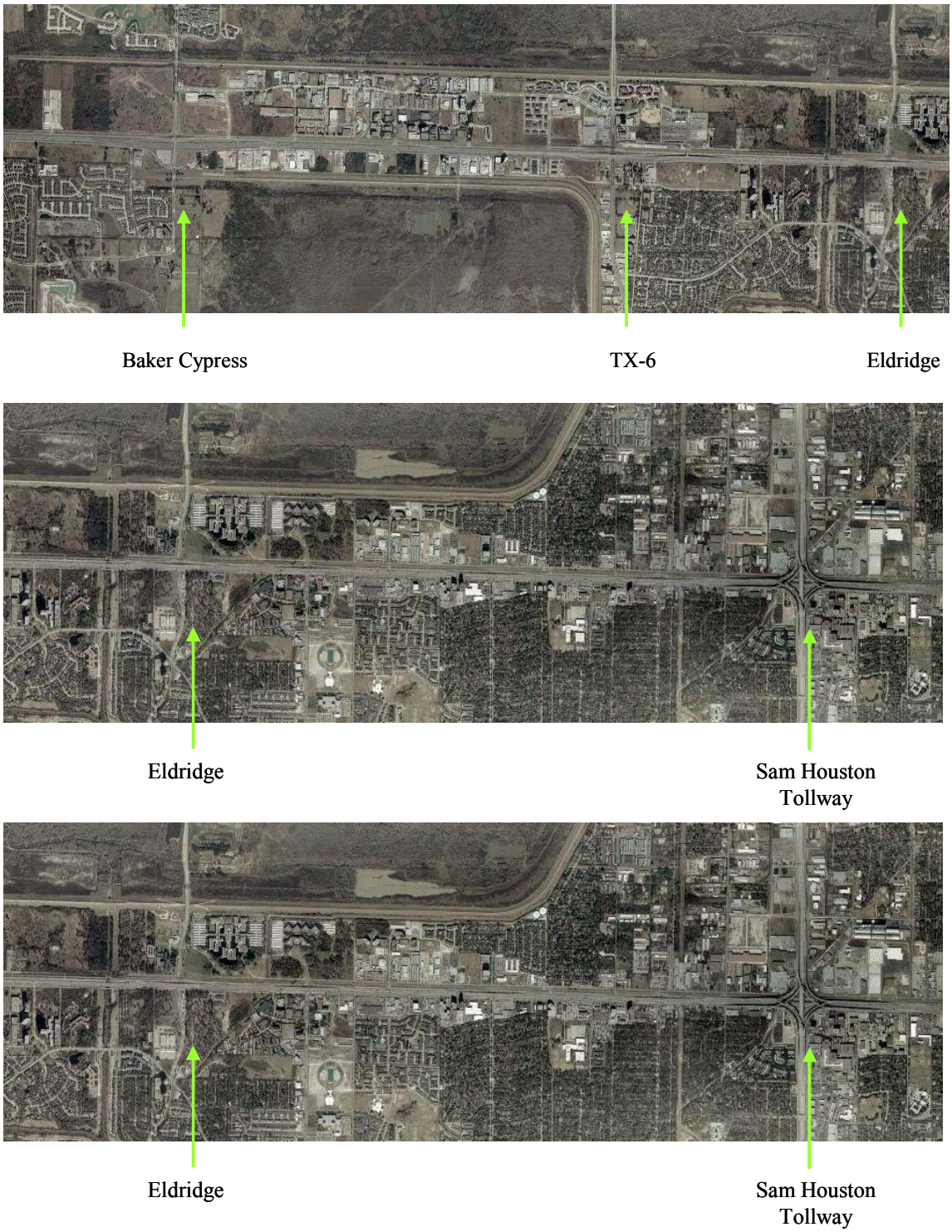

FIGURE B.2 Aerial Photo Map of the I-10 Freeway Test Network in Houston

TABLE B.1 Observed Volume Data for the I-10 Freeway Test Network in Houston

From	To	Link Number (Main or On-ramp)	Volume (veh/hr)		
			6:30~7:00AM	7:00~7:30AM	7:30~8:00AM
Start	AVI 0	10	4069	5296	4174
AVI 0	AVI 1	11	762	929	949
		31	1066	1299	1329
AVI 1	AVI 2	51	777	975	895
		71	797	1000	918
		91	613	769	707
		121	541	679	623
AVI 2	AVI 3	141	744	857	921
		151	757	873	937
		171	927	1069	1147
		181	634	731	785

TABLE B.2 Estimated AVI OD Split Proportion for the I-10 Freeway Test Network in Houston

AVI OD		Time Interval		
Origin	Destination	6:30~7:00AM	7:00~7:30AM	7:30~8:00AM
0	0	0.19	0.20	0.21
0	1	0.43	0.46	0.49
0	2	0.04	0.02	0.03
0	3	0.34	0.32	0.26
1	1	0.58	0.77	0.89
1	2	0.09	0.12	0.11
1	3	0.34	0.11	0.00
2	2	0.59	0.67	0.59
2	3	0.41	0.33	0.41

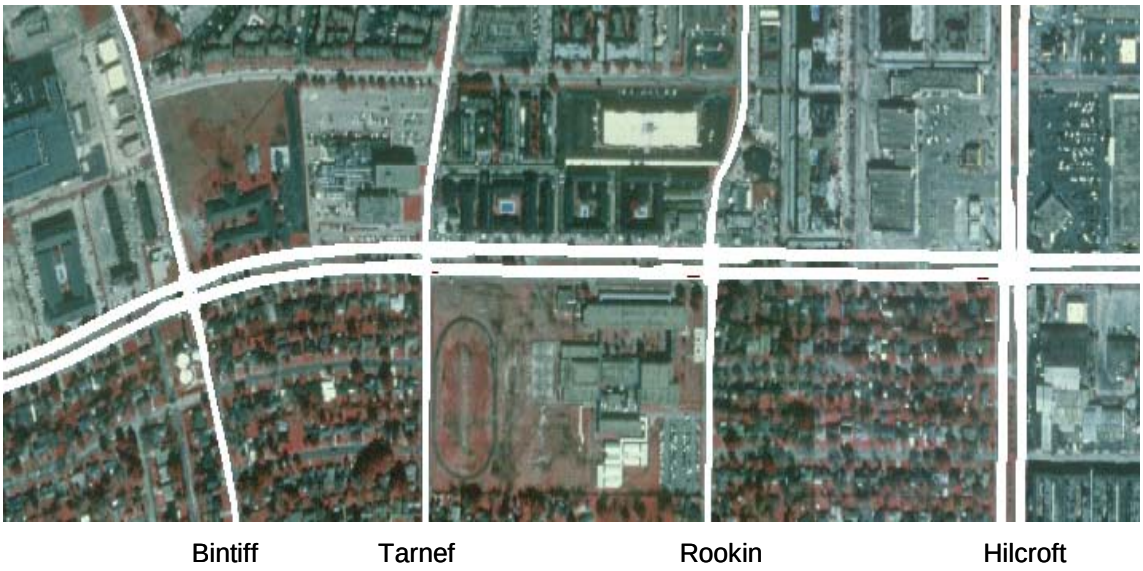

FIGURE B.3 Aerial Photo Map of the Bellaire Arterial Test Network in Houston

* Detailed layout of the Bellaire arterial test network is provided in Section 3.2.1.

TABLE B.3 Observed Volume Data for the Bellaire Arterial Test Network in Houston

Cross Street	Bound	Entering Volume			
		7:30~7:45AM	7:45~8:00AM	8:00~8:15AM	8:15~8:30AM
Bintiff	East	1752	1612	1468	1320
	North	260	184	156	112
	Sourth	160	84	84	72
Tarnef	North	52	40	44	28
	Sourth	48	36	36	28
Rookin	North	232	264	232	168
	Sourth	184	228	276	224
Hilcroft	North	1000	992	1126	1076
	Sourth	648	640	612	552
	West	992	952	976	925

TABLE B.4 Observed Turning Percentage for Each Approach for the Bellaire Arterial Test Network in Houston

Cross Street	Time Interavl	Turning Percentage (%)											
		EB*			NB			SB			WB		
		L**	TH	R	L	TH	R	L	TH	R	L	TH	R
Bintiff	7:30~7:45AM	2	97	1	29	28	43	5	50	45	1	92	6
	7:45~8:00AM	1	98	1	35	22	43	5	19	76	1	95	4
	8:00~8:15AM	1	98	1	33	28	38	5	14	81	2	94	5
	8:15~8:30AM	1	98	2	21	25	54	39	11	50	2	90	8
Tarnef	7:30~7:45AM	1	99	0	38	15	46	58	8	33	0	99	1
	7:45~8:00AM	1	98	0	50	10	40	67	0	33	0	98	1
	8:00~8:15AM	1	99	0	27	27	45	67	11	22	0	99	1
	8:15~8:30AM	1	99	0	29	0	71	71	0	29	0	99	0
Rookin	7:30~7:45AM	3	92	5	17	40	43	15	27	59	13	77	10
	7:45~8:00AM	4	92	3	23	41	36	13	33	54	12	76	12
	8:00~8:15AM	7	90	3	7	55	38	14	32	55	13	71	16
	8:15~8:30AM	9	89	3	10	48	43	13	33	53	7	75	18
Hilcroft	7:30~7:45AM	7	84	9	17	72	12	36	60	4	17	72	10
	7:45~8:00AM	7	87	5	22	66	13	38	53	9	14	69	17
	8:00~8:15AM	10	81	9	17	74	9	32	56	12	16	70	15
	8:15~8:30AM	9	81	9	21	70	9	36	45	19	10	75	16

* EB denotes east bound approach.

** L, TH, and R denote left turn, through, and right turn movements, respectively.

TABLE B.5 Observed Volume Data for the Case Study Test Network in Houston

From	To	Link Number (Main or On-ramp)	Volume (veh/hr)			
			6:30~6:50AM	6:50~7:00AM	7:00~7:10AM	7:10~7:20AM
Start	AVI 0	10	4500	6400	6100	5800
AVI 0	AVI 1	11	750	1200	1150	850
		31	650	750	850	750
AVI 1	AVI 2	51	600	950	1050	900
		71	600	900	1050	900
		91	700	700	850	850
		121	500	500	750	750
AVI 2	AVI 3	141	450	450	500	500
		151	400	400	450	450
		171	700	700	800	800
		181	450	450	500	500

From	To	Link Number (Main or On-ramp)	Volume (veh/hr)			
			7:20~7:30AM	7:30~7:40AM	7:40~7:50AM	7:50~8:00AM
Start	AVI 0	10	5500	5000	4500	4500
AVI 0	AVI 1	11	800	700	700	700
		31	650	600	600	600
AVI 1	AVI 2	51	700	600	600	600
		71	850	800	800	800
		91	750	700	700	700
		121	750	750	700	650
AVI 2	AVI 3	141	500	600	600	600
		151	450	450	500	500
		171	800	800	900	900
		181	500	500	550	550

* The "True" and "Starting" OD split proportions for the case study test network are provided in Chapter VII and Appendix E.

APPENDIX C

STATISTICALLY VALID PARAMETER SETS ON THE BELLAIRE ARTERIAL TEST NETWORK

The definitions of the selected VISSIM parameters are as follows:

P_1	Number of observed preceding vehicles
P_2	Look ahead distance
P_3	Average standstill distance
P_4	Additive part of desired safety distance
P_5	Multiplicative part of desired safety distance
P_6	Lane Change Distance

TABLE C.1 Complete set of Statistically Valid Parameter Sets on the Bellaire Arterial Test Network

No	P1	P2	P3	P4	P5	P6	p_val	MAER
1	1	130	2	5	5	260	0.31	0.06
2	2	240	3	4	4	210	0.08	0.10
3	1	270	2	4	7	280	0.38	0.07
4	4	190	2	5	3	100	0.45	0.02
5	2	240	4	4	4	270	0.13	0.06
6	3	130	1	5	5	80	0.31	0.06
7	3	100	3	4	4	230	0.17	0.05
8	2	240	3	4	4	270	0.17	0.07
9	2	330	1	5	7	250	0.08	0.03
10	2	290	1	8	1	210	0.08	0.02
11	3	310	3	5	2	140	0.10	0.05
12	4	150	2	5	5	260	0.31	0.08
13	3	80	3	5	2	140	0.53	0.08
14	3	90	2	5	4	270	0.78	0.05
15	1	40	4	4	4	290	0.06	0.05
16	3	210	3	5	2	130	0.61	0.03
17	1	90	1	6	6	280	0.17	0.02
18	4	190	2	5	3	90	0.26	0.01
19	2	40	3	4	4	270	0.17	0.01
20	2	90	1	7	2	260	0.08	0.02
21	2	240	3	4	4	260	0.53	0.02
22	0	130	2	5	5	260	0.31	0.06
23	3	130	1	5	3	100	0.21	0.06
24	3	190	2	5	4	230	0.13	0.05
25	4	100	3	4	3	100	0.78	0.03
26	2	230	3	4	4	210	0.61	0.03
27	3	230	4	5	5	80	0.61	0.06
28	4	140	2	5	3	100	0.08	0.06
29	1	240	2	4	7	280	0.17	0.01
30	4	190	2	5	4	100	0.06	0.06
31	1	270	2	4	7	270	0.08	0.06
32	3	300	3	4	4	220	0.31	0.06
33	2	40	3	4	4	280	0.17	0.03
34	4	390	2	5	3	100	0.10	0.03
35	0	270	2	4	7	280	0.13	0.07
36	4	130	1	5	5	80	0.31	0.01
37	3	330	3	5	2	140	0.31	0.06
38	0	100	2	5	5	260	0.61	0.04
39	3	130	1	5	4	80	0.38	0.04
40	3	210	3	4	4	130	0.31	0.06

* p_val : *p*_value from Kolmogorov-Smirnov Test

No	P1	P2	P3	P4	P5	P6	p_val	MAER
41	2	240	3	5	2	260	0.13	0.02
42	1	40	2	5	3	100	0.17	0.06
43	4	180	2	5	3	90	0.31	0.04
44	1	40	4	4	4	230	0.38	0.06
45	3	130	1	5	5	160	0.31	0.06
46	2	240	3	4	4	190	0.26	0.01
47	3	100	3	4	4	100	0.26	0.03
48	1	140	1	5	5	80	0.45	0.03
49	4	190	1	8	1	90	0.53	0.06
50	2	290	2	5	3	210	0.31	0.03
51	3	210	3	5	2	140	0.26	0.06
52	2	330	1	5	7	280	0.06	0.08
53	3	80	1	5	7	130	0.26	0.06
54	3	100	3	4	4	200	0.53	0.03
55	3	310	3	4	4	270	0.45	0.06
56	2	240	3	5	2	140	0.13	0.00
57	2	240	3	4	4	130	0.61	0.06
58	3	310	3	5	2	280	0.21	0.06
59	2	240	3	4	4	280	0.53	0.06
60	2	330	1	5	7	240	0.26	0.02
61	4	110	2	5	5	260	0.26	0.06
62	3	350	3	5	2	140	0.21	0.01
63	2	240	4	5	2	140	0.26	0.06
64	2	380	1	5	7	250	0.38	0.04
65	3	130	2	5	5	80	0.53	0.06
66	4	150	1	5	5	260	0.10	0.07
67	2	210	3	4	4	260	0.08	0.06
68	3	140	1	5	5	80	0.85	0.02
69	3	100	1	4	4	230	0.13	0.06
70	1	270	2	4	4	280	0.70	0.06
71	3	190	2	5	4	280	0.78	0.06
72	1	90	1	6	6	230	0.96	0.03
73	1	270	2	4	7	150	0.31	0.00
74	2	90	1	7	2	270	0.53	0.06
75	3	210	3	10	2	130	0.78	0.06
76	3	140	2	5	3	100	0.38	0.06
77	0	130	2	5	5	140	0.13	0.06
78	4	140	2	5	3	160	0.45	0.04
79	1	130	2	5	4	100	0.31	0.06
80	3	80	3	5	4	140	0.26	0.06
81	3	210	3	5	4	170	0.26	0.06
82	4	130	2	5	5	260	0.06	0.06
83	4	140	2	5	2	130	0.13	0.06
84	2	240	3	5	4	270	0.85	0.03
85	2	250	3	4	4	270	0.06	0.08
86	3	80	3	5	2	270	0.45	0.06
87	2	140	2	5	3	100	0.53	0.06
88	4	150	2	5	5	250	0.78	0.06
89	4	190	2	5	3	110	0.92	0.04
90	3	310	3	5	4	140	0.61	0.06
91	3	190	2	6	6	230	0.70	0.06
92	3	80	3	5	3	160	0.31	0.06
93	2	290	3	4	4	210	0.61	0.06
94	2	290	1	8	1	230	0.17	0.06
95	4	100	3	4	3	90	0.45	0.01
96	2	290	1	8	4	210	0.21	0.06
97	3	80	2	5	4	270	0.13	0.05
98	3	150	2	5	5	260	0.85	0.06
99	1	90	1	6	4	280	0.70	0.06
100	1	290	1	6	6	280	0.08	0.02
101	1	40	2	4	7	280	0.08	0.10
102	0	130	2	5	5	250	0.31	0.06
103	3	90	2	5	4	280	0.53	0.04
104	3	190	2	5	4	290	0.13	0.04
105	2	240	3	4	2	290	0.45	0.06
106	4	340	2	5	3	100	0.38	0.03
107	2	130	2	8	1	210	0.53	0.06
108	2	140	3	4	4	280	0.38	0.03
109	2	190	2	5	7	250	0.61	0.06
110	2	120	3	4	4	260	0.31	0.05
111	3	80	1	7	2	230	0.10	0.02
112	3	90	2	5	4	300	0.70	0.06
113	1	120	1	5	5	210	0.17	0.06
114	3	310	3	5	2	130	0.26	0.02
115	4	310	3	5	2	140	0.45	0.06
116	3	190	4	4	4	230	0.26	0.06
117	2	40	1	5	2	270	0.31	0.06
118	4	190	2	4	3	90	0.26	0.06
119	2	90	2	5	4	210	0.21	0.06
120	4	230	3	4	4	90	0.61	0.06
121	2	40	2	5	4	270	0.26	0.06
122	4	390	3	4	3	100	0.26	0.09
123	2	240	4	4	4	290	0.10	0.06
124	3	190	2	5	4	210	0.31	0.09
125	4	90	2	5	4	100	0.10	0.10
126	3	210	3	5	4	100	0.38	0.06
127	1	240	4	4	4	290	0.17	0.08
128	3	210	3	5	1	130	0.78	0.06

APPENDIX D

CALIBRATION RESULTS FROM THE BI-LEVEL APPROACH FOR THE I-10 FREEWAY TEST NETWORK

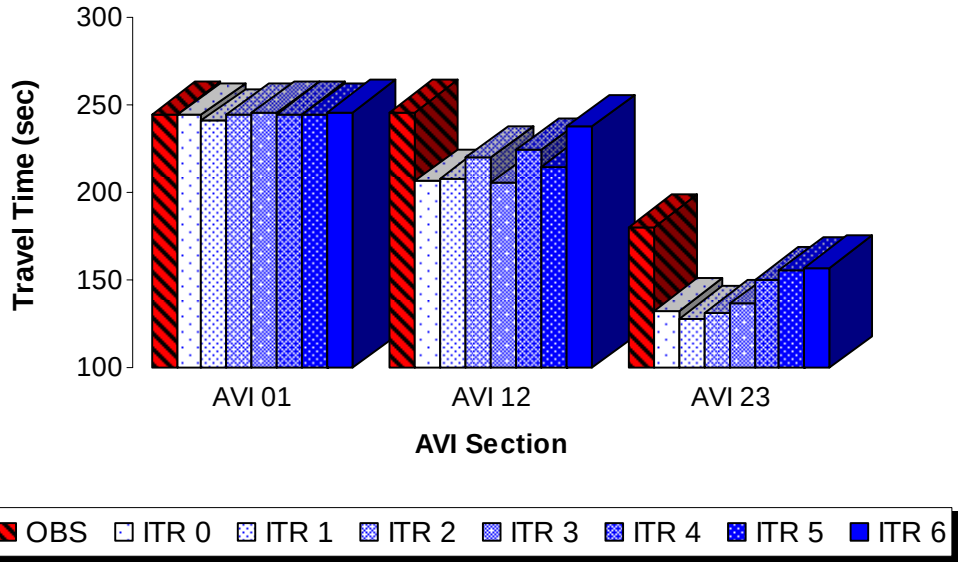

FIGURE D.1 Average Travel Times from the EKF_LTT Algorithm for the I-10 Test Network (7:00AM~7:30AM)

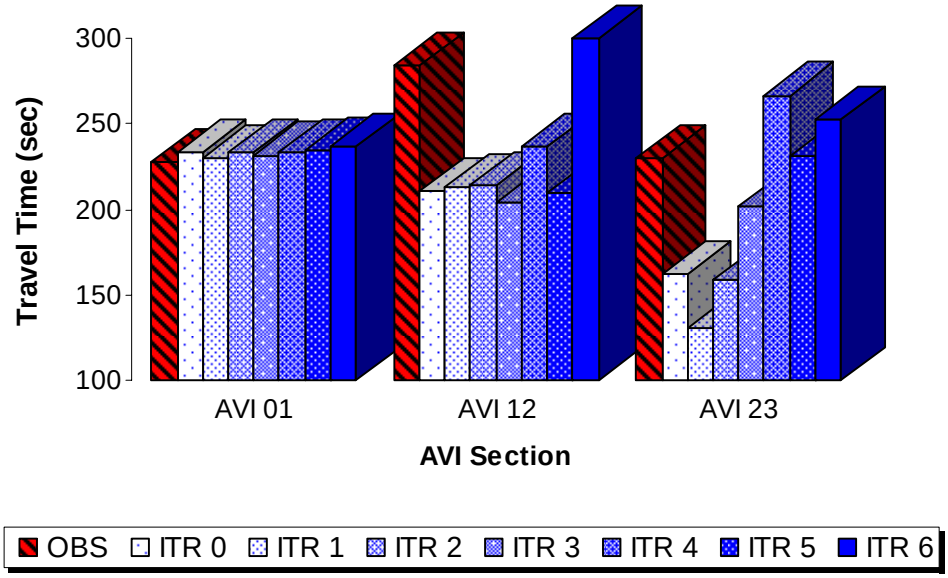

FIGURE D.2 Average Travel Times from the EKF_LTT Algorithm for the I-10 Test Network (7:30AM~8:00AM)

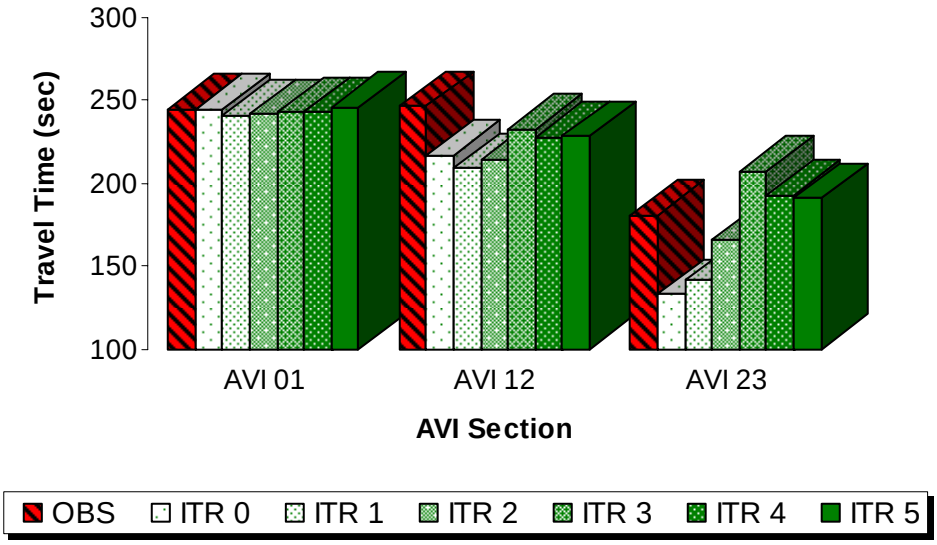

FIGURE D.3 Average Travel Times from the EKF_ODTT Algorithm for the I-10 Freeway Test Network (7:00AM~7:30AM)

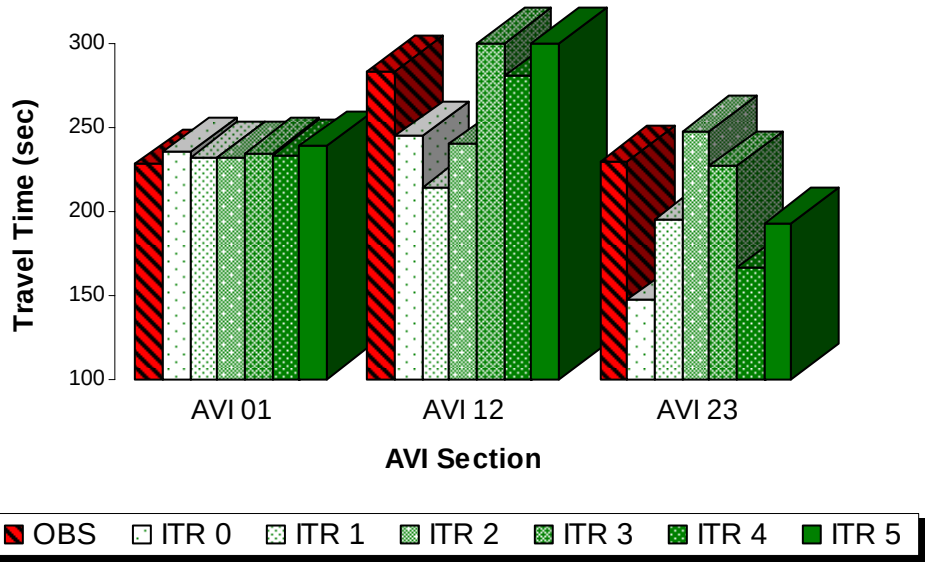

FIGURE D.4 Average Travel Times from the EKF_ODTT Algorithm for the I-10 Freeway Test Network (7:30AM~8:00AM)

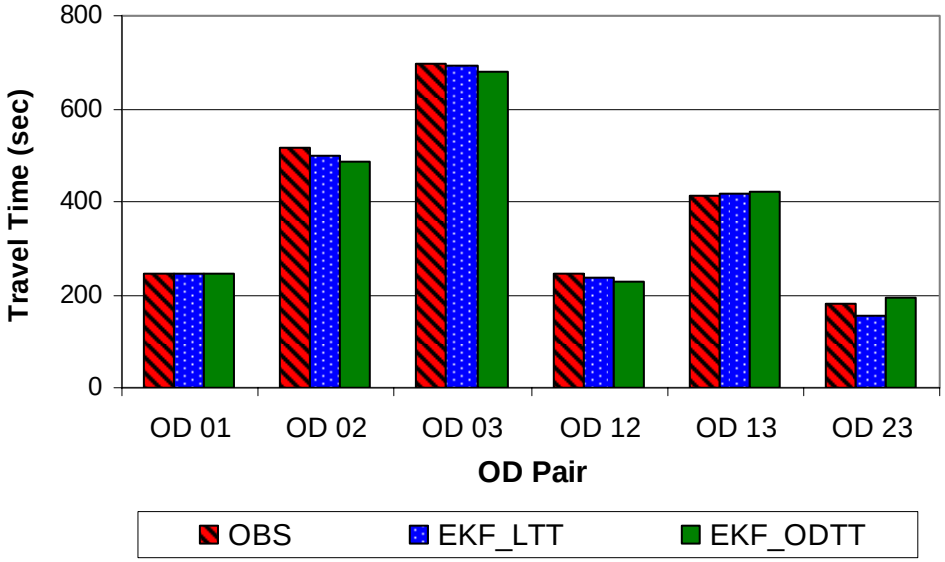

FIGURE D.5 Average Travel Times for OD Pairs for the I-10 Freeway Test Network (7:00AM~7:30AM)

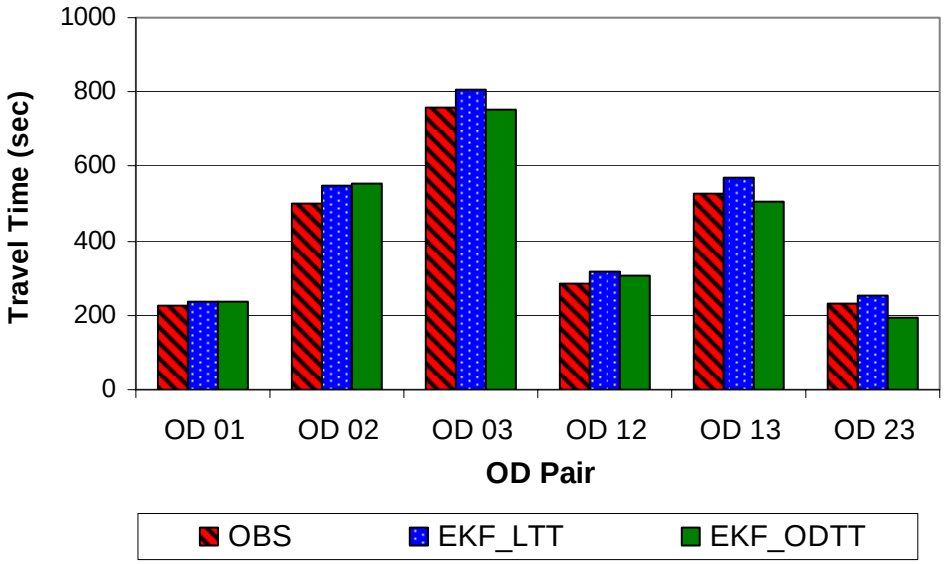

FIGURE D.6 Average Travel Times for OD Pairs for the I-10 Freeway Test Network (7:30AM~8:00AM)

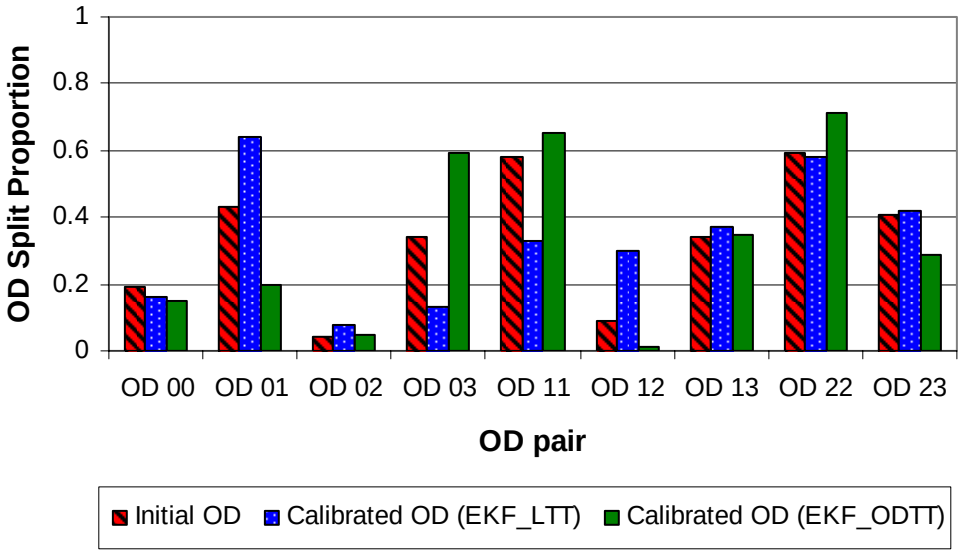

FIGURE D.7 Calibrated OD Split Proportion from the EKF_LTT and EKF_ODTT Algorithm for the I-10 Freeway Test Network (6:30AM~7:00AM)

TABLE D.1 Initial and Calibrated OD Split Proportions at Each Iteration from the EKF_LTT Algorithm for the I-10 Freeway Test Network (6:30~7:00)

Time Interval	OD Pair	0 (Initial)	1	2	3	4	5	6	Diff*
6:30~7:00	00	0.19	0.21	0.17	0.17	0.19	0.17	0.16	-0.03
	01	0.43	0.40	0.47	0.56	0.60	0.61	0.64	0.21
	02	0.04	0.00	0.06	0.05	0.07	0.06	0.08	0.04
	03	0.34	0.39	0.30	0.22	0.14	0.15	0.13	-0.21
	11	0.58	0.52	0.52	0.41	0.39	0.36	0.33	-0.25
	12	0.09	0.08	0.15	0.16	0.25	0.26	0.30	0.21
	13	0.34	0.40	0.34	0.43	0.37	0.37	0.37	0.03
	22	0.59	0.67	0.59	0.59	0.52	0.55	0.58	-0.01
	23	0.41	0.33	0.41	0.41	0.48	0.45	0.42	0.01

TABLE D.2 Initial and Calibrated OD Split Proportions at Each Iteration from the EKF_ODTT Algorithm for the I-10 Freeway Test Network (6:30~7:00)

Time Interval	OD Pair	0 (Initial)	1	2	3	4	5	Diff*
6:30~7:00	00	0.19	0.18	0.18	0.16	0.16	0.15	-0.04
	01	0.43	0.37	0.26	0.23	0.22	0.20	-0.23
	02	0.04	0.00	0.02	0.02	0.02	0.05	0.01
	03	0.34	0.45	0.53	0.60	0.60	0.59	0.25
	11	0.58	0.53	0.62	0.66	0.66	0.65	0.07
	12	0.09	0.00	0.00	0.00	0.03	0.00	-0.09
	13	0.34	0.47	0.38	0.34	0.31	0.35	0.01
	22	0.59	0.68	0.74	0.70	0.69	0.71	0.12
	23	0.41	0.32	0.26	0.30	0.31	0.29	-0.12

* Difference between the initial and final OD split proportions

APPENDIX E

CALIBRATION RESULTS FROM THE BI-LEVEL APPROACH FOR THE CASE STUDY TEST NETWORK

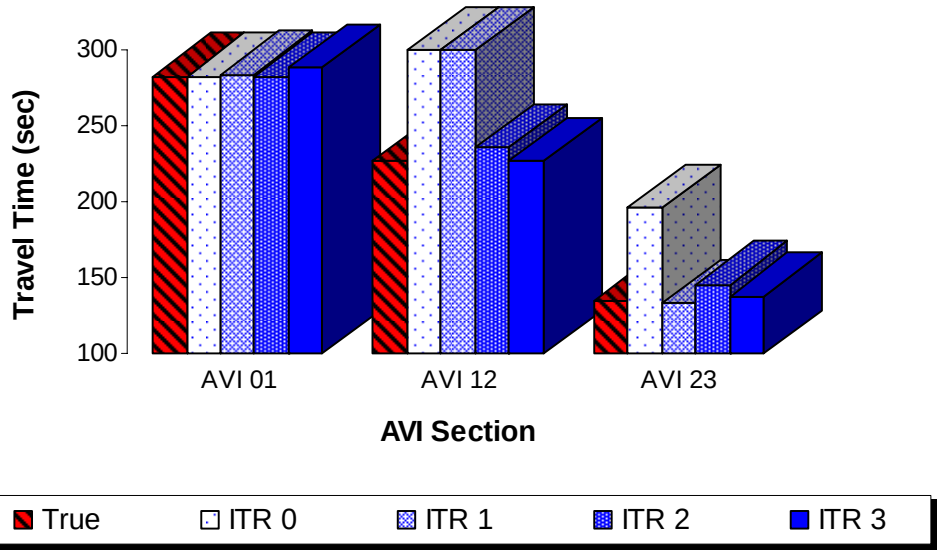

FIGURE E.1 Average Travel Times from the EKF_LTT Algorithm for the Case Study Network (7:00AM~7:30AM)

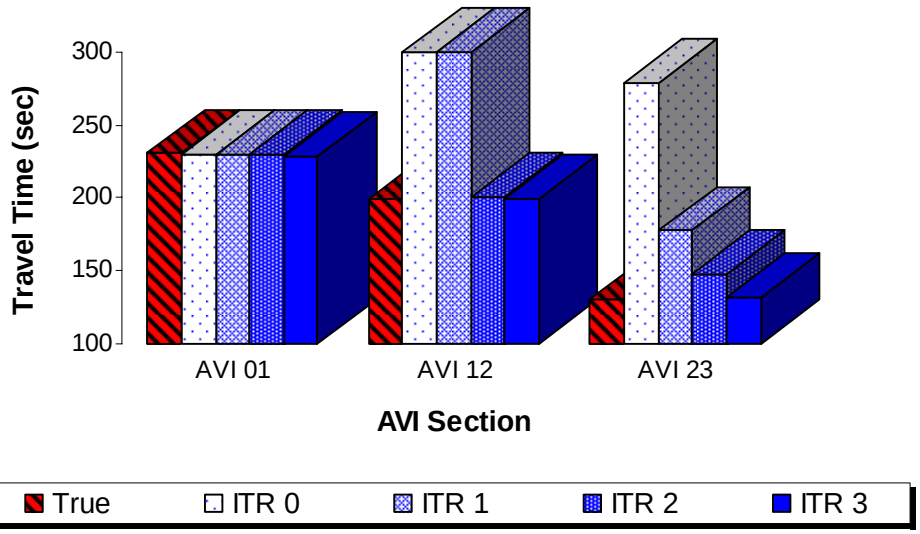

FIGURE E.2 Average Travel Times from the EKF_LTT Algorithm for the Case Study Network (7:30AM~8:00AM)

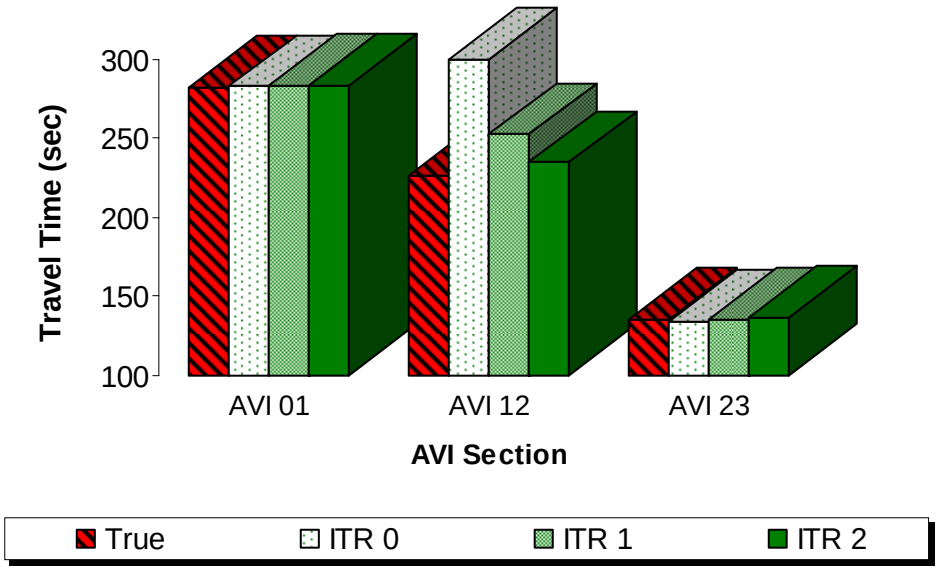

FIGURE E.3 Average Travel Times from the EKF_ODTT Algorithm for the Case Study Network (7:00AM~7:30AM)

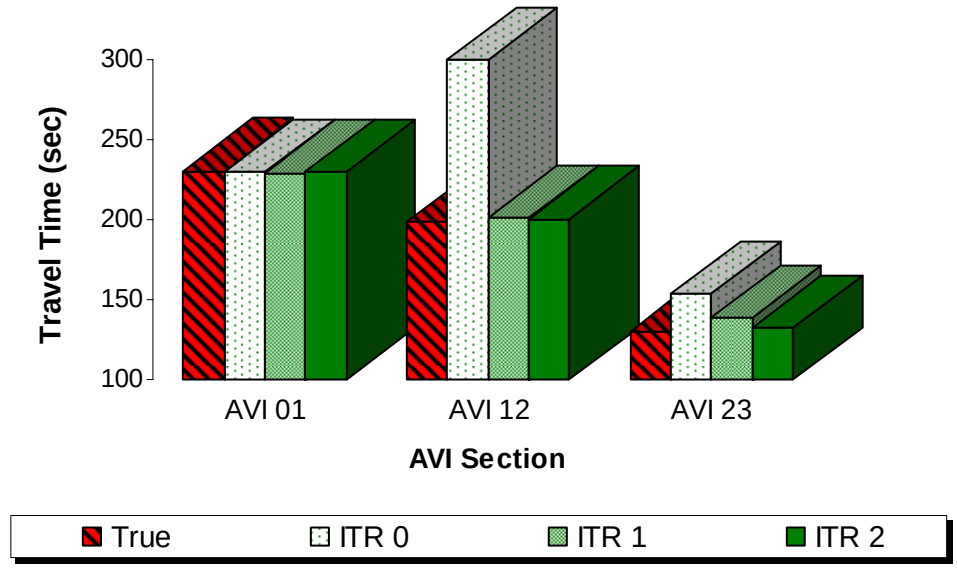

FIGURE E.4 Average Travel Times from the EKF_ODTT Algorithm for the Case Study Network (7:30AM~8:00AM)

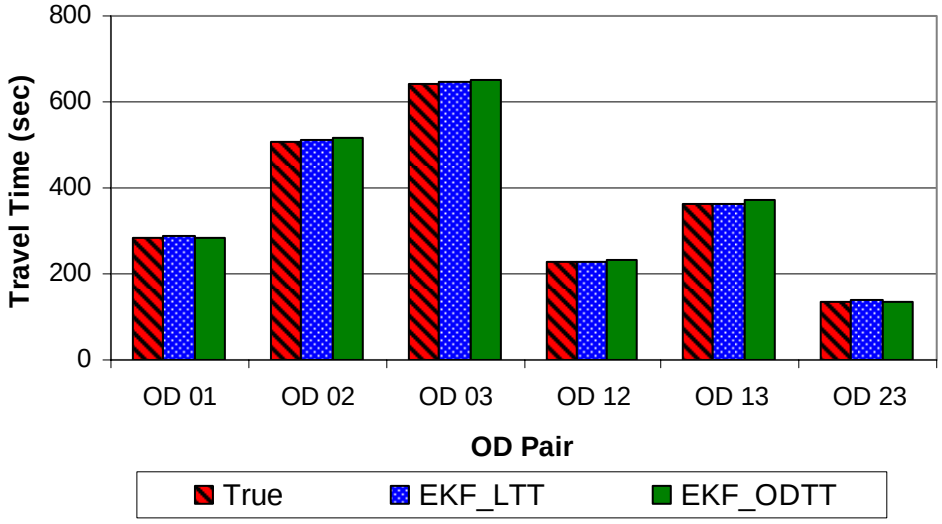

FIGURE E.5 Average Travel Times for OD Pairs for the Case Study Network (7:00AM~7:30AM)

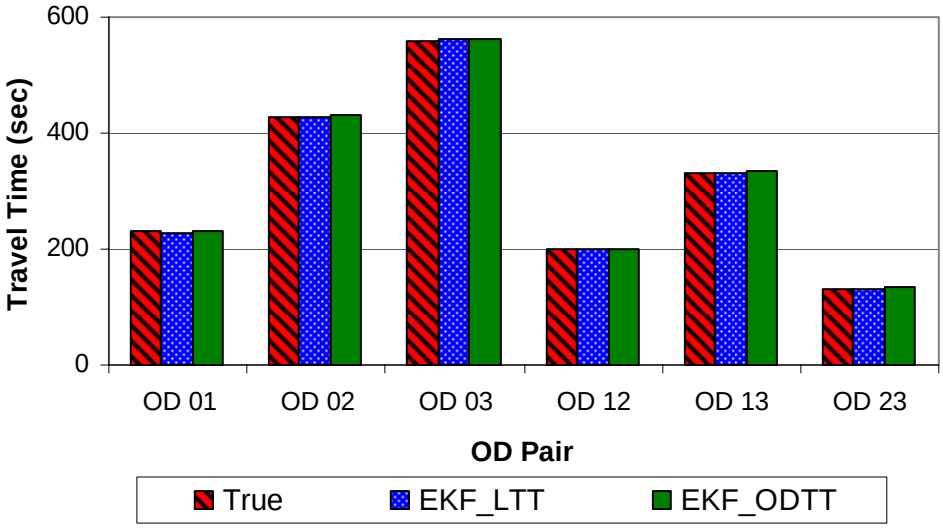

FIGURE E.6 Average Travel Times for OD Pairs for the Case Study Network (7:30AM~8:00AM)

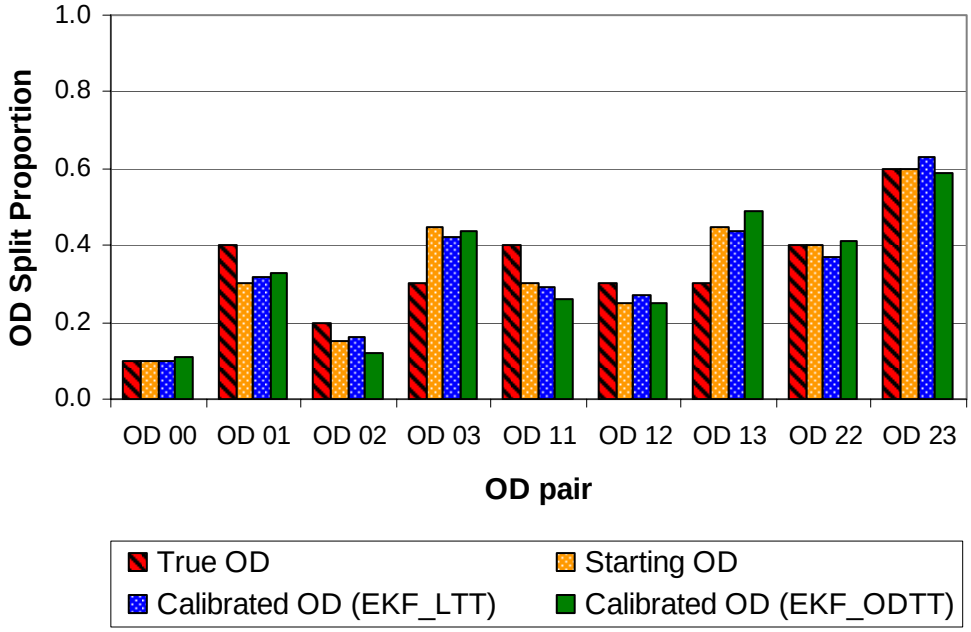

FIGURE E.7 Calibrated OD Split Proportion for the Case Study Network (6:30AM~7:00AM)

TABLE E.1 True, Starting, and Calibrated OD Split Proportions at Each Iteration from the EKF_LTT Algorithm for the Case Study Network (6:30~7:00AM)

Time Interval	OD Pair	True	Starting	1	2	3	Diff*
6:30~7:00	00	0.10	0.10	0.09	0.10	0.10	0.00
	01	0.40	0.30	0.33	0.33	0.32	-0.08
	02	0.20	0.15	0.16	0.16	0.16	-0.04
	03	0.30	0.45	0.41	0.41	0.42	0.12
	11	0.40	0.30	0.28	0.28	0.29	-0.11
	12	0.30	0.25	0.27	0.28	0.27	-0.03
	13	0.30	0.45	0.46	0.44	0.44	0.14
	22	0.40	0.40	0.37	0.35	0.37	-0.03
	23	0.60	0.60	0.63	0.65	0.63	0.03

TABLE E.2 True, Starting, and Calibrated OD Split Proportions at Each Iteration from the EKF_ODTT Algorithm for the Case Study Network

Time Interval	OD Pair	True	Starting	1	2	Diff*
6:30~7:00	00	0.10	0.10	0.11	0.11	0.01
	01	0.40	0.30	0.32	0.32	-0.08
	02	0.20	0.15	0.14	0.13	-0.07
	03	0.30	0.45	0.44	0.44	0.14
	11	0.40	0.30	0.30	0.29	-0.11
	12	0.30	0.25	0.21	0.22	-0.08
	13	0.30	0.45	0.49	0.49	0.19
	22	0.40	0.40	0.41	0.42	0.02
	23	0.60	0.60	0.59	0.58	-0.02

* Difference between the true and final OD split proportions

VITA

Name: Seung-Jun Kim

Address: University of Nebraska at Lincoln, Mid-America Transportation Center, W337 Nebraska Hall, Lincoln, NE 68588

E-mail: kkssjj@hotmail.com

Education: Ph.D., Civil Engineering, Texas A&M University, August 2006
M.S., Civil Engineering, Seoul National University, February 1998
B.S., Civil Engineering, Seoul National University, February 1996

Research Experience:

Graduate Research Assistant, Texas Transportation Institute, April 2001 to August 2004

Graduate Research Assistant, Mid-America Transportation Center, September 2004 to August 2006

Professional Experience:

Researcher, Korea Highway Corporation, February 1996 to November 1996